THE UNIVERSITY OF CHICAGO

MOTILITY OF UNCONVENTIONAL MYOSIN MOTORS RECONSTITUTED ON DYNAMIC ACTIN NETWORKS

A DISSERTATION SUBMITTED TO
THE FACULTY OF THE DIVISION OF THE BIOLOGICAL SCIENCES
AND THE PRITZKER SCHOOL OF MEDICINE
IN CANDIDACY FOR THE DEGREE OF
DOCTOR OF PHILOSOPHY

DEPARTMENT OF BIOCHEMISTRY AND MOLECULAR BIOLOGY

BY

ALICJA SANTOS

CHICAGO, ILLINOIS

MARCH 2017

Copyright © 2016 by Alicja Santos

All Rights Reserved

To Małgorzata Bidzińska & Anna Kosela

“A teacher affects eternity, he can never tell where his influence stops.”

TABLE OF CONTENTS

LIST OF FIGURES……viii

LIST OF TABLES……xi

LIST OF ABBREVIATIONS……xii

ACKNOWLEDGMENTS……xiv

CHAPTER 1: GENERAL INTRODUCTION……1

1.1. Myosin motors, mechano-enzymes that run the cells……2

1.1.1. Overview of myosin motor classes……2

1.1.2. Myosins as transporters, anchors and force generators……4

1.1.3. Myosin domains and their functions……5

1.1.4. ATPase cycle and mechanism of myosin processivity……7

1.2. Actin cytoskeleton: dynamic and complex track system……10

1.2.1. The role of actin rearrangements in eukaryotic cell……10

1.2.2. Compartmentalization of actin cytoskeleton……10

1.2.3. Navigating the complex meshwork of paths……11

1.2.4. The structure of actin……13

1.2.5. Actin polymerization scheme……14

1.2.6. Three phosphate states that define the age of actin……15

1.2.7. Phalloidin preserves phosphate state in actin filament……17

1.3. The unconventional myosin we know the most about: myosin-5……18

1.3.1. Cellular functions of myosin-5……19

1.3.2. Structure of myosin-5……19

1.3.3. Processive movement of myosin-5……20

1.4. Out of the ordinary: myosin-6, the pointed end directed motor 21
1.4.1. From endocytosis to hearing: myosin-6 functions 21
1.4.2.Flexibility in myosin-6 lever arm.....22
1.4.3. Wide range of step sizes and back steps of myosin-6.....23
1.5. Questions addressed in this thesis 23
CHAPTER 2: ACTIN AGE ORCHESTRATES MYOSINS RUN LENGTHS.....26
2.1. Introduction 26
2.2.Reconstitution of native-like actin tracks for myosin motility 28
2.2.1.Single filament elongation in conditions adapted for myosins 28
2.3. Myosin-5 and myosin-6 detect actin nucleotide state aka actin age.....30
2.3.1. Differences in myosin run lengths on assembling vs stabilized actin 30
2.3.2. Myosin response to nucleotide state gradient within filament.....35
2.4. Myosin run lengths are not affected by the stabilizer 38
2.4.1. Distinct phosphate states of phalloidin stabilized filaments.....38
2.4.2. Capping stops growth and sets uniform filament age.....39
2.4.3. Myosin run lengths are dictated by phosphate state, not the stabilizer....39
2.5. Actin nucleotide state affects myosin landing rates 41
2.6. Parameters unaffected in assembling assay and the implications.....43
2.6.1. Velocities of myosins do not change upon different Pi state 43
2.6.2. Actin filament assembly rate remains unchanged 44
2.7. Discussion.....45
CHAPTER 3: SHARING ONE TRACK: BIDIRECTIONAL MOTILITY OF MYOSIN-5 AND MYOSIN-6 ON A SINGLE FILAMENT 50

3.1. Introduction 50
3.1.1. Bidirectional motility of myosin-5 and-6 on single filament 52
3.2. Simultaneous myosin-5 and myosin-6 motility reconstituted on a single filament . 53
3.3.The geometry of the collision 56
3.3.1. Paths available for myosin motor on a single actin filament 56
3.3.2.Defining the ‘head on’ collisions 58
3.4.Outcomes of encounters between myosin-5 and myosin-6 60
3.4.1.Outcomes of ‘head on’ collisions 60
3.4.2. Both myosins continue their runs after encountering each other 61
3.4.3. Only one motor continues the run after the collision 62
3.4.4. Both myosins detach or stall 62
3.4.5. Competition vs blocking 63
3.5. A stochastic simulation that predicts ’head on’ collision outcomes 64
3.5.1. Gillespie's stochastic simulation algorithm 64
3.5.2. Outcome of collision series based on experimental kinetic rates 67
3.5.3. Analysis of collision outcomes with wide range of kinetic rates 67
3.6. Discussion 69
CHAPTER 4: CONCLUDING REMARKS 71
4.1. Synthesis of experimental findings 71
4.2. Biological significance and applications 74
4.3. Recommendations for future research 76
CHAPTER 5: METHOD RATIONALE AND DEVELOPMENT 80

5.1. Objectives of the assay 80
5.2. Construct design, protein purification and labeling 81
5.3.Gliding filament assay and TIRF assay 84
5.4. Data collection and analysis 86
APPENDIX A: MOTILITY OF MYOSIN-10 ON GROWING BUNDLE 88
A.1. Introduction 88
A.2. Finding the way to cell's farthest ends: myosin-10 in filopodia 90
A.3. Evolutionary designation and unique structure of myosin-10 90
A.4. Stepping mechanism adapted for bundle selectivity 92
A.5. Observation of bundle formation and elongation in real time 94
A.6. Reconstitution of myosin-10 motility on assembling bundle 95
A.7. Minimal requirement of filaments in the bundle for processivity 95
A.8. Conclusions and recommendations for future research 96
APPENDIX B: ACTIN FILAMENT BY ATOMIC FORCE MICROSCOPY (AFM) 98
B.1. Introduction 98
B.2. Details of sample preparation for AFM 100
B.3. Principles of imaging by AFM 101
B.4. Structural details of actin filament captured by AFM imaging 103
B.5. Conclusions and recommendations for future research 106
REFERENCES 108

Movies 2-1, 3-1, 3-2, and A-1 available as supplementary files

LIST OF FIGURES

FIGURE 1.1 Phylogenetic tree of the myosin motor domains 3

FIGURE 1.2 The common structural features of myosins. 7

FIGURE 1.3 Myosin chemo-mechanical cycle of myosin motor domain 8

FIGURE 1.4 Cellular actin structures of various organization and functions 12

FIGURE 1.5 Model of the F-actin structure 13

FIGURE 1.6 Three consecutive phases of actin filament assembly 15

FIGURE 1.7 Actin filament aging by ATP hydrolysis and Pi release 17

FIGURE 1.8 Model of dimerized myosin stepping mechanisms along F-actin on example of myosin-5 21

FIGURE 2.1 Schematic of the experiments 27

FIGURE 2.2 Time-lapse fluorescence micrographs of a single myosin-6 motor moving along single assembling actin filament 29

FIGURE 2.3 In vitro reconstitution of myosin-5 or myosin-6 motility on assembling F-actin 29

FIGURE 2.4 Experimental time course for obtaining desired filament phosphate state. 31

FIGURE 2.5 Run lengths of myosins along the F-actins listed in Figure 2.4 33

FIGURE 2.6 A schematic kymograph of myosin-6 runs on a growing filament 36

FIGURE 2.7 Run lengths 36

FIGURE 2.8 Five distinct phosphate states of actin filaments used in experiments ..38

FIGURE 2.9 The actin filament stabilizer does not affect myosin run lengths 40

FIGURE 2.10 Myosin-5 lands more frequently on ADP•Pi F-actin, whereas myosin-6 lands more frequently on ADP 42
FIGURE 2.11 Myosin speed on ADP•Pi decay and static ADP F-actin remains the same 43
FIGURE 2.12 Growth rates of assembling F-actin in the presence of myosin-5 or myosin-6 remain the same.....45
FIGURE 3.1 Schematic of the experiments 50
FIGURE 3.2 Myosin-5 and myosin-6 sharing the same elongating actin filament in vitro for the bidirectional motility 52
FIGURE 3.3 Representative kymographs showing simultaneous motility of myosin-5 and myosin-6 on elongating filaments. 54
FIGURE 3.4 Spatial arrangement of myosin-5 and myosin-6 during bidirectional motility along a single filament. 57
FIGURE 3.5 Visualization of accessible tracks for myosin walking along the filament... 59
FIGURE 3.6 Collisions between myosin-5 and myosin-6 lead to five possible outcomes 61
FIGURE 3.7. Collisions outcomes.....63
Figure 3.8. A stochastic simulation predicts that the faster myosin should detach more frequently when colliding with a slower myosin.....66
FIGURE 3.9 A contour plot of the probability of myosin-5 detaching first at a collision, detachment and rebinding rates 68
FIGURE 5.1 Fractions of TMR labeled actin via SDS-PAGE 82

FIGURE 5.2 Concentrations of myosin-5 (M5) and myosin-6 (M6) by SDS-PAGE 83
FIGURE 5.3 Gliding filament assay.....85
FIGURE 5.4 TIRF set-up to study myosin motility on elongating F-actin 86
FIGURE A.1 Myosin-10 HMM localizes to the tips of filopodia and retraction fibers..89
FIGURE A.1 A model of myosin-10 bundle selectivity mechanism. Adapted from Nagy et al. and Vavra et al. 93
FIGURE A.2 A scheme of a bundle assembling from de novo polymerizing filaments..94
FIGURE A.3 Kymographs showing motility of myosin-10 HMM GCN4 construct across assembling fascin-actin bundle 96
FIGURE B.1 Cryo-EM reconstruction of F-actin decorated with tropomyosin 100
FIGURE B.2 Schematic of tapping-mode AFM setup.....102
FIGURE B.3 The topography of actin filaments via AFM 104
FIGURE B.4 Series of close-up images of the region along actin filaments via AFM.....105

LIST OF TABLES

TABLE 1. Run length summary statistics for myosin motors moving along F-actin with the set of nucleotide states and filament stabilizers. 32

TABLE 2. Run length summary statistics for myosin-5 and myosin-6 moving along assembling actin within bands of different nucleotide states along the filament. Mean and madian runlength as well as the confidence interval (CI) also shown. 37

TABLE 3. Velocity summary statistics for myosin motors moving along F-actin with the set of nucleotide states and filament stabilizers. 44

LIST OF ABBREVIATIONS

ABD	Actin Binding Domain
ABP	Actin Binding Protein
ADP	Adenosine Diphosphate
ADP•Pi	Adenosine Diphosphate with Inorganic Phosphate Bound
ATP	Adenosine Triphosphate
BME	2-Mercaptoethanol
BSA	Bovine Serum Albumin
CaM	Calmodulin
C_c	Critical Concentration
EM	Electron Microscopy
FERM	Four-point-one/ Ezrin/ Radixin/ Moesin
FPLC	Fast Protein Liquid Chromatography
F-actin	Filamentous Actin
G-actin	Globular Actin
GFP	Green Fluorescent Protein
HMM	Heavy Meromyosin
HPLC	High Performance Liquid Chromatography
LMM	Light Meromyosin
MyTH4	Myosin Tail Homology 4
MT	Microtubule
P_i	Inorganic Phosphate
PDB	(RCSB) Protein Data Bank

PSPD	Position-Sensitive Photo Diode
S1	Subfragment 1
S2	Subfragment 2
SDS-PAGE	Sodium Dodecylsulfate Polyacrylamide Gel Electrophoresis
SD	Standard Deviation
SE	Standard Error of the Mean
SEM	Standard Error
QDot	Quantum Dot
TIRF	Total Internal Reflection Fluorescence
TMR	Tetramethyl Rhodamine
WT	Wild-type

ACKNOWLEDGEMENTS

The research presented in this Thesis has been catalyzed by multiple people: I am very thankful for the inspiration and support I have received over the years from my instructors, teachers, mentors, co-workers, friends and family.

Firstly, I would like to thank Prof. Ronald Rock for the open-minded and patient guidance that helped me gain confidence as an independent researcher. While working in Ron's group I was always given the chance to be in charge of designing experimental approach and follow my scientific interests. Ron's trust in my capacity was one of the greatest motivations and propellers of professional and personal growth over all the years I worked in his group.

I have had an honor to be advised by an extraordinary Thesis Committee, that kept my research in line and provided me with in depth feedback. Therefore I would like to thank Prof. Erin Adams, Prof. Shohei Koide and Prof. David Kovar. Erin, the Committee Chair, always had her doors open for me to step by to discuss science and any other aspect of my graduate training at the University of Chicago. Erin's supportive words, amplified by an example of her spectacular career in academic research, have always empowered me as a female scientist. Enormous insights given by Shohei improved the scientific approach and broaden the horizons for the scientific discoveries presented here. Shohei taught me how extremely meaningful scientific questions are and that as scientists, asking the right questions is equally important to answering them correctly. I am very thankful to David for inviting me for the rotation to his group, where my PhD project sprouted from an idea to the hands-on experiments.

From there, a new collaboration emerged between Rock & Kovar labs in reconstituting actin networks for myosin motility assessment.

Prof. Anthony Kossiakoff deserves a special mention for all his support along stages of my scientific career. Collaborations with Kossiakoff lab were critical for development of synthetic antibodies presented in the Appendix of this Thesis and laid the groundwork for major future directions emerging from my PhD work.

Next, I would like to thank the members of the University of Chicago Cytoskeletal groups: Gardel, Glotzer, Gupta, Kovar, Munro and Voth labs. The positive feedback loops and creativity sparks during our biweekly meetings were extremely valuable to the progress of my project.

Pursuing my scientific goals was possible thanks to the personal funding sources supporting the work presented in this Thesis: Dean's International Student Fellowship at The University of Chicago and The American Heart Association Predoctoral Fellowship Program, no 16PRE26850006.

Many thanks to colleagues of mine, which I worked back to back with and shared many scientific discussions that shaped this Thesis. These include many members of Rock, Kosiakoff, Kovar and Keenan labs: Dr. Alex French, M.Sc. Natalia Plewa, M.Sc. Natalia Zapiórkowska, M.Sc. Łukasz Truszkowski, Dr. Gosia Nocula-Ługowska, Dr. Mateusz Ługowski, Dr. Dennis Zimmermann, Dr. Agnieszka Mateja-Paduch, M.Sc. Szymon Kordon, Dr. Marcin Ura, Dr. Annika Sääf, Dr. Marcin Paduch, Dr. Crista Brawley, Dr. Stanislav Nagy, Dr. David Courson, Dr. Benjamin Ricca & many others. Very special thanks to M.Sc. Joanna Kalita, co-worker and close friend, that made the lab an effect and joyful work place. I also thank my cohort of PhD

Candidates: May Gu, Tylor Starr, Molly Evans, Matthew Tien, Louesa Akin, Ronnie Almonte and Jordan Sullivan for their support at all times and for making the graduate school an unique experience.

From my first day of PhD program I had great friends and inspiring scientists at my side, serving with their advice and presence. I would not achieve my goals withouth Dr. Paweł Dominik, Dr. Agnieszka Misiura-Hyde, Dr. Clark Hyde, Dr. Anna Łuchniak and soon-to-be Dr. Marta Borowska.

I would like to acknowledge my family and their contribution to my PhD. I would like to thank my parents: Grażyna and Tadeusz Janik and my brother Mateusz for always being there for me. Finally, special thanks to my husband Igor and daughter Natalia, who gave me everlasting motivation that helped in gaining the kind of focus that accelerates the researchers: I am grateful for their love.

CHAPTER 1: GENERAL INTRODUCTION

Cellular interior is organized on a scaffold constructed of cytoskeletal proteins. Apart from maintaining the shape and providing mechanical support, the cytoskeleton enables cells to carry out fundamental processes such as division or movement. In response to cell's needs two proteins, actin and tubulin, assemble into polarized polymers. Actin forms thin, flexible, helically twisted fibers called actin filaments. Tubulin arranges into long cylinders of outer diameter about three times wider than the actin filament. These structures are called microtubules (MTs). Both, actin filaments and MTs serve as tracks for the transport on molecular level. MTs support motility of motor proteins called kinesins and dyneins, actin is a platform for myosin motors proteins. There are numerous other participating factors associated with cytoskeleton that influence both the track and the motor components. Overall, the nature of protein interactions within the cellular cytoskeleton is complex and dynamic, however organized with distinct precision. In the work described here I will focus on actin based motility. Myosin motors, functioning on actin, emerge as main players in maintaining cellular shape and transport in eukaryotic cells. Even slight perturbations of myosin-actin interplay result in serious defects of cellular function. The disruptions entail severe global effects, that lead to multitude of diseases ranging from deafness to cancer metastasis. Despite their importance, little is known about how distinct myosin motor families navigate to find their proper cellular destination.

1.1. Myosin motors, mechano-enzymes that run the cells

1.1.1. Overview of myosin motor classes

Myosins are a large superfamily of motor proteins that generate force by ATP hydrolysis during an interaction with actin filaments. The most recent report, through sequence alignment from genes encoding myosin motor domains of over 300 eukaryotic organisms, emerges with an impressive phylogenetic tree of myosin motors (Figure 1.1) (Odronitz & Kollmar, 2007). Myosin motor domains are classified into 35 classes, of which 16 newly discovered ones have unique domain organizations that are defined based on sequence analysis (Odronitz & Kollmar, 2007). Each myosin class has subsets of different types. A human genome itself contains more than 40 different types of myosin genes, organized into at least 18 different classes (Berg et al., 2001).

Myosins are best known for their role in muscle contraction, as the first identified and studied for over 150 years motor protein is skeletal myosin, representing class 2. Myosin-2 is responsible for generating the force in muscle movement. Several hundred myosin-2 molecules bound by their C-terminal tails build thick filaments in muscles. The N-terminal motor domains pull on and slide thin filaments composed of filamentous actin (F-actin), resulting in powerful collective motion fueling the muscle. The relatively well known mechanism in which myosin motor domains derive force from energy contained in ATP is in fact widespread well beyond muscle tissues, as myosins are known to be present in all eukaryotic cell types. The myosins that are found in nonmuscle cells, including even certain protozoan cells, are called unconventional myosis. They also generate force during their ATPase cycle, quite like skeletal myosins and the ‘feet’ are very closely related, with rather minor structural differences.

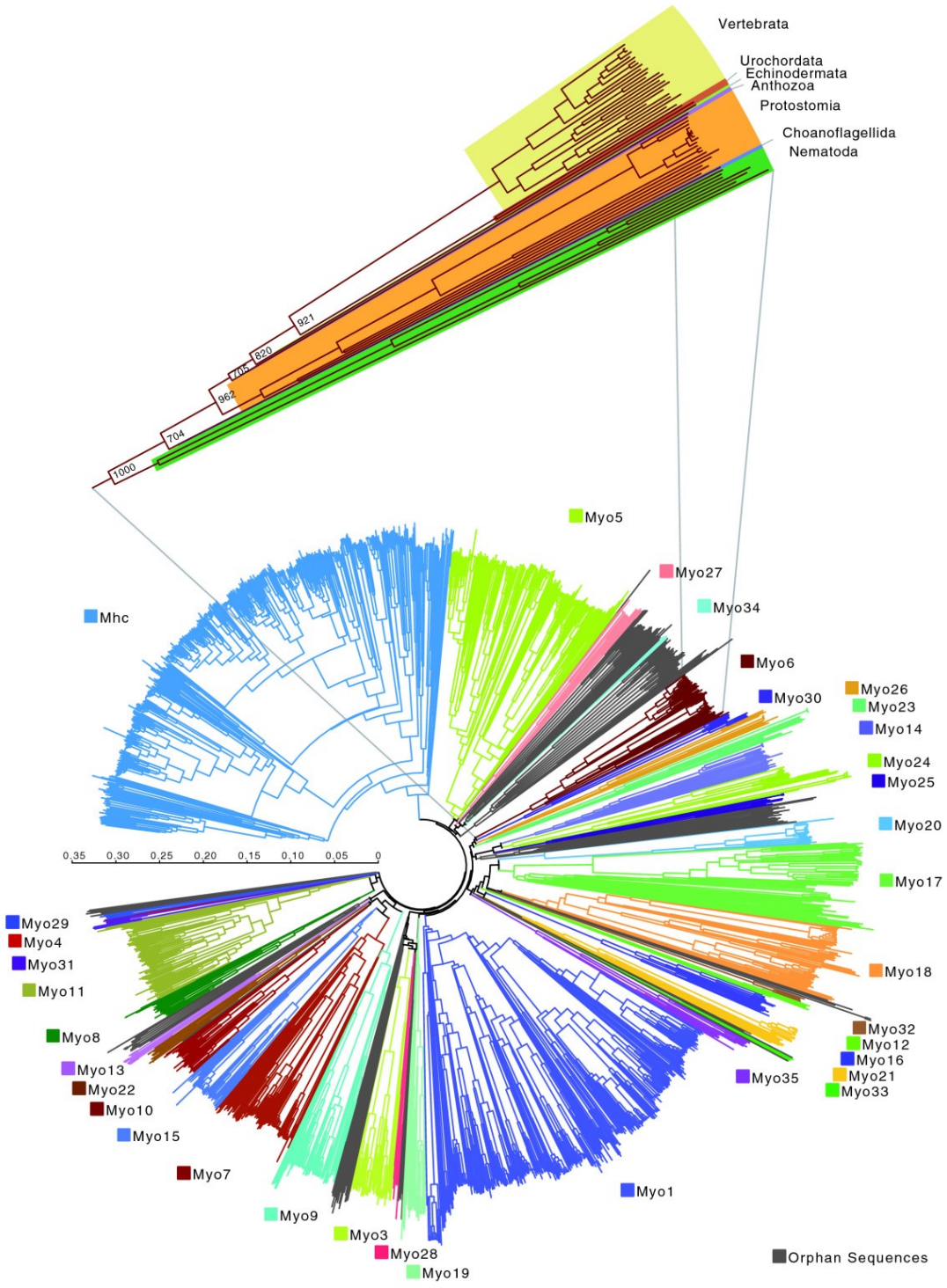


FIGURE 1.1 Phylogenetic tree of the myosin motor domains
The non-rooted phylogenetic tree built from the sequence alignments of myosin motor domains. The expanded view shows myosin-6 class sequences and their distribution in taxa. SOURCE: (Odronitz & Kollmar, 2007)

The defining property for this large subset of myosin superfamily is the fact that unconventional myosins do not form filaments like conventional myosin do in muscles, but go through their kinetic cycle as monomers or dimers. The ubiquitous presence of unconventional myosins is extremely important for variety of cellular process. These myosis function in cellular transport, anchoring/tethering, tension sensing, actin organization and cell motility/adhesion (Hartman et al., 2011). With the myosin motor domains conserved, the multitude of functions assigned is a result of tailored structural details and evolutionary adaptations that differ myosin classes from each other.

1.1.2. Myosins as transporters, anchors and force generators

The multitude of specialized tasks that unconventional myosin motors perform, has been studied for nearly 40 years. Detailed knowledge about members of the myosin superfamily leads to a comprehensive understanding of the cytoskeletal system as a whole. To exemplify the versatility of myosin motors, we may look at a few representatives of the superfamily: Myosin-1 class plays a role in membrane dynamics and actin organization at the cell cortex, thus affecting cell migration, endocytosis, pinocytosis and phagocytosis (Goodson et al., 1996; Ostap & Pollard, 1996; Yamashita & May, 1998); Myosin-3 class is required for phototransduction and maintenance of the rhabdomere in flies (Ng et al., 1996; Porter & Montell, 1993); Myosin-7 is found in the inner ear in vertebrates, and certain mutations in the gene coding for myosin-7 cause deafness in mice and humans (Liu et al., 1997); Myosin-9 negatively regulate the small G-protein Rho, a signaling molecule that regulates the organization of the actin cytoskeleton. (Chieregatti et al., 1998). In this work I am considering two other

unconventional myosin motors: myosin-5 and myosin-6. The multifaceted roles of myosins used in this dissertation will be discussed later in this chapter.

1.1.3. Myosin domains and their functions

All myosins share similar basic features in their overall structure. The N-terminal motor domain, also called a 'foot', is followed by the extended 'leg' region with IQ motifs that bind calmodulin or calmodulin-like light chain, and finally the tail region with dimerization and cargo binding domains at the C-terminus (Figure 1.2). According to older terminology myosin foot could be also referred to as a 'head', the leg region was called the 'neck' region. These terms are used exchangeably in the cited literature, however for the purposes of this dissertation the names foot and leg will be used, as they were acknowledged by the field in recent years as more accurate representation for unconventional myosins walking along actin.

Each of the three major myosin domains, foot, leg and tail, plays a different function. In brief, the motor domain contains the actin binding site that binds to the track and nucleotide binding site responsible for ATPase activity. Next are the light chains, bound to the IQ motifs along the leg region. The light chains regulate the motor domain. The tail domain governs dimerization and cargo binding properties, ultimately dictating the specific role of each myosin in the cell. More details on the myosin domains functions specifically for myosin-5 and myosin-6 will be provided later in this chapter.

Another way to differentiate the structure of myosin is a conclusion from enzymatic proteolysis of the motor. Myosin can be cleaved at the base of the leg region, before tail domain into paired-foot and leg fragment, called heavy meromyosin

(HMM), and a rodlike tail fragment, called light meromyosin (LMM). Further digestion of HMM splits off the neck region (S2 fragment) and leads to separation of the two feet domains into single myosin foot fragments (S1 fragments). This classification is an important one, because for a single molecule studies HMM portions of the myosins are used in majority of cases. Typically two HMMs of unconventional myosin are fused with additional dimerization domains in place of natural occurring lower affinity dimerization domain. The artificial dimerization domains are typically high affinity structures to ensure that homodimers of the myosins are formed and sustained in the low concentration of proteins required for majority of experimental set ups and in absence of cargoes that are thought to assist or even induce dimerization of myosin (Yu et al., 2009).

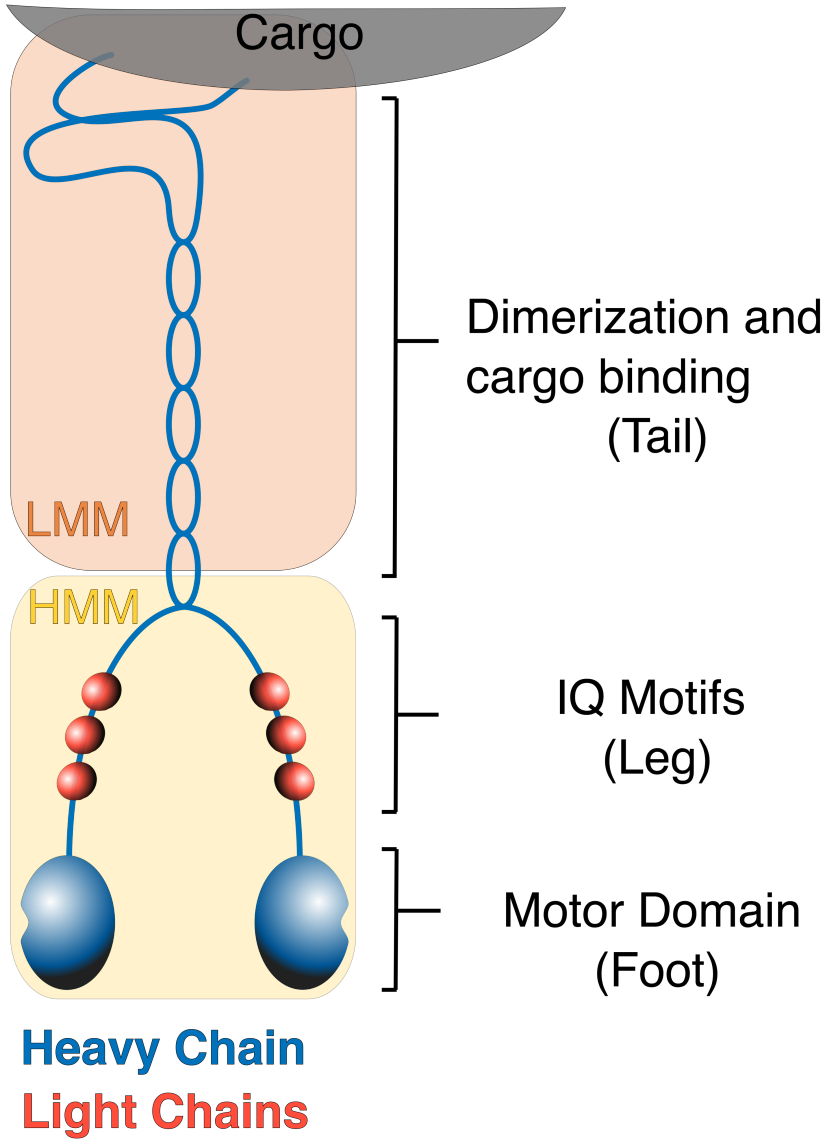


FIGURE 1.2 The common structural features of myosins.
Example of a generic myosin presented here is a homo-dimer, dimerized within its tail domain when bound to a cargo. IQ motifs in the leg region bind, in this case, three light chains that regulate the function of N-terminal motor domain (the foot). Domains are not to scale.

1.1.4. ATPase cycle and mechanism of myosin processivity

As mentioned before, the ATPase cycle is conserved for all myosin isoforms in terms of the order in which the kinetic intermediates occur (De La Cruz & Ostap, 2004) (Figure 1.3). In the absence of ATP, myosin foot is bound tightly to actin. ATP binding

induces a conformational change in myosin that weakens its actin affinity and causes the myosin foot to detach from the filament. ATP is subsequently hydrolyzed to ADP•Pi, with the hydrolysis product remaining bound to myosin.

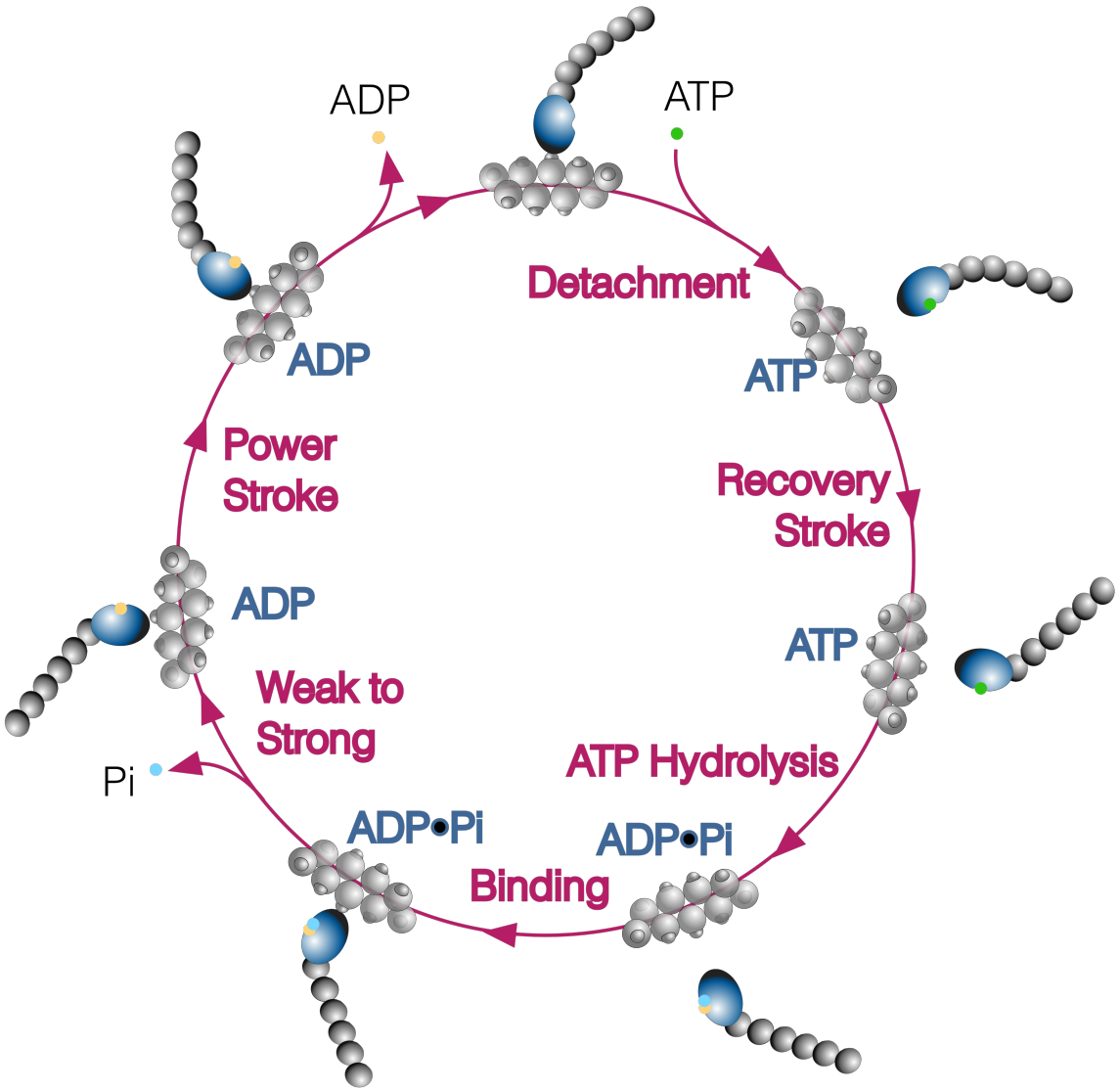


FIGURE 1.3 Myosin chemo-mechanical cycle of myosin motor domain
The scheme shows phases of ATP-ase cycle for a single motor domain in relation to nucleotide and actin binding.

Myosin with ADP•Pi rebinds to actin filament and the force generating power-stroke is originated by the phosphate release. During such phosphate release the myosin feet transitions from a weakly bound state to being strongly bound to actin. Once the foot is bound, ADP is released, causing unbinding from the filament and preparing the myosin motor domain to receive new portion of energy in new ATP molecule. The cycle repeats upon ATP binding.

The myosins studied here are high duty ratio motors, which means that most of their kinetic cycle is spent bound to the actin filament. The duty ratio can be simply defined as the fraction of the total time in the chemo-mechanical cycle that motor domain spends in an ATP hydrolysis state with high affinity for actin. The other term that describes myosins studied here is processivity, which means they are able to take subsequent steps, moving along the filament withouth detachment. The processivity is possible because the myosin undergoes multiple catalytic cycles. Each catalytic cycle is coupled with the power stroke and subsequent diffusional search by the leading foot for the proximal binding side on actin. The longer time which the trailing myosin foot spends bound to the actin filament, keeping entire protein in proximity to the track, allows the leading foot to search efficiently for the next binding spot. Therefor the hight duty ratio results in more binding events for the leading foot and more processive steps. Additional factor that promotes processivity is coordination of the two feet during stepping, as it happens in case of e.g. myosin-5 (Sakamoto et al., 2008). This coordination involves intramolecular strain generated between both feet when they are attached to actin. This strain differentially affects trailing and leading foot. All those mechanisms are enabling single motors, such as unconventional myosins or kinesins,

to support movement of cargoes along cytoskeletal tracks (Hancock & Howard, 1998; Mehta et al., 1999).

1.2. Actin cytoskeleton: dynamic and complex track system

1.2.1. The role of actin rearrangements in eukaryotic cell

The cytoskeleton of each living cell is a dynamic structure with multiple proteins acting together in the concert. The actin meshwork undergoes constant changes that enable essential processes like motility, polarization and cell division (Pollard & Cooper, 2009). Motor proteins are actively 'walking' and transporting cargoes around the cell, but they are not the only highly dynamic element of the meshwork. Actin tracks are also 'on the move', being assembled in one part of the cytoskeleton and disassembled in the other part. This is a peculiar mechanism, in which the cell addresses its local needs by utilizing the globular actin (G-actin) subunits reclaimed from disassembled filaments. Since cells have relatively limited pool of G-actin available as a building block, the dynamic rearrangements are happening constantly in each living cell.

1.2.2. Compartmentalization of actin cytoskeleton

Cellular actin meshwork is not an uniform structure, but a compartmentalized space that with each region playing different role for cellular physiology. At the cell's forefront actin network stays spread close to the surface, with filaments that are branched and crosslinked, forming the lamellipodium. The lammellipodium is the region where cell movement starts, since the filaments push the cell membrane by polymerizing against it (Figure 1.4). A structures that emerge from lammellipodium as bundled filament extending into the environment are filopodia — cell's fingertips

important for directional response of the cell. Plasma membrane at the back and sides of the cells is covered in a thin layer of actin meshwork called a cell cortex, important for cell shape maintenance and changes. The cell body contains a network of cross-linked filaments interspersed with contractile bundles, including stress fibers that connect the cell cytoskeleton to the extracellular matrix via focal adhesion sites (Blanchoin et al., 2014). Myosin motors respond to these differences in structure and they are thought to be optimized by evolution to fulfill particular roles at specific places in the cell. An example of such adaptation is myosin-10, that co-localizes with tips of filopodia and plays a role in building and transporting cargoes to those cellular fingers, assisting in cell migration (Berg & Cheney, 2002; Bohil et al., 2006). In this work I am investigating basis of adaptive behavior that myosin-5 and myosin-6 present as well.

1.2.3. Navigating the complex meshwork of paths

In cells actin is arranged in a network of highly dynamic polymers that undergo rapid cycles of assembly and disassembly. The ability to rearrange filaments depending on state of cell cycle and subcellular localization is an intrinsic property of cellular actin. As mentioned, inside the cell, actin matrix is shaped differently in particular cytoskeletal regions, creating distinct local environments such as stress fibers, lamellipodia or filopodia (Figure 1.4). The process of forming and differentiating these characteristic features brings another level of dynamicity of cytoskeleton driven and controlled by set of actin binding proteins (ABPs). Attempts to capture the dynamic properties of cytoskeletal meshwork *in vitro* in order to identify how they are fine-tuning myosin motility is one of the goals of the cytoskeletal field (Brawley & Rock, 2009).

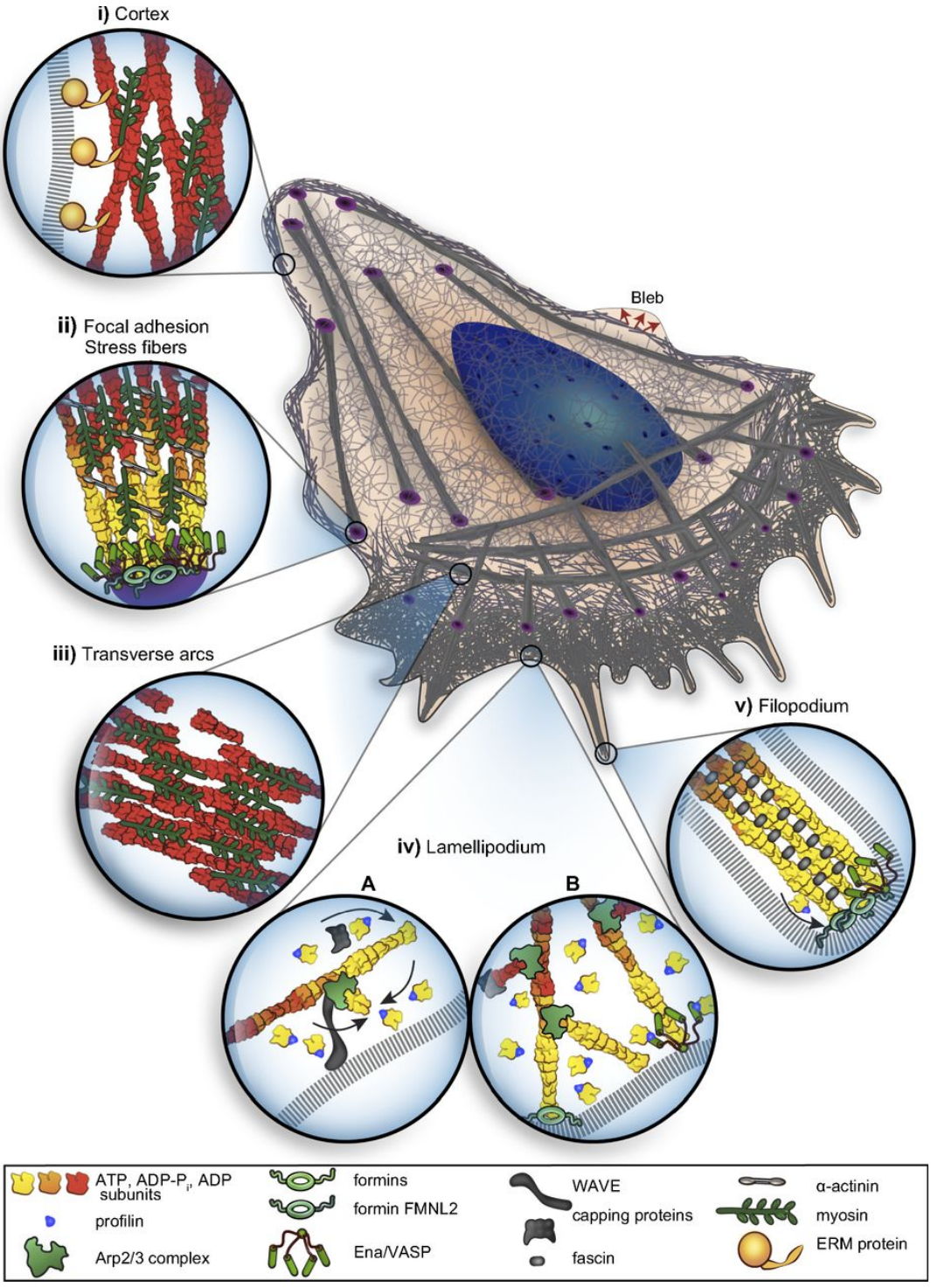


FIGURE 1.4 Cellular actin structures of various organization and functions
Depicted cell has distinguished sub-regions of actin cytoskeleton, with structures like stress fiber, lamellipodium or filopodia build with assistance of various actin binding protein. It illustrates the variety of possible compartments that myosin motors encounter while traveling along cellular meshwork. SOURCE: Blanchoin et al. Physiol Rev 2014

1.2.4. The structure of actin

The main proteins that myosins interact with is the actin. Intricacies that govern myosin behavior are hypothetically encoded in the bare actin track itself. Actin is abundant in all eukaryotic cells, and particularly prevalent in muscle, where it comprises about 20% of the total mass. As mentioned before, actin which is present in non-muscle cells forms a meshwork of filaments, that serve as track for myosin based transport. Actin comes in two forms: monomeric, globular G-actin; and polymeric, filamentous F-actin. Actin filaments are composed of a chain of monomeric actin building a two-start helix with a pseudo repeat of 36 nm (Figure 1.5) (Oda et al., 2009). It is a polar filament, with opposite ends termed 'barbed' and 'pointed' that are defined by direction and speed of polymer assembly. The length of the filaments and the architecture of their attachments determine the shape and consistency of a cell.

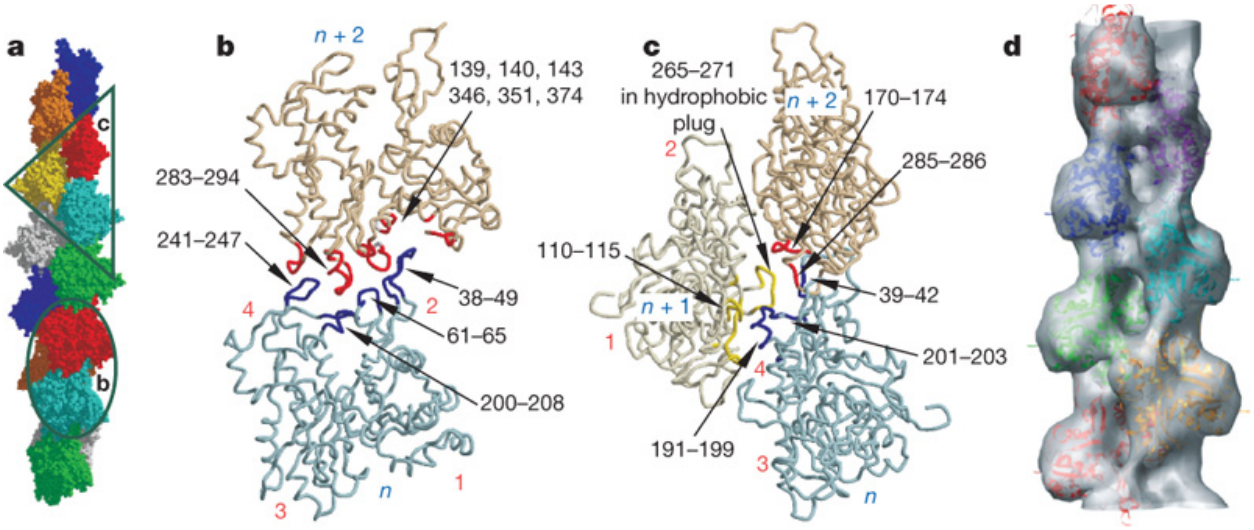


FIGURE 1.5 Model of the F-actin structure
(A) A model of 13 subunits of F-actin length with the blue actin monomer at the barbed end and the green actin monomer at the pointed end of the filament (B) Intra- strand contacts within an F-actin model with contributing residues marked (C) Residues facilitating the inter-strand contacts (D) The three-dimensional map independently reconstructed from cryoelectron micrographs is superposed with the F-actin model; pdb code: 2zwh, (Oda et al., 2009).

1.2.5. Actin polymerization scheme

Actin meshwork is a very dynamic system of tracks for the myosins, as it is constantly assembled and disassembled depending on the cellular needs. The polymerization of actin filaments proceeds in three sequential phases (Figure 1.6). The filaments start forming when the total actin concentration of G-actin exceeds the critical concentration (C_c) for assembly (Oosawa & Kasai, 1962). C_c depends on the nucleotide bound by the monomer (ATP, ADP•Pi or ADP) and the type and concentration of ions in solution (Kang et al., 2012; Pollard, 1986; Pollard & Weeds, 1984). The salt-dependent C_c in physiological condition has been attributed to divalent cation (e.g. Mg^{2+}) binding at discrete sites (Estes et al., 1987; Frieden, 1983). Early steps of actin polymerization require a conformational change in actin induced by an interaction with cations. At first a lag period can be distinguished, in which G-actin aggregates into short, unstable dimers. Once the oligomer reaches three subunits in length, it can act as a stable seed, or nucleus, which in the second phase rapidly elongates into a filament by the addition of actin monomers to both of its ends (Sept & McCammon, 2001). Barbed end has a higher affinity for monomeric subunits. Because elongation progresses rapidly at the barbed end it is also referred to as 'the fast growing end'. The pointed end is also elongating, but with significantly lower assembly rate, making it 'the slow growing end' (Carlier, 1991). As F-actin filaments grow, the concentration of G-actin monomers in local environment decreases until it is in steady state with the filament. This third phase is called steady state because G-actin monomers exchange with subunits at the filament ends but there is no net change in the total mass of filaments.

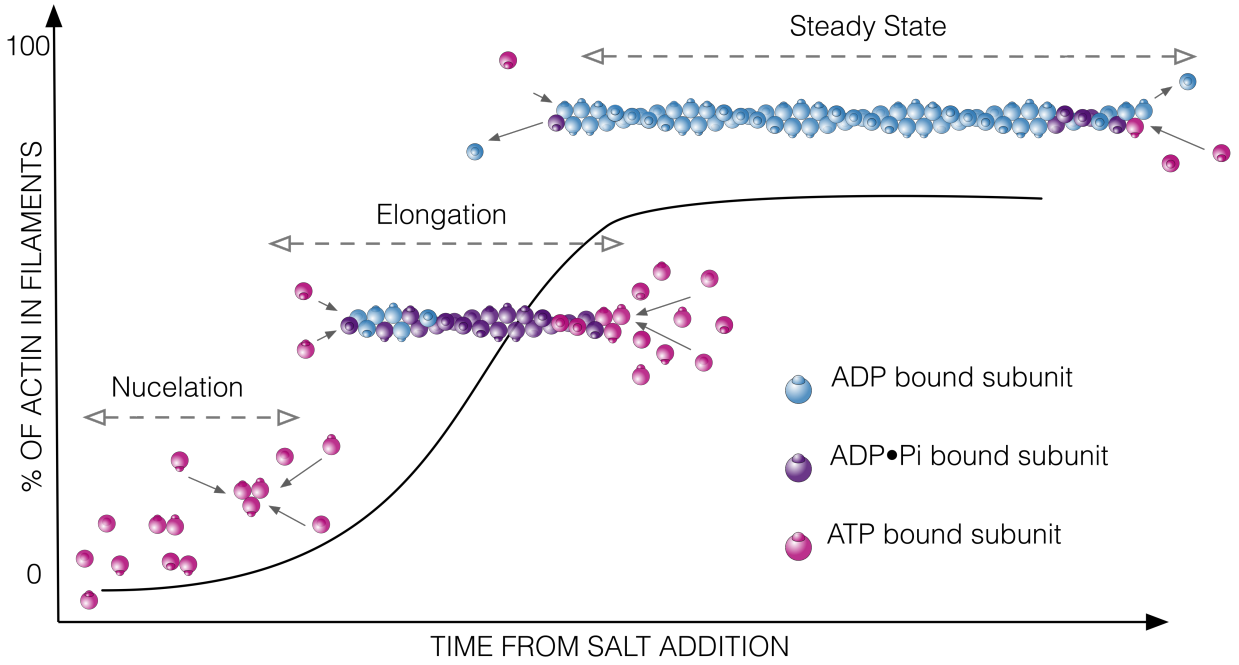


FIGURE 1.6 Three consecutive phases of actin filament assembly
The scheme presents three phases of actin polymerization: nucleation, elongation, and steady state. The nucleation is dependent on presence of G-actin above C_c in given experimental condition and presence of salt ions that induce conformational change in an early step of actin polymerization. With energetic barrier of trimer formation crossed, elongation phase starts with rapid assembly on the pointed end and slower at pointed end. When the pull of G-actin is exhausted filaments remain in the steady state.

1.2.6. Three phosphate states that define the age of actin

Monomers of actin that have highest binding affinity to filamentous actin are in an ATP state, meaning that they have ATP bound in their nucleotide binding pocket (Pollard, 1986; Carlier, 1987). After a set of ATP-bound globular subunits are incorporated into a filament, they create so called 'ATP cap' — a region of a filament that sustains ATP phosphate state. ATP bound portion of filament is the first defined by nucleotide state actin age (Figure 1.7). This region is only couple nanometers long and short-lived. At typical filament growth rates of 10 monomers/s at 1.0 mM G-actin present in the buffer, the barbed end ATP cap has 30 monomers and is 100 nm long.

The ATP is hydrolyzed to ADP•Pi within seconds, bringing the filament to the second 'age' defined by the nucleotide with hydrolyzed nucleotide with inorganic phosphate still bound (Figure 1.7). Release of inorganic phosphate (P_i) from F-actin is up to even 100-fold slower, with half-life of ca. 350 seconds. and yielding ADP F-actin that persists for the lifetime of the filament. ADP is the third and final phosphate state — aka age of F-actin (Figure 1.7). Process of ATP hydrolysis and Pi release is stochastic, meaning that there is no specific order for the monomers to undergo these changes. There is only a time frame within which the phosphate state changes will occur independently from each other. It is a mechanism distinguish from microtubules, which have a similar GTP hydrolysis process but the hydrolysis and product release along the aging microtubule is vectorial. As a result of the ATP hydrolysis and Pi release, most of the filament consists of ADP monomers after minutes from the moment of being incorporated into the polymer. However, it is noted that ATP hydrolysis or Pi release is not essential for polymerization to occur, as evidenced by the ability of G-actin containing ADP or a non-hydrolyzable ATP analog to polymerize into filaments (Kudryashov & Reisler, 2013).

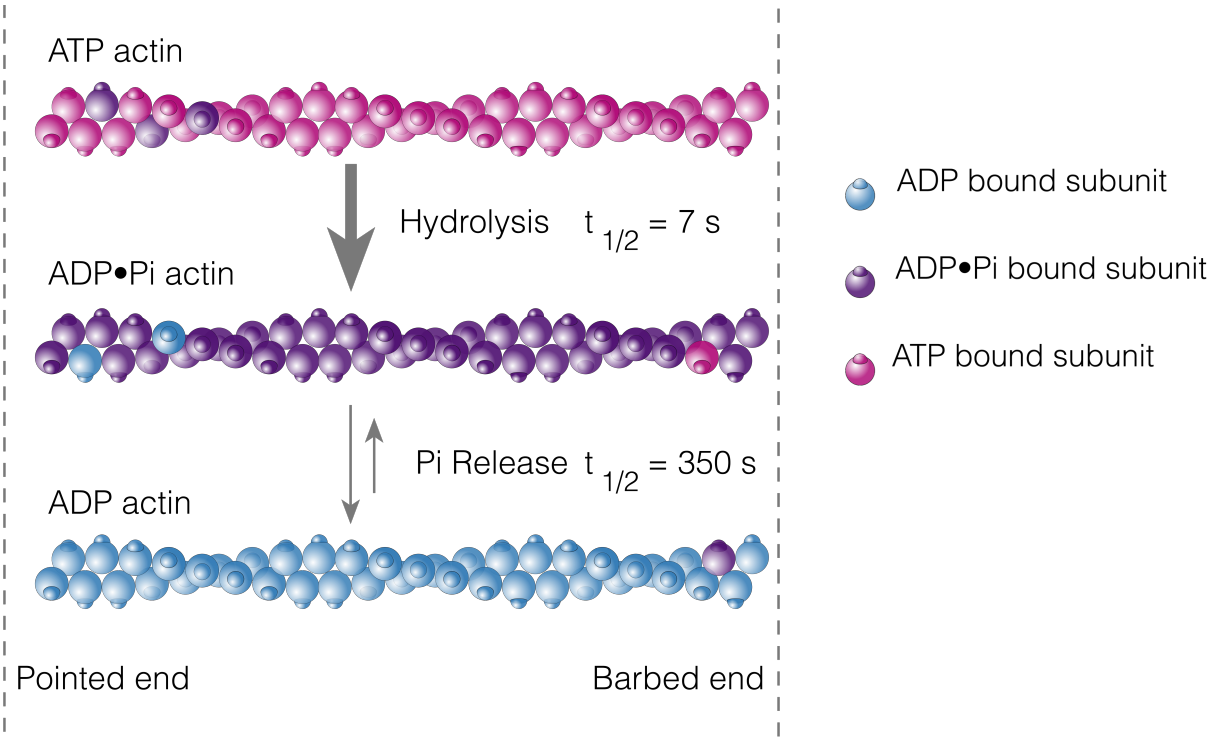


FIGURE 1.7 Actin filament aging by ATP hydrolysis and Pi release
Filament aging is a process that occurs in three sequential events. At barbed end of the filament ATP actin monomers are added preferentially, as shown on Figure 1.6. Overtime in ATP actin subunits, initially incorporated into a filament in ATP state, the nucleotide is hydrolyzed and changed to ADP•Pi state. Inorganic phosphate is subsequently released, leaving subunits in filament in their final ADP state. Both, ATP hydrolysis and Pi release are stochastic processes. Phosphate state of the monomers in filament marks time passed from the monomer binding to filament, and as such it is also a filament age indicator.

1.2.7. Phalloidin preserves phosphate state in actin filament

Important, but often omitted aspect of investigating myosin and actin interactions is the kind of stabilizer used in the experiments. Utilized for decades motility assays are performed with the filamentous actin stabilized via addition of phalloidin (Kron & Spudich, 1986) (Sellers, 2001). Phalloidin, a toxin from mushroom *Amanita Phalloides,* slows elongation at the barbed end by almost half, and increases the rate of the spontaneous polymerization of pure actin at actin concentrations greater

than 0.6 μM. Spontaneous polymerization is faster, because phalloidin strongly promotes nucleation (Dancker et al., 1975). Phalloidin also inhibits subunit dissociation at both ends of actin filaments (Coluccio & Tilney, 1984). The reagent is known to bind and affect activities of other cytoskeletal elements. Most important of all of its properties however is that the presence of the toxin strongly retards the release of the hydrolysis product Pi. At the same time phalloidin does not inhibit ATP hydrolysis during actin polymerization (Dancker & Hess, 1990). Therefore by using phalloidin in canonical single molecule myosin motility assays, actin is captured in a 'frozen' state, either ADP or ADP•Pi. I utilized this property of phalloidin for ensuring appropriate phosphate state of filaments in the researched described here. However, the toxin could possibly affect the nature of interactions between myosin motor and actin, and fail to reproduce acto-myosin dynamics observed in live cells. Therefore I controlled for phalloidin's influence in stabilized F-actin and its direct effects on myosin motors, which will be addressed in later chapters.

1.3. The unconventional myosin we know the most about: myosin-5

Myosin-5 that functions as dimeric cargo transporter is arguably the most well-studied unconventional myosin. It is a barbed end directed ATPase with the large step size of 36 nm that is easily distinguishable from Brownian motion noise in single molecule assays. It is an easiest motor protein to visualize by cryo-electron microscopy (cro-EM) with its long leg regions and ability to bind actin filament with both motor domains at the same time (Vale, 2003). It is also relatively easy to express and purify active myosin-5 using the baculovirus system.

1.3.1. Cellular functions of myosin-5

Myosin-5 is known as a transporter of verity of cargoes, therefore a contributor to multitude of cellular processes. This myosin is responsible for transport of organelles, membranous cargo, secretory vesicles, mRNA, lipids and proteins vesicles on actin tracks (Reck-Peterson et al., 2000; Trybus, 2008). Humans have three myosins from class 5: myosin 5a, myosin 5b and myosin 5c (Rodriguez & Cheney, 2002). Myosin 5a is found in melanocytes and brain cells, where its trafficking malfunctions result in pigmentation defects and neurological symptoms that ultimately cause the Griscelli syndrome (Ménasché et al., 2003). Myosins 5b and myosin 5c function in epithelial cells, and have been implicated as motors involved in recycling of endosomes (Swiatecka-Urban et al., 2007; Roland et al., 2007).

1.3.2. Structure of myosin-5

Myosin-5, out of the unconventional myosins group, has structural information available to a considerable level of detail. Thanks to X-ray crystallography structures of myosin-5 major structural domains were revealed without the nucleotide bound (Coureux et al., 2004; Coureux et al., 2003). Thanks to cryo-EM it was possible to observe the motor domain bound to actin with nucleotide analogues (Volkmann et al., 2005). The structural studies of the last decade allowed a better understanding of mechanisms by which myosin-5 functions. Myosin-5 motor domain is followed by an extended α-helical lever arm that is stabilized by IQ motifs that bind six calcium binding proteins — calmodulins (CaM), or related light chains (Koide et al., 2006). The lever arm amplifies small nucleotide-dependent changes that originate at the active site, allowing a large powerstroke to occur following ATP hydrolysis. The next important

structural domain is the rod region that contains α-helical coiled-coils that are responsible for dimerization of the molecule. At the C-terminus there is a globular tail which binds adapter proteins that link myosin-5 to cargo, supporting the transporter function of the motor (Pashkova et al., 2005). The globular tail also plays a role by binding to the motor domain in the folded, auto-inhibited state (Li et al., 2006). Myosin-5 ATPase activity of the motor domain can be activated when the motor domain is 'freed' from the tail domain, so from folded, inactive state to extended, functional state. The unbinding of the tail domain from the motor domain happens by either calcium binding to CaMs or alternatively by cargo binging (Trybus et al., 2007; Li et al., 2005).

1.3.3. Processive movement of myosin-5

Activated, myosin-5 dimer is bound to the filament with both feet that are in ADP state. Dimeric nature of myosin allows the two feet to exert intramolecular strain on each other, so that ADP is first released from the trailing foot. The trailing foot rapidly dissociates from the actin, as the ATP is bound in the nucleotide binding pocket. The attached foot undergoes a power stroke, becoming the new trailing foot and positioning the new, unbound leading foot ahead. By rapid hydrolysis of ATP in the unbound, now leading foot, conformational change occurs rotating the lever arm to the pre-power stroke position (De La Cruz et al., 1999). The detached foot state is of high affinity for actin now and the diffusive search of the next binding site begins. Upon binding to actin, the leading foot rapidly releases Pi and transitions from weak to strong binding conformation, which brings the whole motor myosin to the starting position with

ADP bound, but translated forward by 36 nm along filament (Mehta et al., 1999). Stepping mechanism is depicted on Figure 1.8.

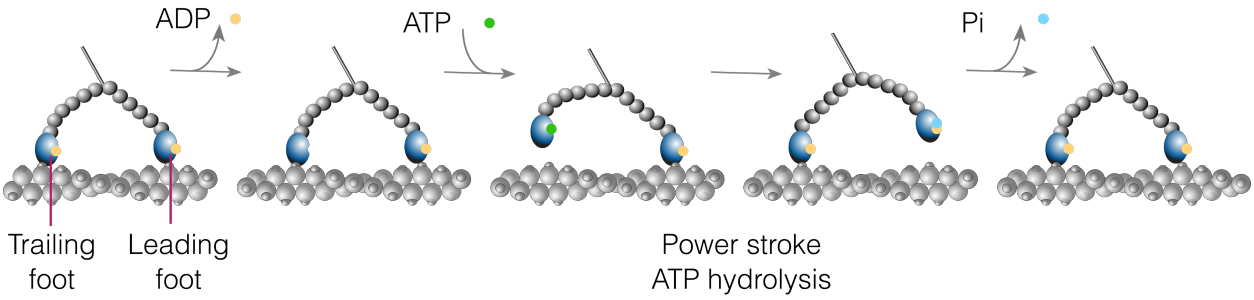


FIGURE 1.8 Model of dimerized myosin stepping mechanisms along F-actin on example of myosin-5
Myosin motor domain could have following nucleotides bound in the nucleotide binding pocket: ATP (green dot), ADP (yellow dot), ADP•Pi (yellow and blue dots) or no nucleotide.

1.4. Out of the ordinary: myosin-6, the pointed end directed motor

1.4.1. From endocytosis to hearing: myosin-6 functions

Recent studies indicate that myosin-6 plays a multitude of roles in intracellular trafficking (Buss et al., 2004) (Tumbarello et al., 2013). Foremost, myosin-6 participates in endocytosis by assisting clathrin-coated vesicle formation and by trafficking of uncoated nascent vesicles (Geisbrecht & Montell, 2002) (Hasson, 2003) (Altman et al., 2007). In endocytosis myosin-6 likely plays an accessory role, enhancing the efficiency of endocytosis or sorting and directing cargo either to be recycled back to the plasma membrane or targeted for the lysosomal degradation. Myosin-6 has a potential impact on membrane trafficking required for the maturation of autophagosome and is indicated to be crucial, along with its adaptor proteins, for autophagy process (Tumbarello et al., 2012). Furthermore, as load increases on myosin-6, it may switch

from its transport function to actin as an anchor (Altman et al., 2004). This enables myosin-6 to play a set of structural roles in cells, e.g. in the overall organization of the Golgi and in the last step of secretion (Sahlender et al., 2005) (Bond et al., 2011).

Myosin-6 is also expressed within the sensory hair cells of the inner ear, maintaining their structural integrity. Mutations of the genes encoding myosin-6 results in hearing loss, starting form a null mutation in myosin-6 results in the congenitally deaf Snell's waltzer mice (Avraham et al., 1995) and ending on the newly identified gene mutation that lead to hereditary hearing loss in humans (Brownstein et al., 2014). Thus myosin-6 is thought to fulfill fundamental functions in the auditory system. More specifically, myosin-6 is suggested to organize the stereocilia in their early development and participate in membrane trafficking as well as anchoring the apical hair cell membrane (Pylypenko et al., 2015). These diverse roles of myosin-6 are facilitated its versatile nature, myosin-6 takes part and assists in a variety of intracellular processes: vesicular membrane traffic, cell migration, and mitosis.

1.4.2.Flexibility in myosin-6 lever arm

The general structure of the unconventional myosin dimer, with the N-terminal motor domain followed by IQ motifs, lever arm up to dimerization and cargo binding domains is similar between myosin-5 and myosin-6. However, myosin-6 is an unique, pointed end directed motor. This fundamental functional difference from myosin-5 is achieved by structural adaptations in myosin-6. Motility in the opposite way from the other myosin motors is possible due to the ‘reverse gear’ mechanism inserted between the converter domain and the lever arm, which swings the arm in the opposite direction to that of all the other myosins. Myosin-6 has only two calmodulin bindings sides, first

calmodulin stabilizes the reverse swing of the lever arm. Second calmodulin is bound by canonical IQ motif, followed by a extendable lever arm that allows to achieve the large step size of 36nm (Spudich & Sivaramakrishnan, 2010).

1.4.3. Wide range of step sizes and back steps of myosin-6

The extendable lever arm is an impactful structural feature of myosin-6 and it underlies the adaptive stepping mechanism of this reversed directionality myosin. Whereas myosin-5 for the forward step binds with the leading foot to the monomer 36 nm ahead from the trailing foot, myosin-6 uses one of approximately six accessible monomers for the forward step, stretching its short lever arm in reach for the binding spot on actin (Rock et al., 2005; Mukherjea et al., 2009; Dunn et al., 2010). The trailing foot has also an ability to unbind, while leading foot is still bound to actin and to re-bind to one of three accessible monomers behind initial binding site for the backward step (Ikezaki et al., 2013). Moreover, myosin-6 is prone to take short back steps under the load (Chuan et al., 2011). Side and back stepping extend the possible step sizes range and allow stepping patterns that characterize this peculiar and remarkably adaptable motor protein.

1.5. Questions addressed in this thesis

The work presented here is a comprehensive study for myosin motility on assembling actin filaments. I propose a novel method of reconstructing actin tracks to recapture cytoskeletal complexity *in vitro* to higher extend than traditional myosin motility assays. By use of polymerizing actin filament and controlling the phosphate state of F-actin I am able to ask questions about intrinsic properties of unconventional

myosin motor activity that govern its behavior *in vivo*. The reconstitution method is building the bridge between the *in vitro* tests and the experiments done in the cell's complexity background. By reconstituting cytoskeletal structures to resemble the environments of the cell more faithfully I intended to reveal the behaviors of myosin and actin that are often too subtle, therefore extremely challenging to detect, when investigating cellular interior with its immense amounts of interactions and factors influencing each other. These characteristics of myosin and actin are also not possible to observe in classical *in vitro* tests, because the experimental set ups omit vast numbers of native cytoskeletal aspects to achieve the desired simplicity of the assay. In here I added back layers of cellular complexity and asked questions about specific effects these extra interactions have on the system.

The first question addressed in this dissertation is whether myosin motors and native-like polymerizing actin influence each other in the reconstituted environment that mimics cell interior more faithfully than other assays used currently in the field. The approach taken to answer this question reveals if myosin-5 and myosin-6 properties, such as velocities, run lengths and processive run initiation rates sense the distinct properties of polymerizing actin filament. I also can observe any impact that myosin motors have on actin polymerization dynamics, in terms of increasing up or slowing down polymerization rates of the observed filaments. In this approach I have an opportunity to evaluate the level to which phalloidin could be affecting myosin's activity.

The second point addressed in this work deals with elevating the complexity of reconstituted *in vitro* environment. I introduced, apart from utilizing polymerizing actin filaments and observing motility of one unconventional myosin, additional actin binding

protein. A representative of second myosin motor class, either myosin-5 or myosin-6 added to the experimental environment with the other myosin class already present tests the interaction between the two ABPs — myosin-5 and myosin-6. Both of the motors are arguably the best studied unconventional myosins and belong to the classes thought to utilize the same cellular actin filaments for their *in vivo* activity. As they walk and carry their cargos in opposite directions along the filament, it is not known whether they can share the same exact filament at the same time. If they can, the nuances of how they encounter each other on that shared track are not known. By reconstituting the simultaneous motility of myosin-5 and myosin-6 on the same filament I was able to perform an exhaustive analysis of myosin-5 and myosin-6 crossing mechanisms. This information delineates how the bidirectional transport is achieved in the multi myosin cell interior. I learnt how myosins utilize the same actin track while moving along it in opposite directions. The microscopy observation as well as stochastic simulation model of the bidirectional motility show which of the myosins is dominating in case of an encounter when both myosins trajectories come to spatial and temporal overlap. By dissecting the differences between the two myosin classes I am also able to hypothesize on what are the advantages that allow the more successful myosin pass and what are the implication for the cellular transport effectiveness.

CHAPTER 2: ACTIN AGE ORCHESTRATES MYOSINS RUN LENGTHS

2.1. Introduction

Unlike a static and immobile skeleton, the actin cytoskeleton is a highly dynamic network of filamentous polymers that continuously turn over. In addition to generating mechanical forces as well as driving and sensing deformations, dynamic F-actin networks serve as cellular tracks for myosin motor traffic. However, much of our understanding of processive myosins behavior comes from *in vitro* studies in which motility was examined on pre-assembled and artificially stabilized, static F-actin tracks. On the other hand actin polymerization assay was used over decades to study the behavior of a multitude of other ABPs. In single molecule studies of actin associated proteins and actin itself, dynamic properties of actin are not omitted and often play crucial role in identifying physiologically relevant interactions. There are examples of groundbreaking discoveries that reveal properties of cellular cytoskeleton that were achieved with microscopic observation of polymerizing actin and interacting proteins. Moreover, activity of other motor proteins, MT based kinesins, was investigated in pioneering *in vitro* reconstitutions of dynamic MT track (Kinoshita et al., 2001). The *in vitro* experiments showed that beads coated with motor proteins can follow a shrinking MT (Grissom et al., 2009; Riemslag et al., 2004), or that the nucleotide-binding state of MTs modulates kinesin processivity itself (McVicker et al., 2011).

However corresponding *in vitro* assays with reconstitution of actin polymerizing track was never used to study behavior of myosins. This makes myosin motors the sole ABPs that were characterized in single molecule technique exclusively on phalloidin

stabilized actin. In this chapter, I examine the role of actin dynamics in single-molecule myosin motility using assembling F-actin and two highly processive motors, myosin-5 and myosin-6. I also evaluate the influence of the actin condition on the functionality of myosin-5 and myosin-6 (Figure 2.1).

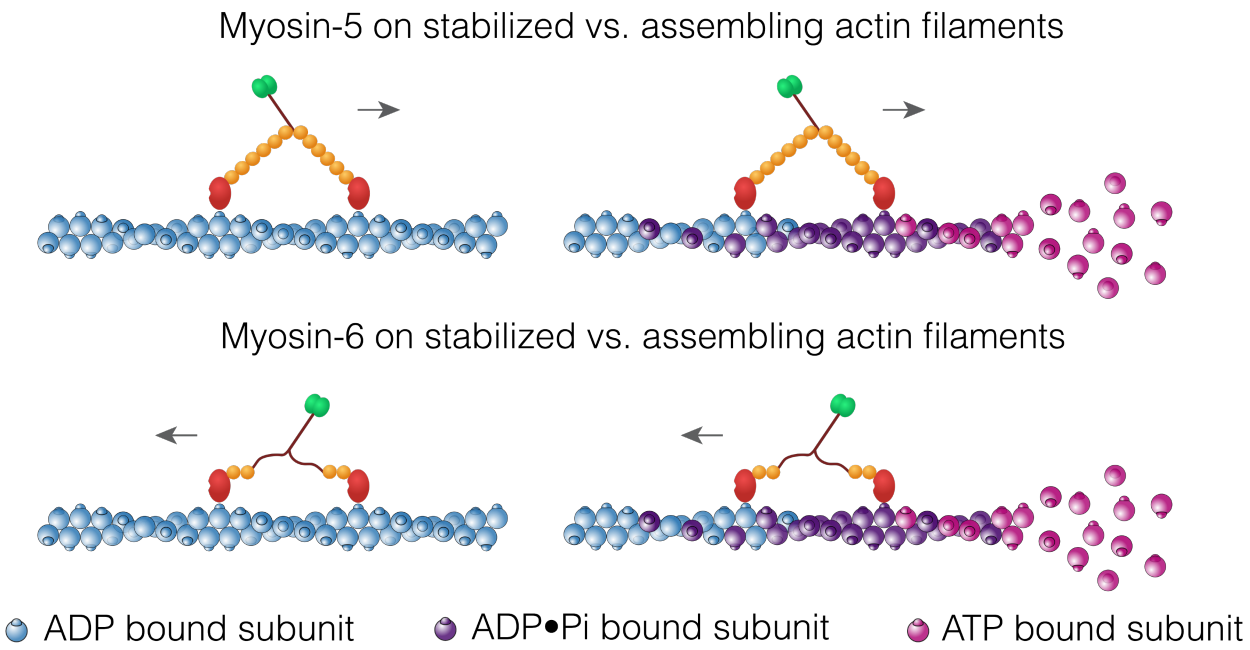


FIGURE 2.1 Schematic of the experiments
Fluorescently labeled myosin-5 (top) and myosin-6 (bottom) walk along two kinds of actin tracks: phalloidin stabilized F-actin (left) and assembling F-actin (right). Nucleotide turnover on actin is illustrated by the transition from pink to blue subunits.

The two myosins investigated here have distinct functions in the cell and travel in opposite directions along actin filaments (Sellers & Goodson, 1995) (Berg et al., 2001) (Buss et al., 2004). Myosin-5 walks toward the barbed ends of F-actin, traveling to sites of intense actin polymerization and depolymerization at the cell periphery (Reck-Peterson et al., 2000). Myosin-6 walks toward the pointed end of F-actin (Wells et al., 1999), traveling toward the cell center along older segments of the actin, where

the cytoskeletal network is more established and does not undergo such extreme changes as at the cell's forefront.

In collaboration with Dennis Zimmerann from Kovar Lab we were able to reconstitute the motility of both of the myosins *in vitro* along the single polymerizing actin filament, with the participating proteins fluorescently labeled. Actin polymerization form the time of nucleation and myosin motility were visualized via TIRF microscopy, recorded and analyzed (Supplementary Movie 2-1). We find that myosin-5 takes 1.3- to 1.5-fold longer runs on ADP•Pi (young) F-actin, whereas myosin-6 takes 1.7- to 3.6-fold longer runs along ADP (old) F-actin. These results suggest that conformational differences between ADP•Pi and ADP F-actin tailor these myosins to walk farther toward their preferred actin filament end. Taken together, these experiments define a new mechanism by which myosin traffic may sort to different F-actin networks depending on filament age of the environment.

2.2.Reconstitution of native-like actin tracks for myosin motility

2.2.1.Single filament elongation in conditions adapted for myosins

My work is the first report of myosin motor utilizing elongating actin reported via single molecule techniques, where myosin-5 or myosin-6 can be observed walking towards barbed or pointed end of elongating filament, respectively. An exemplified time-lapse of myosin-6 moving away from the growing barbed end of a filament is shown on Figure 2.2. Motility of both myosin-5 and myosin-6 on elongating filament are also shown *via* the kymographs on Figure 2.3.

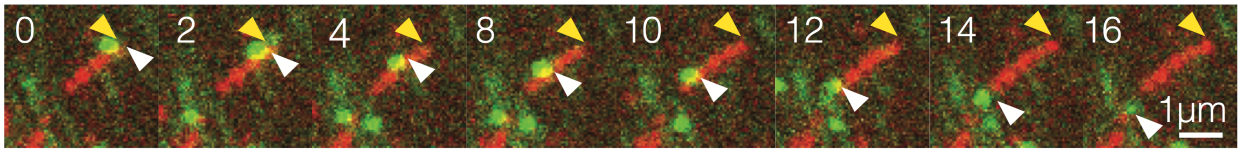


FIGURE 2.2 Time-lapse fluorescence micrographs of a single myosin-6 motor moving along single assembling actin filament

Myosin is shown in green, actin in red. Yellow arrowheads mark the growing barbed end of the filament, white arrowheads mark displacement of individual myosin molecules towards pointed end of the growing filament. Micrographs show motility of myosin-6 at concentration of 1 nM, time stamp is in seconds.

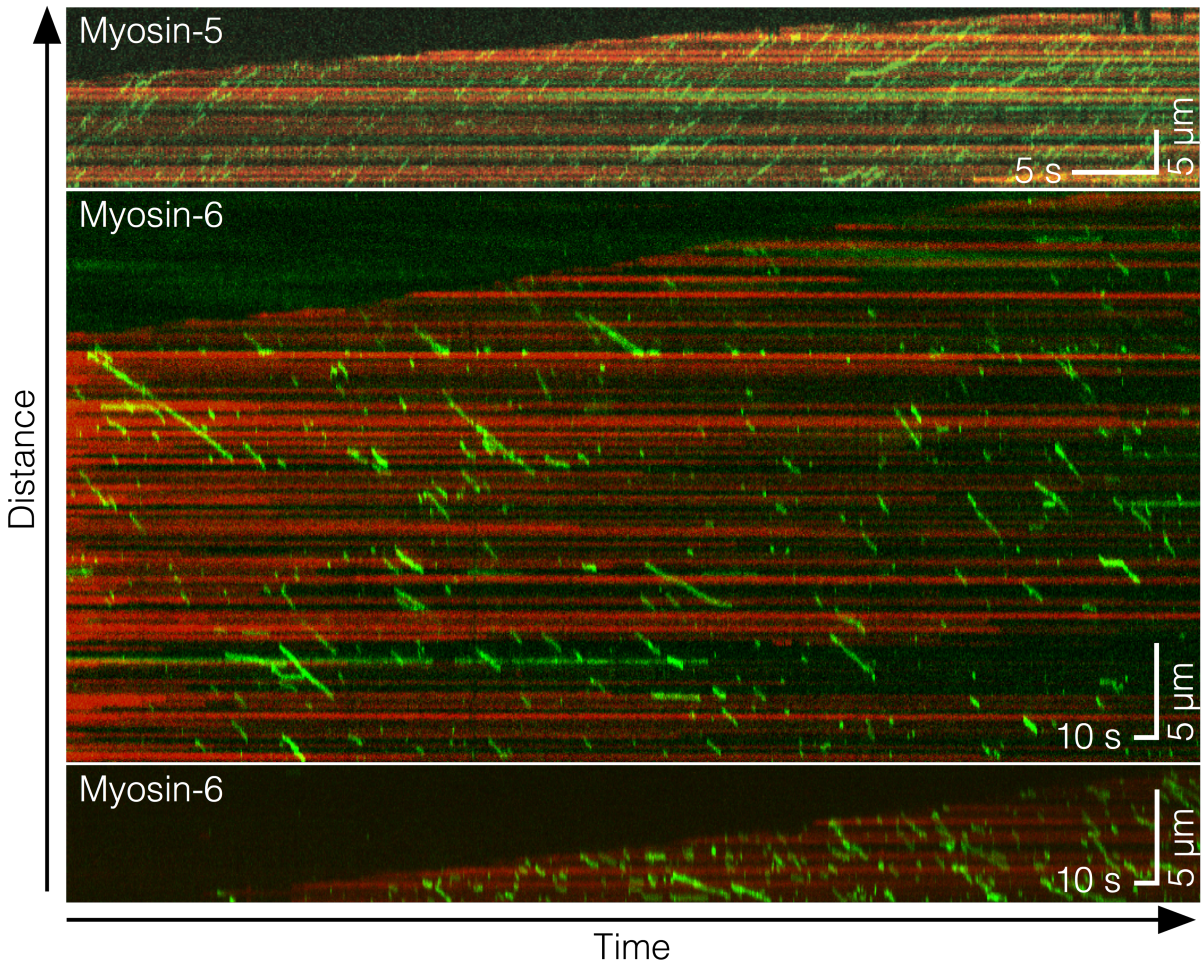


FIGURE 2.3 *In vitro* reconstitution of myosin-5 or myosin-6 motility on assembling F-actin

Representative kymographs showing processive motility of 5 nM myosin-5 and myosin-6 on growing F-actin. Processive runs of myosins appear as green diagonal lines. Actin is shown in red, illustrating elongation of the barbed end toward the kymograph top.

The experimental setup established in this work has significant advantages over traditional *in vitro* motility assays. Qualitatively, in the assembling actin assays I note a reduced incidence of 'dead' myosins that adhere to the coverslip away from long filaments, with an overall improvement in imaging quality. This observation suggests that many of these dead myosins actually bind to unresolved, short segments of actin under the standard phalloidin-stabilized filament condition.

2.3. Myosin-5 and myosin-6 detect actin nucleotide state aka actin age

2.3.1. Differences in myosin run lengths on assembling vs stabilized actin

Actin filaments in eukaryotic cells are typically born near the plasma membrane and age as they travel inward by retrograde flow (Blanchoin et al., 2014). Concomitantly, they acquire diverse actin-binding proteins that tune F-actin organization and dynamics, defining subcellular actin compartments. These actin-binding proteins could alter myosin motility, direct myosins to separated cytoskeletal regions, and ultimately serve to organize the cell. One example is tropomyosins, which differentially direct myosin-1 s and myosin-2 s (Fanning et al., 1994; Tang & Ostap, 2001), are essential for the processivity of budding yeast myosin-5 (Hodges et al., 2012) and bias bias actin track selection by vertebrate myosin-5a (Sckolnick et al., 2016)

Here, I consider a simple process that might generate distinct F-actin populations independent of ABPs, namely actin filament aging. As new ATP-actin monomers add to the barbed end of a nascent filament, aging begins with ATP turnover serving as an internal molecular clock. ATP hydrolysis and P_i release are

stochastic processes, so the ATP and ADP•Pi populations decay from the barbed to the pointed end as approximately single exponential functions. Whereas ATP and ADP•Pi F-actin are structurally similar, ADP F-actin is less stable and more flexible (Orlova & Egelman, 1993) (De La Cruz et al., 2010). Thus, I focus on the transition from ADP•Pi to ADP actin. With the use of phalloidin or capping protein I am able to preserve desired phosphate state of the F-actin during the experiment course. With varying the experimental condition and actin stabilizers I am operating among three actin phosphate states: uniform ADP, uniform ADP•Pi and ADP•Pi Decay states (Figure 2.4).

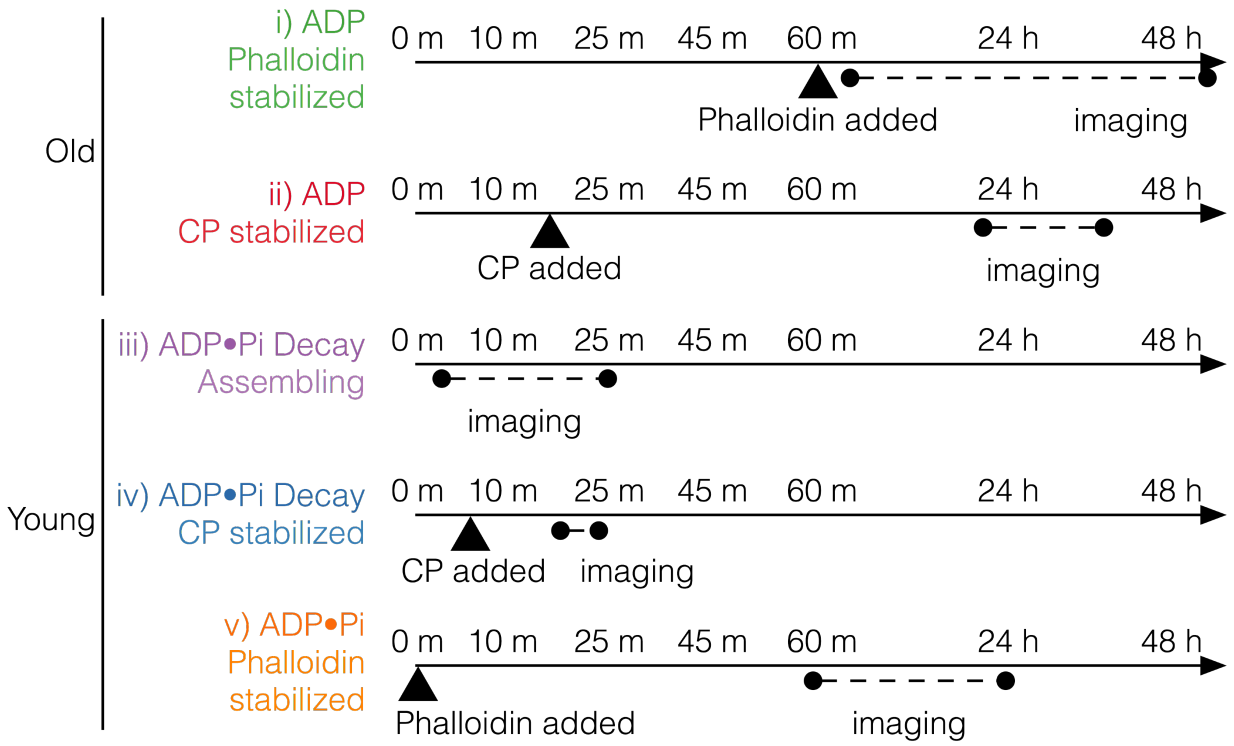


FIGURE 2.4 Experimental time course for obtaining desired filament phosphate state
Actin polymerization begins at time zero. Experimental conditions are listed that yield: ADP F-actin (i and ii), mixed ADP and ADP•Pi F-actin (iii and iv), and uniform ADP•Pi F-actin (v)

At first I compared ADP•Pi Decay where no stabilizer was present with uniform ADP actin stabilized with phalloidin. Both, myosin-5 and myosin-6 had changed run lengths with the change of phosphate state of the actin in the experiment. Myosin-5 runs has a tendency to get longer on the ADP•Pi Decay actin vs the ADP filaments. Myosin-6 behaves in the opposite way, executing longer run lengths on the ADP actin as compared to shorter runs on ADP•Pi Decay tracks (Figure 2.5, Table 1).

Motor	Actin State	Actin Stabilizer	n	Mean run length (nm, ± SEM)	Median run length (nm)	0.95 CI (nm)
myosin-5	**ADP**	**Phalloidin**	315	790 ± 40	600	540 - 670
myosin-5	**ADP**	**CP**	146	890 ± 60	740	620 - 910
myosin-5	**ADP·Pi Decay**	**None**	989	1100 ± 40	760	700 - 820
myosin-5	**ADP·Pi Decay**	**CP**	428	1200 ± 50	900	800 - 990
myosin-5	**ADP·Pi**	**Phalloidin-Copoly**	263	1200 ± 60	910	790 - 1100
myosin-6	**ADP**	**Phalloidin**	476	1300 ± 90	680	610 - 800
myosin-6	**ADP**	**CP**	279	1300 ± 120	600	530 - 730
myosin-6	**ADP·Pi Decay**	**None**	707	770 ± 50	380	360 - 430
myosin-6	**ADP·Pi Decay**	**CP**	133	650 ± 60	380	300 - 470
myosin-6	**ADP·Pi**	**Phalloidin-Copoly**	249	360 ± 30	220	170 - 260

TABLE 1. Run length summary statistics for myosin motors moving along F-actin with the set of nucleotide states and filament stabilizers.

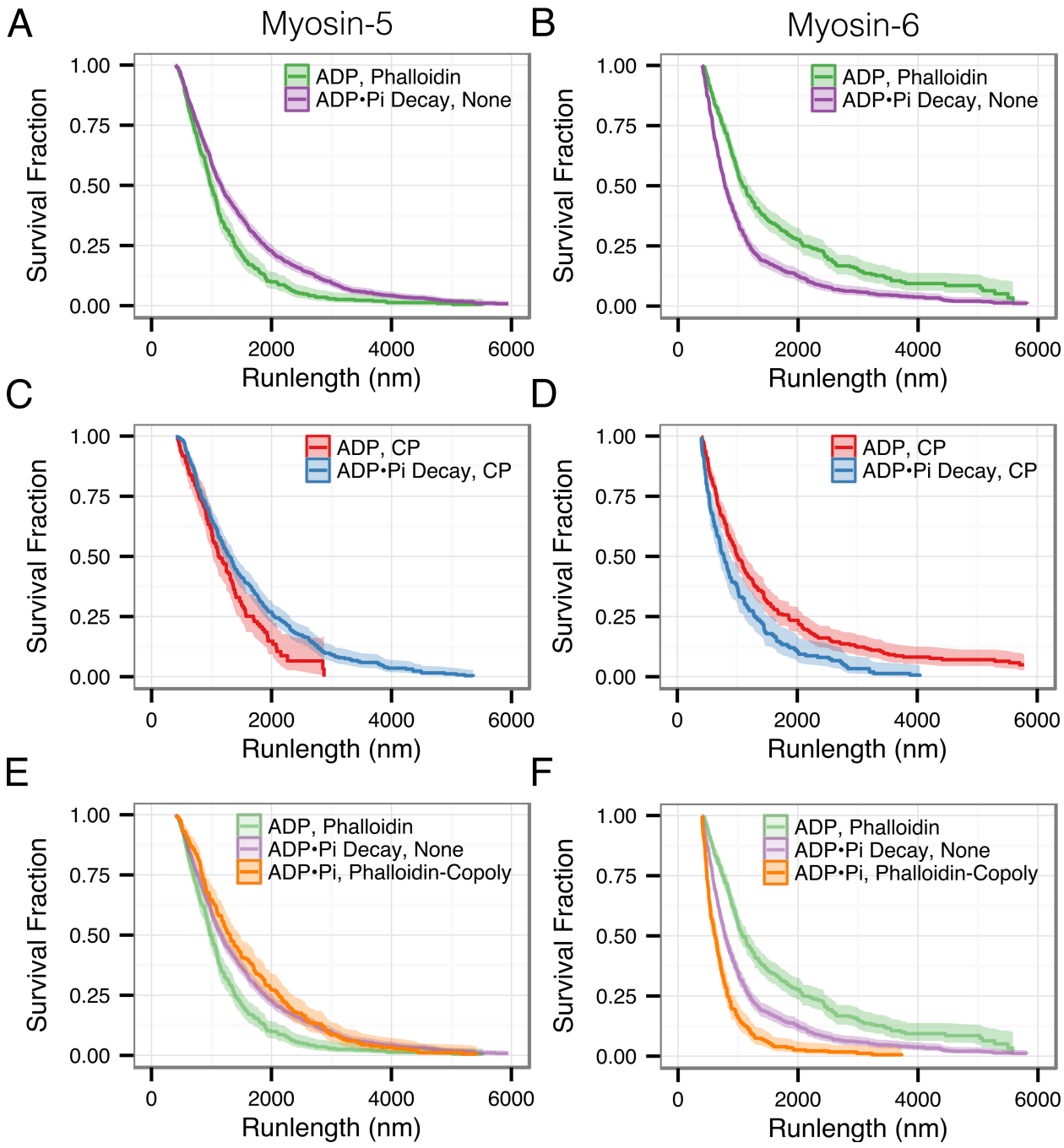


FIGURE 2.5 Run lengths of myosins along the F-actins listed in Figure 2.4
(A)Run lengths of myosin-5 on filaments assembled without stabilizer (iii) or stabilized with phalloidin after aging (i) are shown. Myosin-5 runs 1.4-fold farther on assembling actin ($p = 2\ 3\ 10^{8}$). (B) Run lengths of myosin-6 are shown, as in (A). Myosin-6 runs 1.7- fold farther on aged, phalloidin-stabilized actin ($p = 0$). (C) Run lengths of myosin-5 on capped (iv) or capped and aged (ii) F-actin are shown. Myosin- 5 runs 1.3-fold farther on younger filaments ($p = 7\ 3\ 10^{4}$). (E) Run lengths of myosin-6 are shown, as in (C). Myosin-6 runs 2-fold farther on the older filaments ($p = 1\ 3\ 10^{7}$). (F) Myosin-5 run lengths on F-actin co-polymerized with phalloidin to trap the ADP•Pi state

FIGURE 2.5 Caption Continuation
(v) are shown. Myosin-5 runs 1.5- fold farther on the trapped ADP•Pi F-actin than on the ADP phalloidin F-actin ($p = 3\ 3\ 10^{9}$). Run length curves from (A) are shown for comparison. (F) Run lengths of myosin-6 are shown, as in (E). Myosin-6 runs 3.6-fold farther on the ADP phalloidin F-actin ($p = 0$). All curves show the Kaplan- Meier estimator of the run length survivor function; bands report the 0.95 CI. Events are left truncated at 400 nm and are right censored at filament ends. Reported fold differences apply to mean run lengths, and p values report the log rank test. See Table 1 for summary statistics.

Mean run length of myosin-5 raises by 40% when presented with filaments of preferred phosphate state: ADP•Pi Decay. Myosin-6 has run lengths longer by 70% on the preferred ADP phosphate state of filaments in this experiment. The stabilizer has not changed the tendency of either of the myosins. Additionally both of the myosins have opposite preference changing runlengths in contrary ways. Therefore this dramatic difference is hypothesized to be solely a result of each myosins preference towards the phosphate state within the actin filaments. In order to explore this idea I took a closer look at the changing factor in the experimental set-ups: the phosphate state of F-actin.

Since the results suggest that the actin nucleotide state itself influences myosin-5 and myosin-6 processivity. I tested this hypothesis using phalloidin to generate actin filaments containing exclusively ADP•Pi or ADP subunits. Phalloidin dramatically slows P_i release, inhibiting the transition from ADP•Pi to ADP actin (for >20 hr), but leaves ATP-hydrolysis unaffected (Dancker & Hess, 1990). Thus, copolymerization of actin with phalloidin yields uniform ADP•Pi filaments (Figure 2.4 v). In contrast, addition of phalloidin after filaments have assembled and aged yields exclusively ADP filaments (Figure 2.4 i). I rejected alternative approaches involving nucleotide analogs or P_i competition because of their direct effects on myosin activity.

Myosin motility on phalloidin-stabilized, uniformly ADP•Pi or uniformly ADP actin filaments show that run length trends follow the nucleotide state. Myosin-5 mean run lengths are 1.5-fold longer on ADP•Pi than on ADP phalloidin filaments. Conversely, myosin-6 run lengths are 3.6-fold longer on ADP than on ADP•Pi phalloidin filaments (Figure 2.5 E and F; Table 1).

2.3.2. Myosin response to nucleotide state gradient within filament

Given their preference for different actin nucleotide states, I looked at myosin-5 and myosin-6 run lengths on different regions of individual growing filaments. Myosins that travel near the growing barbed end sample predominantly ADP•Pi -actin, whereas those near the pointed end sample predominantly ADP-actin. To correlate myosin run lengths to actin nucleotide state, I associated each point in a myosin run with the age of the actin monomer at that point. From the actin age and the reported phosphate release decay rate, I calculated the probability of each actin subunit being in the ADP•Pi -actin state (P(ADP•Pi)). The schematic kymograph in Figure 2.6 of a representative assembling F-actin track shows P(ADP•Pi) along an aging filament.
The heat map across the filament shows the probability of that contour region to be in ADP•Pi state.

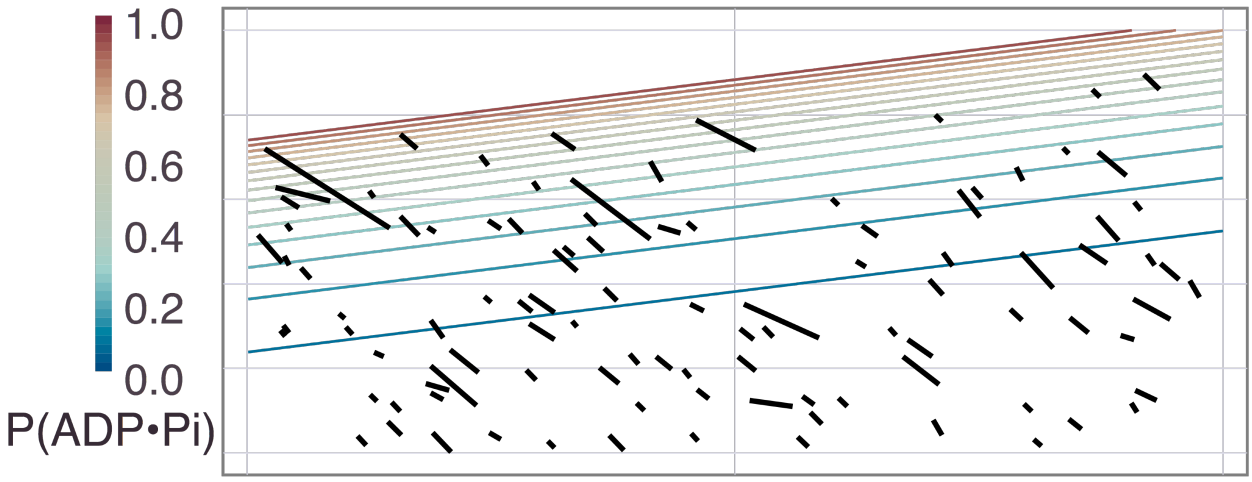


FIGURE 2.6 A schematic kymograph of myosin-6 runs on a growing filament
The scheme of actin filament growth with unperturbed phosphate decay and myosin-6 runs along it (compare to Figure 2.4 iii), based on the kymograph in Figure 2.3. Black lines indicate motor runs, and contour lines indicate the nucleotide state probabilities along the actin filament. The P(ADP•Pi) values decay from one to zero from the barbed to the pointed end.The last red lane is the edge of the filament's barbed end, where the probability of ADP•Pi state is always 1, as it is equivalent to ATP bound subunits of ATP cap.

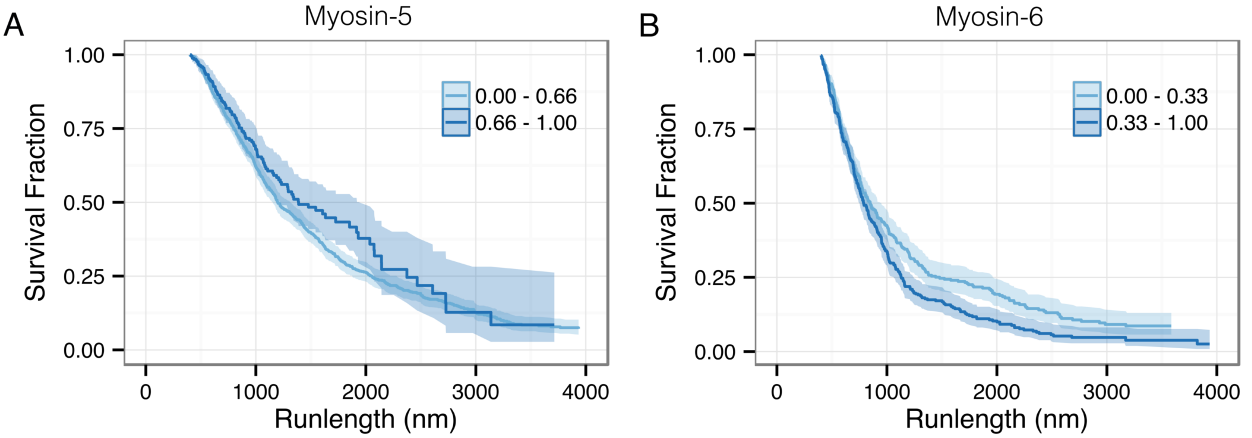


FIGURE 2.7 Run lengths
(A) Myosin-5 run lengths, separated into two classes of P(ADP•Pi) values. Myosin-5 runs farther along stretches of F-actin in the upper third of P(ADP•Pi) values ($p = 0.05$; log rank test). (B) Myosin-6 run lengths, separated into two classes. Myosin-6 moves farther along the stretches of actin in the lower third of P(ADP•Pi) values ($p = 0.002$; log rank test).

Myosin-5 and myosin-6 runs along growing filaments were grouped into two categories: low or high P(ADP•Pi) actin. Consistent with the earlier findings, the myosins exhibit opposite run length preferences. Myosin-5 takes 1.1-fold longer runs in the actin zone with the upper 33% of P(ADP•Pi) values (Figure 2.7 A; Table 2), where myosin-6 runs are 1.8-fold longer in the bottom 33% of P(ADP•Pi) values (Figure 2.7 B; Table 2). Thus, these two myosins can sense the F-actin nucleotide state in different regions of the same set of filaments. This finding rules out a concerted, all-or-none conformational change in the filament; instead, the structural features of F-actin that these two myosins sense must be local in nature.

Motor	Actin P(ADP•Pi)	n	Mean run length (nm, ± SEM)	Median run length (nm)	0.95 CI (nm)
myosin-5	**0.00 - 0.66**	853	1200 ± 50	800	760 - 910
myosin-5	**0.66 - 1.00**	256	1300 ± 110	990	820 - 1500
myosin-6	**0.00 - 0.33**	405	1200 ± 140	450	380 - 550
myosin-6	**0.33 - 1.00**	397	660 ± 50	390	350 - 450

TABLE 2. Run length summary statistics for myosin-5 and myosin-6 moving along assembling actin within bands of different nucleotide states along the filament. Mean and madian runlength as well as the confidence interval (CI) also shown.

2.4. Myosin run lengths are not affected by the stabilizer

2.4.1. Distinct phosphate states of phalloidin stabilized filaments

There are five distinct phosphate states of actin filaments that were used in discussed here experiments (Figure 2.8). The first state is to allow the decay of phosphate state occur as the filaments elongates, much like in the cellular environment. Next is the addition of phalloidin at appropriate times. To obtain ADP•Pi state phalloidin is added before polymerization. Adding the toxin when filaments reached steady state produces predominantly ADP state filaments. Additional capping protein experiments involve phosphate decay imitating state when the filament is capped with capping protein and imaged right away or left to age prior imaging. These phosphate states correspond to specific conditions that were used to obtain each particular filament kind (Figure 2.4).

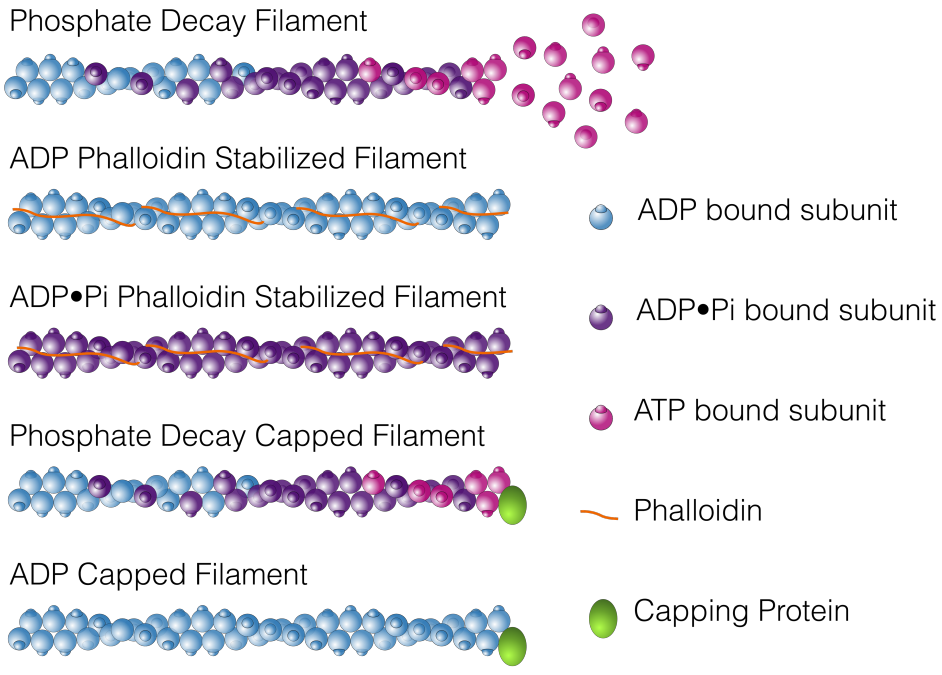


FIGURE 2.8 Five distinct phosphate states of actin filaments used in experiments

2.4.2. Capping stops growth and sets uniform filament age

As mentioned before, elongating filaments affect myosin run lengths with approximately equal magnitude but in opposite directions for the two myosins. Myosin-5 mean run lengths are 1.4-fold longer on growing filaments (ADP•Pi decay) compared to phalloidin-stabilized filaments (ADP; Figures 2.4 i), iii), and 2.5. A; Table 1). Conversely, myosin-6 mean run lengths are 1.7-fold longer on phalloidin-stabilized filaments (ADP) compared to growing actin (ADP•Pi decay Figures 2.4 i), iii), and 2.5 B; Table1. Two primary features differ between the growing and stabilized filaments: the nucleotide state of the filament and the presence or absence of phalloidin.

To determine the basis of the run length effect, I stabilized actin filaments without phalloidin. I added 10 nM capping protein after initial filament assembly to prevent the depolymerization of aged filaments upon dilution. Capping protein is thought not to affect the structure of the filaments like phalloidin does, because it is a barbed end associated protein and does not bind to the entire length of the filament like the toxin does. Although elongation is terminated by capping, this arrangement produces F-actin with an ADP•Pi decay along its length (Figure 2.4 iv). To emulate the phalloidin-stabilized filaments in the ADP state, I simply aged the capped filaments before imaging (Figure 2.4 ii).

2.4.3. Myosin run lengths are dictated by phosphate state, not the stabilizer

I observed the same trends on capped and aged filaments as on phalloidin-stabilized filaments. Myosin-5 runs 1.3-fold farther on capped ADP•Pi -actin decay filaments (Figure 2.5 C), whereas myosin-6 runs 2-fold farther on capped ADP actin filaments (Figure 2.5 D). I expect weaker run length effects here, because after

capping the filament decays to the ADP state without replenishment of ATP-monomers at the barbed end. Myosin run lengths on freshly capped filaments resemble the run lengths on growing actin tracks, whereas aged and capped filaments resemble aged and phalloidin-stabilized filaments (Figure 2.9). I conclude that phalloidin does not directly alter myosin run lengths.

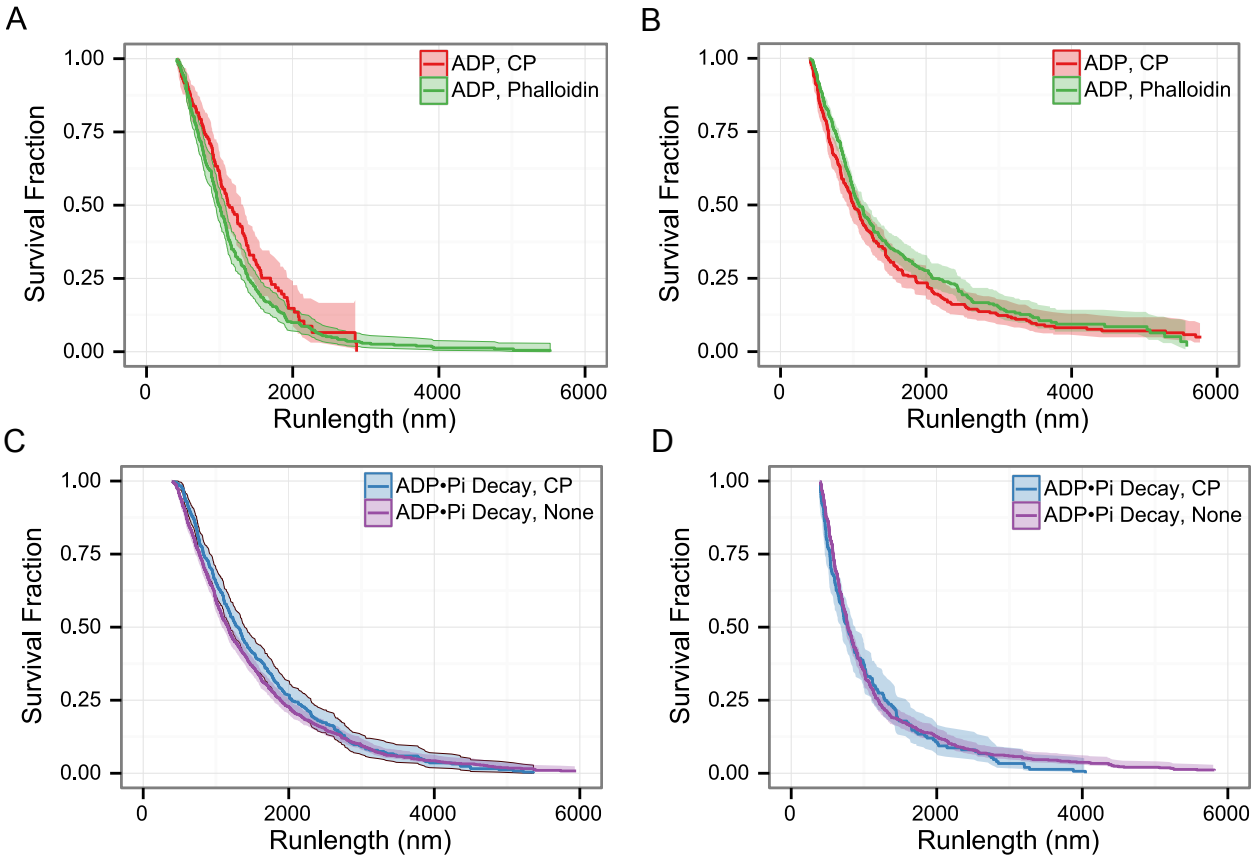


FIGURE 2.9 The actin filament stabilizer does not affect myosin run lengths
Run length measurements of myosin-5 (left) and myosin-6 (right) on F-actin assembled, aged, and stabilized with phalloidin; vs. F-actin assembled to desired filament length, capped with CP and aged. Both conditions yield ADP F-actin. Myosin-5 and myosin-6 take runs of similar length on both types of ADP actin. (B) Run length measurements of myosin-5 (left) and myosin-6 (right) on F-actin assembled without stabilizer (ADP•Pi Decay, None) or assembled to the desired length and capped with CP (ADP•Pi Decay). Myosin-5 and myosin-6 run lengths are similar on both types of ADP•Pi F-actin. Taken together, these observations rule out either stabilizer as the source of the altered run lengths. The Kaplan-Meier estimate of the run length survivor function is shown. Events are left truncated at 0.4 μm and are right censored at filament ends. Bands indicate the 0.95 CI (Confidence Interval)

2.5. Actin nucleotide state affects myosin landing rates

Overall cellular transport may be regulated by controlling either the run length or the frequency of myosin runs. To determine whether actin nucleotide state also regulates run frequency, I examined the rate at which myosins encounter F-actin and start a processive run, also known as the landing rate (Figure 2.10). In general, conditions that favor increased run lengths also favor increased landing rates. For example, median myosin-5 landing rates are 4-fold enhanced on ADP•Pi , phalloidin-copoly F-actin over ADP, phalloidin F-actin (Figure 2.10 A). Likewise, median myosin-6 landing rates are 2-fold enhanced on ADP, phalloidin filaments, compared to ADP•Pi , filaments copolymerized with phalloidin (Figure 2.10 B). Increased landing rates drive myosins to the filament populations that they are tailored for, as it causes longer run lengths, leading to an overall increase in trafficking capacity.

I speculate that the increase landing rate, as well as the elevated run lengths on filaments of preferred phosphate state are caused by the same factors. These factors would include sensing by myosin of structural differences between the different phosphate states of the targeted actin tracks and would facilitate binding on the favored binding sites. As such, this result confirms my reasoning for search of underlying actin structural differences that might be differentially recognized by myosin 5 and myosin-6 feet while searching for the appropriate spot to bind.

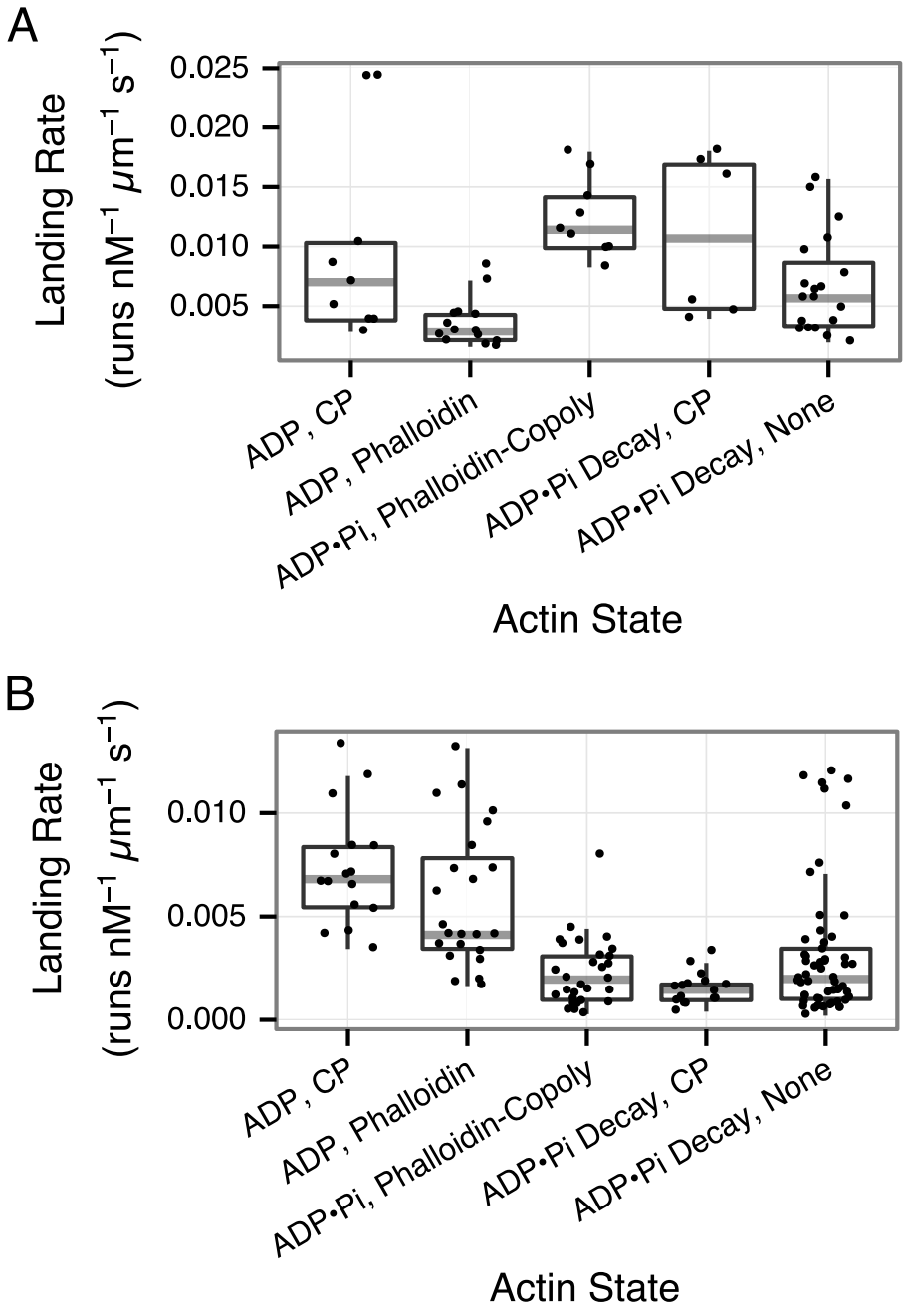


FIGURE 2.10 Myosin-5 lands more frequently on ADP•Pi F-actin, whereas myosin-6 lands more frequently on ADP

F-actin landing rates (the rate of initiating a processive run) are shown for myosin-5 (A) and myosin-6 (B). Myosin-5 lands significantly more often on ADP•Pi, phalloidin-copoly F-actin versus ADP, phalloidin F-actin (Figure 2.4 v versus 2.4 i; $p = 5\ 3\ 10^{6}$; Wilcoxon rank-sum test). Conversely, myosin-6 lands significantly more often on ADP, phalloidin F-actin versus ADP•Pi , phalloidin-copoly F-actin (Figure 2.4 i versus 2.4 v; $p = 2\ 3\ 10^{10}$; Wilcoxon rank-sum test).

2.6. Parameters unaffected in assembling assay and the implications

2.6.1. Velocities of myosins do not change upon different Pi state

As mentioned before, there is no significant change in either motor's speed with the change of actin phosphate state of filaments used for the motility assay (Figure 2.11, Table 3.). Since the rate limiting step for myosin-5 and myosin 6 is the nucleotide release (De La Cruz et al., 1999; De La Cruz et al., 2001), lack of change in the myosin velocity has much significance. I conclude that the unbinding of myosin feet is not the reason for extended runs lengths. Since it is not the unbinding that is affected here for achieving the longer run lengths, it is implied that the binding probability changes in response to actin phosphate state change. It is most likely that myosin's feet have higher affinity to preferred phosphate state of the actin subunits ahead in the filament. That change in attachment dynamic is caused by the structural nuances upon phosphate release from the actin subunits.

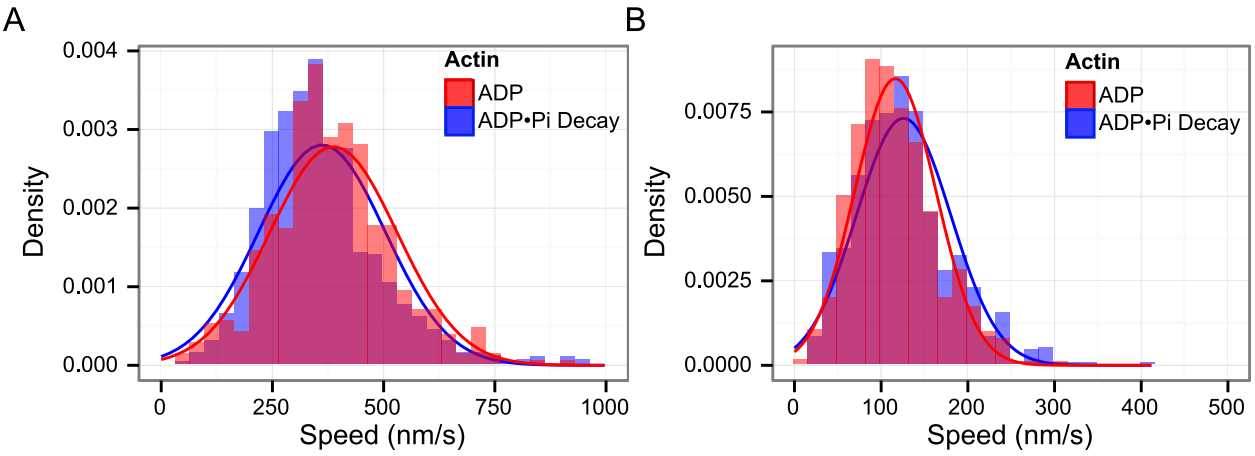


FIGURE 2.11 Myosin speed on ADP•Pi decay and static ADP F-actin remains the same
Histograms of speed distributions of (A) myosin-5 and (B) myosin-6 along assembling ADP•Pi decay (blue) and phalloidin-stabilized ADP (red) F-actin. Values are fit to a Gaussian distribution (mean and standard deviations reported in Table 3). Speeds are

FIGURE 2.11 Caption Continuation
unaltered for both myosins on either F-actin. Speeds are unaltered for either motor under either F-actin condition and correspond to what has been reported previously (Ali et al., 2013).

Motor	Actin State	Actin Stabilizer	n	Mean Speed (nm/s, ± SD)
myosin-5	**ADP**	**Phalloidin**	315	360 ± 130
myosin-5	**ADP**	**CP**	146	410 ± 180
myosin-5	**ADP•Pi Decay**	**None**	989	370 ± 130
myosin-5	**ADP•Pi Decay**	**CP**	428	350 ± 150
myosin-5	**ADP•Pi**	**Phalloidin-Copoly**	263	420 ± 130
myosin-6	**ADP**	**Phalloidin**	476	120 ± 51
myosin-6	**ADP**	**CP**	279	110 ± 40
myosin-6	**ADP•Pi Decay**	**None**	707	130 ± 56
myosin-6	**ADP•Pi Decay**	**CP**	133	110 ± 44
myosin-6	**ADP•Pi**	**Phalloidin-Copoly**	249	140 ± 54

TABLE 3. Velocity summary statistics for myosin motors moving along F-actin with the set of nucleotide states and filament stabilizers.

2.6.2. Actin filament assembly rate remains unchanged

One more factor that I am observing in the experiments is the behavior of actin filaments. Since the experiments performed here visualize for the first time unconventional myosin walking along the single elongating actin filament, I have a chance to evaluate the influence that dimeric myosins might have on the actin assemble process. However comparing assembly rates of actin filaments in experiments where myosin-5 or myosin-6 is present and actively processive on

elongating filaments versus control set up with no myosins present, I do not see significant changes of the assembly rates. F-actin assembly rates are unaffected by either myosin motor and in agreement with literature values (Figure 2.12).

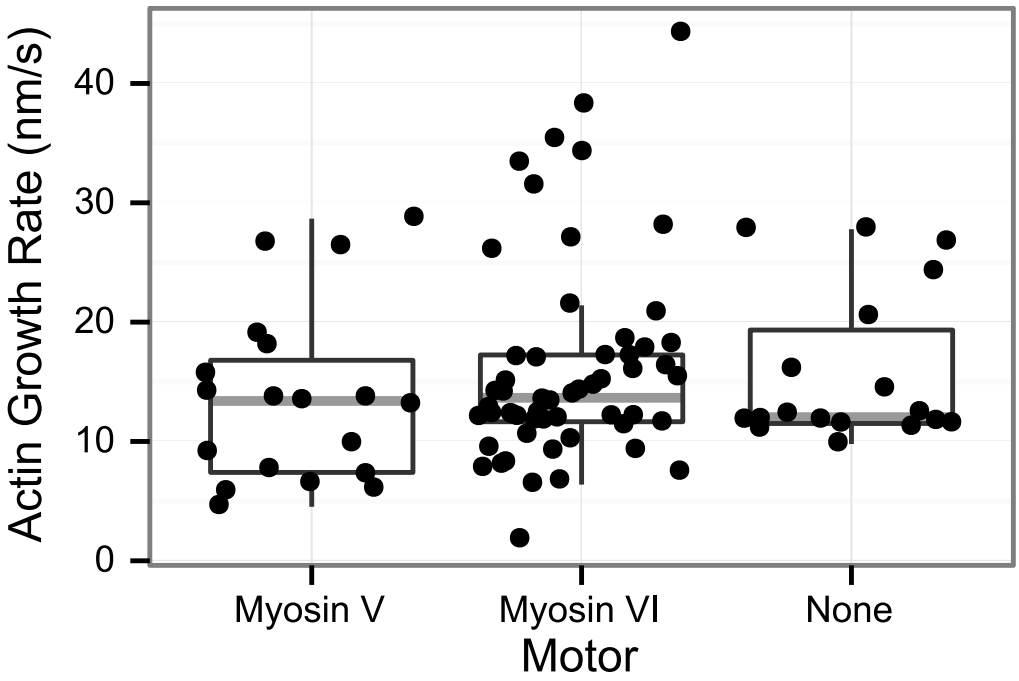


FIGURE 2.12 Growth rates of assembling F-actin in the presence of myosin-5 or myosin-6 remain the same
Growth rates of assembling F-actin were determined in the presence and absence of myosin-5 or myosin-6. The average growth rate of assembling F-actin remains unchanged under the influence of myosin-5 or myosin-6.

2.7. Discussion

The main finding of this work it that myosin-5 runs farther on the younger, ADP•Pi-rich actin, whereas myosin-6 travels farther on older, ADP-rich actin. Interestingly, one study found that the myosin-5 run length in untreated cells was 1.5-fold higher than in cells with blocked F-actin dynamics (Semenova et al., 2008). This difference is strikingly similar to what I find here, under conditions where F-actin growth

rates are also similar (20 monomers/s versus 10 monomers/s). The results of my thesis work are also consistent with a 20% reduction of kinesin processivity on GMPCPP MTs versus Taxol-stabilized GDP MTs (McVicker et al., 2011) illustrating that similar principles apply to MT tracks and motors.

Coupling of myosin motor activity to actin's nucleotide state suggests two guidelines for future work. First, because order of addition matters, it is important to state when phalloidin is added in F-actin polymerization. I suspect that phalloidin is typically added after completion of polymerization. Second, when myosin motility is examined at high P_i concentrations, secondary actin effects should be considered alongside the primary myosin effects on force generation and stiffness (Caremani et al., 2008).

I find that myosin run lengths are affected by the actin nucleotide state, whereas myosin speeds are not. Myosin run lengths increase with the duty ratio, defined as fraction of the ATPase cycle time when the motor is bound to its filament. An increased duty ratio decreases the period in which the myosin is vulnerable to detach. The two ways to increase the myosin duty ratio are to accelerate rebinding to F-actin or to inhibit F- actin detachment. Because the speed does not change, and because ADP release gates detachment while being rate-limiting for both of these myosins (De La Cruz et al., 1999; De La Cruz et al., 2001), the F-actin nucleotide state likely affects the overall rate of strong binding to actin. This accelerated binding scenario is consistent with the increases in myosin landing rates in Figure 2.12, on opposite types of actin for myosin-5 and myosin-6.

Myosins may sense the actin nucleotide state in two ways. The first is a classical molecular recognition mechanism involving actin subdomain 2 (SD2), a key determinant of filament flexibility and stability. Release of P_i causes SD2 to rotate 15°, closing the nucleotide-binding cleft (Isambert et al., 1995) (Belmont et al., 1999). In addition, the DNase-I-binding loop folds into an alpha helix upon P_i release (Graceffa & Dominguez, 2003), changing the longitudinal subunit contacts within the filament and affecting filament bending stiffness (Chu & Voth, 2005). Myosin-5 and myosin-6 may directly sense the orientation of actin SD2. Recent work revealed that strong binding of myosin to F-actin involves interactions between actin SD2 and myosin loop 2, loop 3, and the cardiomyopathy loop (Lorenz & Holmes, 2010). There are many sequence differences between myosin-5 and myosin-6 at the actin-binding interface that could influence sensing of the SD2 orientation. In particular, loop 2 is longer in myosin-5, and changes in the loop 2 region are known to affect actin binding (Murphy & Spudich, 1999) (Yengo & Sweeney, 2004).

Alternatively, these two myosins may recognize flexibility differences between the stiffer ADP•Pi state and the softer ADP state of F-actin. Stiffened F-actin inhibits gliding filament motility on skeletal myosin-2, without affecting myosin enzymatic activity (Prochniewicz & Yanagida, 1990). Furthermore, both myosin-5 and myosin-6 decoration increase the torsional dynamics of F-actin, whereas myosin-2 has the opposite effect (Prochniewicz et al., 2010; Prochniewicz et al., 2011). By thermodynamic linkage, I expect that changes in filament dynamics also affect myosin binding in an isoform-specific manner. One difficulty with this argument is that myosin-5 and myosin-6 both increase torsional dynamics. However, one significant difference is

that these studies used monomeric motor domain S1 fragments, whereas ours used dimerized myosins. Dimeric myosin-5 may prefer stiffer filaments, because its long and stiff lever arms would serve to buttress the actin filament. In contrast, dimeric myosin-6 has more flexible lever arms that are oriented nearly parallel to the filament (Ménétrey et al., 2007) and therefore provide little additional stiffening.

Regulation of myosin motility by the nucleotide state of F-actin is expected to be important in cells. Although the nucleotide state of actin filaments in cells has not been experimentally determined, different F-actin networks are enriched for ADP•Pi or ADP F-actin (Bindschadler et al., 2004). Because P_i release takes 6 min (Melki et al., 1996), networks that turnover in seconds at the leading edge of migrating cells consist primarily of ADP•Pi filaments. Remodeled networks farther from the leading edge turn over slowly and are likely to have ADP filaments. Given that the severing protein ADF/cofilin binds tighter to ADP F-actin than ADP•Pi F-actin (Carlier et al., 1997), ADF/cofilin localization might indicate the cellular nucleotide state of F-actin. As predicted, ADF/cofilin is absent from F-actin at the leading edge of migrating cells but strongly localizes to F-actin deeper into the cell (Svitkina & Borisy, 1999). Actin-binding proteins may also regulate myosin activity in cells by indirectly affecting the nucleotide state of F-actin. For example, ADF/cofilin allosterically increases the amount of ADP F-actin by accelerating the rate of P_i release from unoccupied filament subunits (Suarez et al., 2011). Because myosin-5 moves 10-fold faster than the elongation rate of the barbed end (300 nm/s versus 30 nm/s), myosin-5 is able to overtake the F-actin ADP•Pi decay and reach increasingly younger actin subunits as it walks. Myosin-6 travels in the direction of aging and therefore reaches older actin subunits with each step. I find it

interesting that each myosin has evolved to move in a direction that carries it to more favorable transport conditions. Thus, myosin-5 and myosin-6 both head toward greener pastures, allowing enhanced transport of myosin-5 cargoes to the cell periphery and myosin-6 cargoes to the cell interior. Although I fully expect that ABPs in the cell further modulate myosin activity, such effects would be in addition to the inherent ability of these myosins to discriminate filaments based on age.

CHAPTER 3: SHARING ONE TRACK: BIDIRECTIONAL MOTILITY OF MYOSIN-5 AND MYOSIN-6 ON A SINGLE FILAMENT

3.1. Introduction

In the previous chapter I used assembling F-actin to test how actin tracks modulate myosin motility. I discovered that myosin-5 and myosin-6 detect the age of actin tracks via the actin nucleotide state, and adjust their processivity accordingly (Zimmermann et al., 2015). Myosin-5 has longer runs on young filaments, corresponding to leading edge in the cell. Myosin-6 has longer runs on old filaments, as found in the cell interior away from sites of filament nucleation. Here, I consider another aspect of myosin-5 and myosin-6 motility that has been omitted in *in vitro* assays . Namely, I looked at simultaneous motility of two oppositely directed myosins along assembling filaments, as shown on Figure 3.1 (Santos et al. 2016). Because myosin-5 and myosin-6 travel in opposite directions, they should encounter each other frequently and eventually compete for the same binding site along actin.

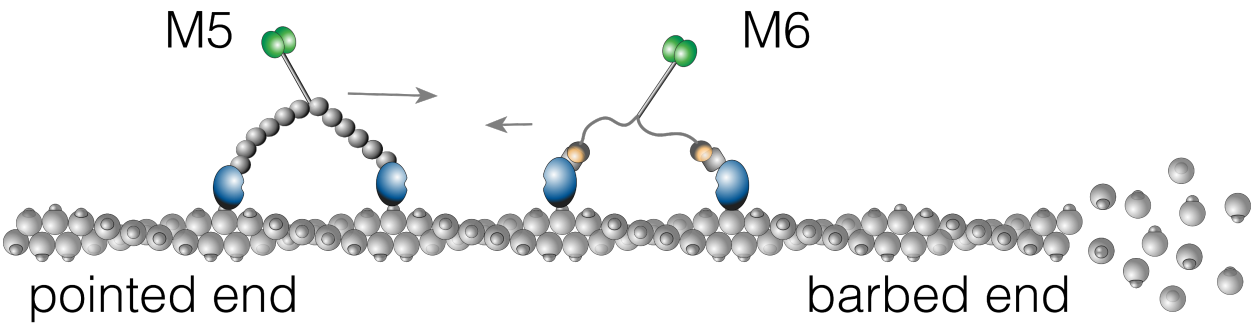


FIGURE 3.1 Schematic of the experiments
Fluorescently labeled myosin-5 and myosin-6 walk along the same assembling actin filament.

The ‘two-way’ traffic that myosin-5 and myosin-6 are responsible for is of great importance for efficient transport in the cell. In this work I seek to answer two main questions about myosin-5 and myosin-6 motility. The first is whether a single F-actin track supports the simultaneous traffic of myosins traveling in opposite directions. The second is how such opposing motility is resolved to ensure effective myosin-5 and myosin-6 based transport.

In cellular environment multiple myosins use the same filamentous actin (F-actin) tracks, yet little is known about how this track sharing is achieved and maintained. To assess the influence that different myosin classes have on each other, I developed an assay that combines two dynamic elements: elongating actin filaments with identified barbed and pointed ends, and myosins moving along these filaments. I studied two different myosins, myosin-5 and myosin-6. These myosins have distinct functions in the cell and are known to travel in opposite directions along actin filaments. Myosin-5 generally walks towards the barbed end of F-actin into dynamically rearranging actin at the cell periphery. Myosin-6 is a pointed-end myosin that generally walks towards the cell center. I successfully reconstituted simultaneous bidirectional motility of myosin-5 and myosin-6 on single polymerizing filaments of actin. I report and provide statistical analysis of encounters between myosin-5 and myosin-6 walking along the single filaments. When myosin-5 and myosin-6 collide, myosin-5 detaches more frequently than myosin-6. The experimental observations are consistent with a stochastic stepping model based upon known kinetic characteristics of each myosin. The observations from *in vitro* experiments are consistent with the *in silico* stochastic model based on kinetic characteristics of each myosin.

3.1.1. Bidirectional motility of myosin-5 and-6 on single filament

I successfully reconstituted simultaneous motility of myosin-5 and myosin-6 on single growing filaments (Figure 3.2 & 3.3). By using the assembling filament assay (Zimmermann et al., 2015) I am able to easily identify barbed and pointed ends of each filament (Supplementary Movie 3-1). To simplify the recording and analysis, I label myosin-5 and myosin-6 with the same fluorophore. I then assign motility towards the barbed end as myosin-5 runs (Sellers & Goodson, 1995), and motility towards the pointed end as myosin-6 runs (Wells et al., 1999). Because myosin-5 and myosin-6 move at different speeds, I can use speed as a second means to identify the myosin class. Both assignments agreed in every case.

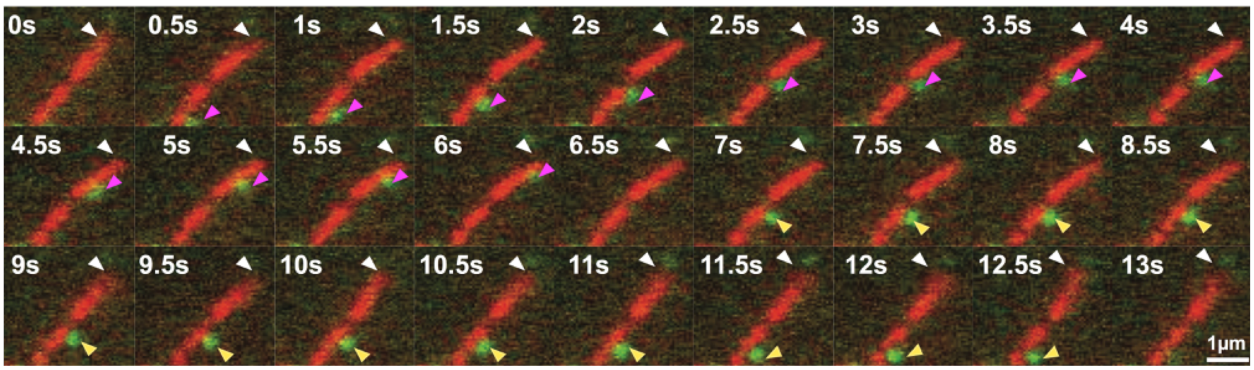


FIGURE 3.2 Myosin-5 and myosin-6 sharing the same elongating actin filament *in vitro* for the bidirectional motility
Time-lapse fluorescence micrographs featuring myosin-5 motors and myosin-6 motors (both in green) traveling on the same assembling actin filament (red). White arrowheads mark the growing barbed end of the filament; magenta and yellow arrowheads mark the displacement of individual myosin-5 and myosin-6 molecules, respectively. Micrographs show motility of both motors at equal concentration of 1 nM.

3.2. Simultaneous myosin-5 and myosin-6 motility reconstituted on a single filament

Myosin motor classes co-exist in the cell and use the same F-actin tracks to transport material and to apply forces to the cytoskeleton. It is currently unclear how these myosins react when they encounter obstacles, even though these obstacles can be common in the cell. The F-actin networks have different composition in subcellular regions, creating distinct local environments (Blanchoin et al., 2014). In some areas of the cell, where F-actin tracks are limiting, myosins could crowd onto single tracks. Determining the accessible myosin binding sites on actin and the outcome when myosins compete for the same site should reveal important aspects of self-organization in the eukaryotic cytoskeleton.

In Figure 3.3 I show representative kymographs of bidirectional motility. The diagonal front showing F-actin elongation is marked in red, and diagonal myosin paths are shown in green. Myosin-5 moves faster than myosin-6, resulting in a diagonal line that appears thinner despite carrying the same fluorophore as myosin-6. To optimize the number of myosin encounters, I increased the concentration of each myosin from 1 nM to 5 nM. A comparison of myosin density between the 1 nM and 5 nM in a presence of TMR phalloidin conditions is shown in the kymographs (Figure 3.3). This 5-fold increase in concentration resulted in a 24-fold increase in the encounter frequency (from number of collisions n=21 for 1nM myosins to n=500 for 5nM myosins), as expected for a process that is first order in each myosin.

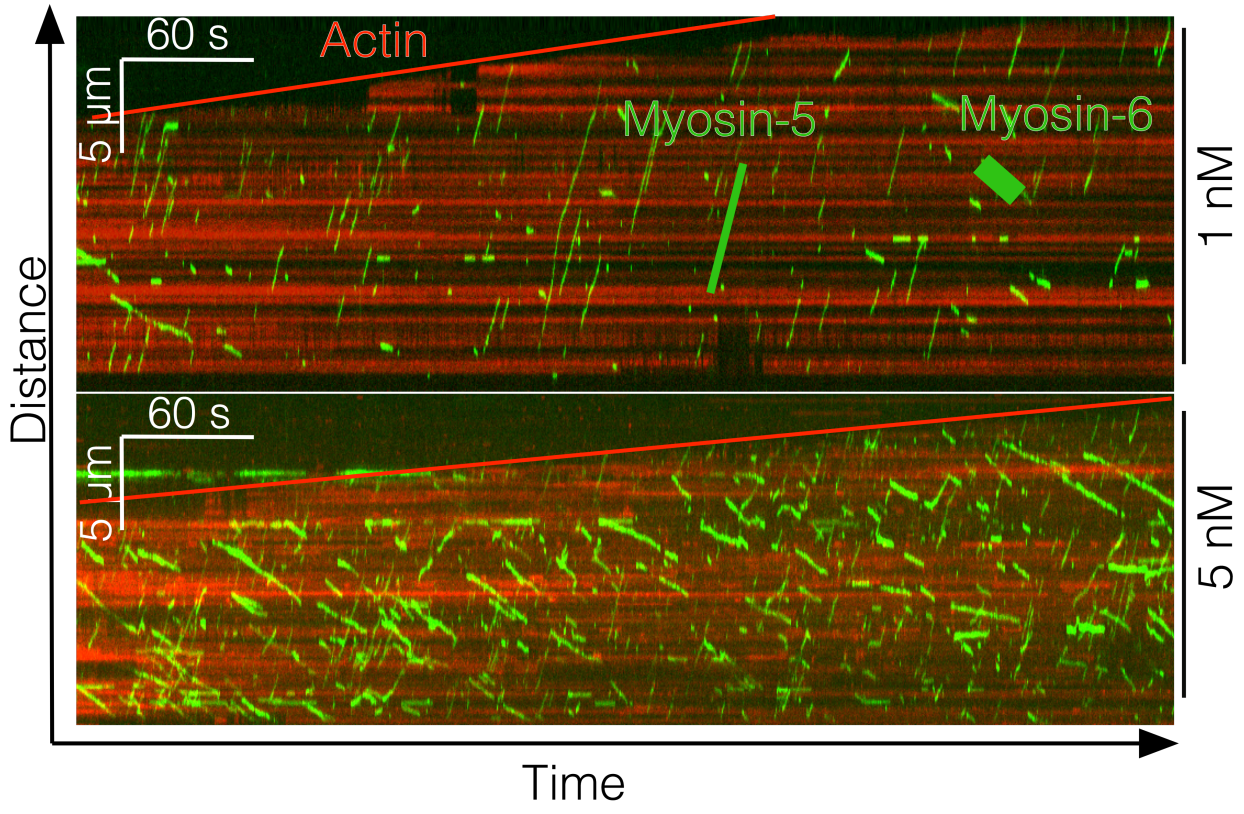


FIGURE 3.3 Representative kymographs showing simultaneous motility of myosin-5 and myosin-6 on elongating filaments.
Although myosin-5 and myosin-6 are labeled with the same fluorophore, they can be distinguished by the direction of their runs. Myosin-5 and myosin-6 travel towards barbed and pointed ends, respectively. Kymographs show the relative motility of both myosins at equal motor concentrations of either 1 nM or 5nM. Collisions between myosin-5 and myosin-6 can be observed.

The main technical challenge in reconstituting the motility of oppositely directed myosins is establishing the polarity of the F-actin. Several groups have devised approaches to distinguish the barbed and pointed ends of actin filaments in a motility assay. The main approach is to use an anchoring particle on one end of F-actin, followed by solution flow to orient filaments in the image plane of the microscope (Spudich et al., 1985) (Wei et al., 2011) (Yuan et al., 2013). Only one of these studies examined motility of myosin-5 and myosin-6 on the same filament (Yuan et al., 2013).

This study by Yuan *et al.* focused on the shear flow methodology with anchored gelsolin used to orient the filaments. These elaborate preparation challenges resulted in a low number of myosin-5 / myosin-6 encounters (n=26). Moreover, Yuan *et al.* used quantum dots to label their myosin motors. Here I am interested in how the myosin motor domains compete for the same binding-sites along actin, and how this competition is resolved. To examine these features of motor-domain competition, it is important to avoid bulky fluorophores like quantum dots, which may present steric interference and affect the processivity of the myosins. On the other hand, quantum dots would mimic cellular cargo to a certain extent, so each approach has its merits.

Here, I monitor myosins on polymerizing F-actin as in the prior work (Zimmermann et al., 2015). The rapidly elongating end of actin is the barbed end. Myosins that travel toward the elongating end are myosin-5s (Sellers & Goodson, 1995), and those that travel away from the elongating end are myosin-6s (Wells et al., 1999). This system does not require flow to align the filaments, nor does it need an anchor or a fluorescent marker to cap the barbed end. I use the same fluorophore on each myosin: a small, Cy5-labeled affinity clamp (Huang et al., 2009). The affinity clamp is comparable in size to a GFP label and much smaller than a quantum dot. This labeling approach simplifies the imaging conditions and ensures equivalent labeling of each myosin.

To examine the features of motor-domain competition, it is important to avoid bulky fluorophores such as quantum dots (QDots), which may present steric interference. Instead I used single organic fluorophores attached to affinity clamp protein that is from 5 to 10 times smaller from QDots (Huang et al., 2009). Use of the

same monovalent labeling agent ensures identical labeling efficiency between myosin-5 and myosin-6.

I successfully reconstituted simultaneous motility of myosin-5 and myosin-6 on single polymerizing filaments (Figure 3.2 and 3.3). By observing the elongation of actin from the start of the experiment, I can ensure that myosin-5 and myosin-6 travel along the same single F-actin. I easily identify barbed and pointed ends of each filament and the myosin identity for each myosin run (Supplementary Movie 3-2). Because myosin-5 and myosin-6 move at different speeds, I can use the speed to verify the myosin class assignment. The assignments agreed in every case.

3.3.The geometry of the collision

3.3.1. Paths available for myosin motor on a single actin filament

I can distinguish two broad behaviors of myosin-5 and myosin-6 walking toward each other on one filament. In half of the encounters, the myosins pass each other like ‘two ships that pass in the night’. The other half of encounters result in what I call a 'collision,' where myosins interfere with each other at the encounter site. In a 'head on' collision between myosin-5 and myosin-6, the two myosins compete for the same binding site on actin as they approach from opposite sides (Figure 3.4). Note that collisions here refer only to the competition for binding sites, and do not involve an exchange of momentum.

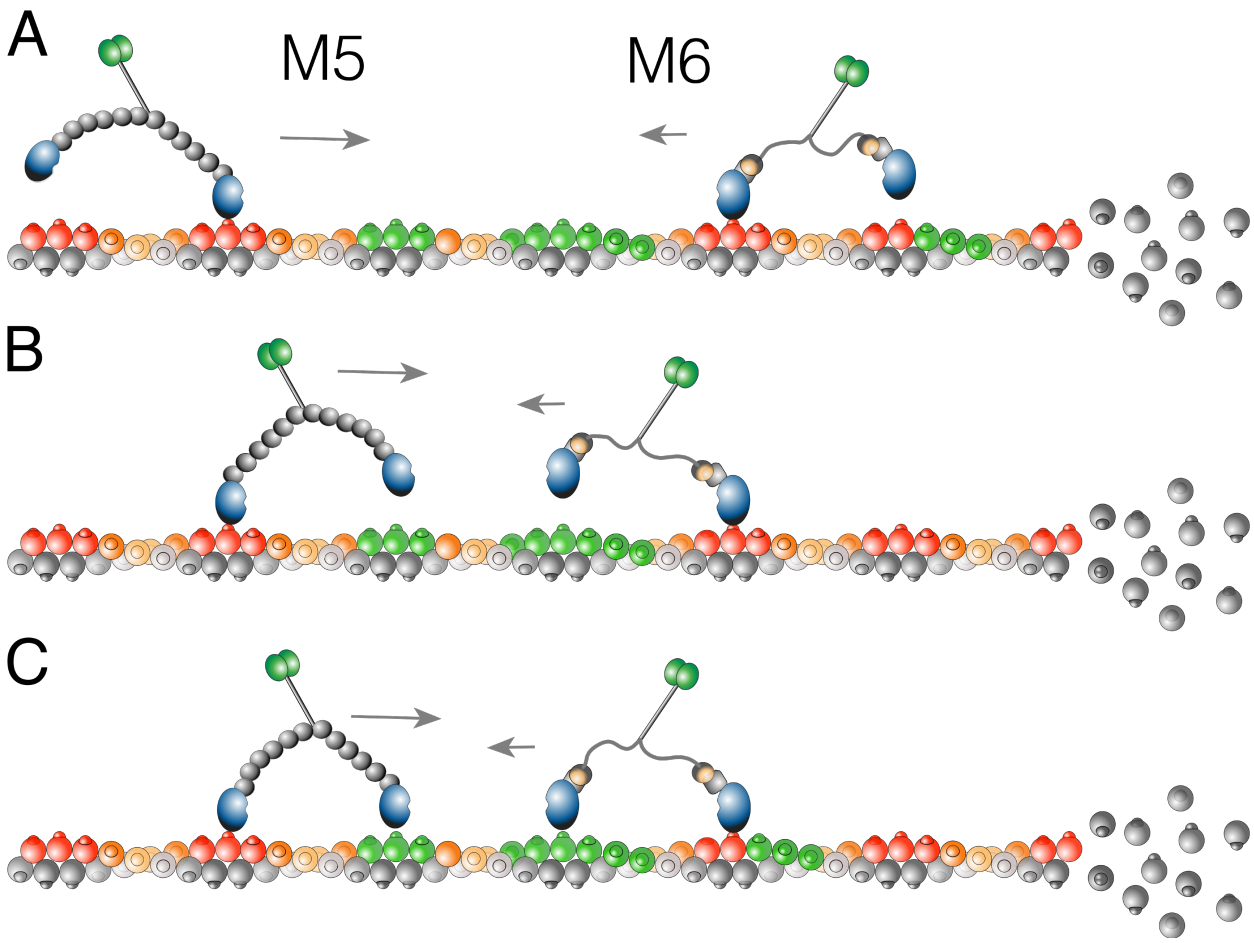


FIGURE 3.4 Spatial arrangement of myosin-5 and myosin-6 during bidirectional motility along a single filament.
Stages of myosin-5 and myosin-6 approaching collision event on a growing actin filament. (A) Myosin-5 and myosin-6 are aligned along the top of the filament, within the plane of the page, and will eventually compete for the same actin-binding site if they continue along those paths without sidesteps. Accessible binding sites on actin are emphasized by green monomers. Myosin-5 uses one of three accessible actin monomers for forward steps, with a strong bias toward the central monomer of the three. Myosin-6 uses one of approximately six accessible monomers for the forward step and one of three accessible monomers for the backward step. (B) Myosin-5 and myosin-6 both complete their working strokes, positioning their free motor domains near their next target binding sites along actin. (C) Myosin-5 and myosin-6 rebind to the filament. With this alignment of the two myosins, one of the myosins must detach in the next cycle unless a sidestep occurs and the lane is cleared.

Myosin-5 has one preferred actin binding site when it takes a forward step, however it can bind one monomer before or after the preferred binding site with lower probability (Uemura et al., 2004). Myosin-6 has a broader range of target binding sites along actin, and can take frequent backsteps as well (Rock et al., 2001). Stepping off the preferred binding site will cause the two myosins change lanes. However, sidesteps that avoid a collision are likely balanced by sidesteps that lead to a collision. Therefore I expect that sidesteps have a negligible effect on the stepping outcomes, and I omit an explicit treatment of sidesteps here.

3.3.2.Defining the 'head on' collisions

Passing events occur somewhat less frequently than expected considering the actin filament geometry. The actin filament forms a 13/6 helix, with 13 actin monomers per pseudohelical repeat. Thus, I expect that F-actin would present a maximum of 13 separate lanes for myosin traffic (Figure 3.5). Filaments in the experiment are attached to the coverslip surface through streptavidin links. Even though the attachment sites are sparse, with actin biotinylation at 0.1%, I expect that half of the lanes are occluded due to proximity to the glass (Figure 3.5). If seven F-actin lanes are accessible, I would predict that under 14% of runs would result in a collision and 86% of myosins would pass each other at the encounter site. Collisions might be more prevalent if each myosin occludes more than one lane, or if myosin landing events are biased toward a smaller number of more exposed lanes (perhaps the ones farthest from the coverslip), or through a combination of these two mechanisms. *In vivo* enhancer of this effect is the presence of steric hindrance caused by the cargos. The cargo obstacle could

increase probability of falling off due to the collision, even if the motors do not share the same ‘path’ on actin.

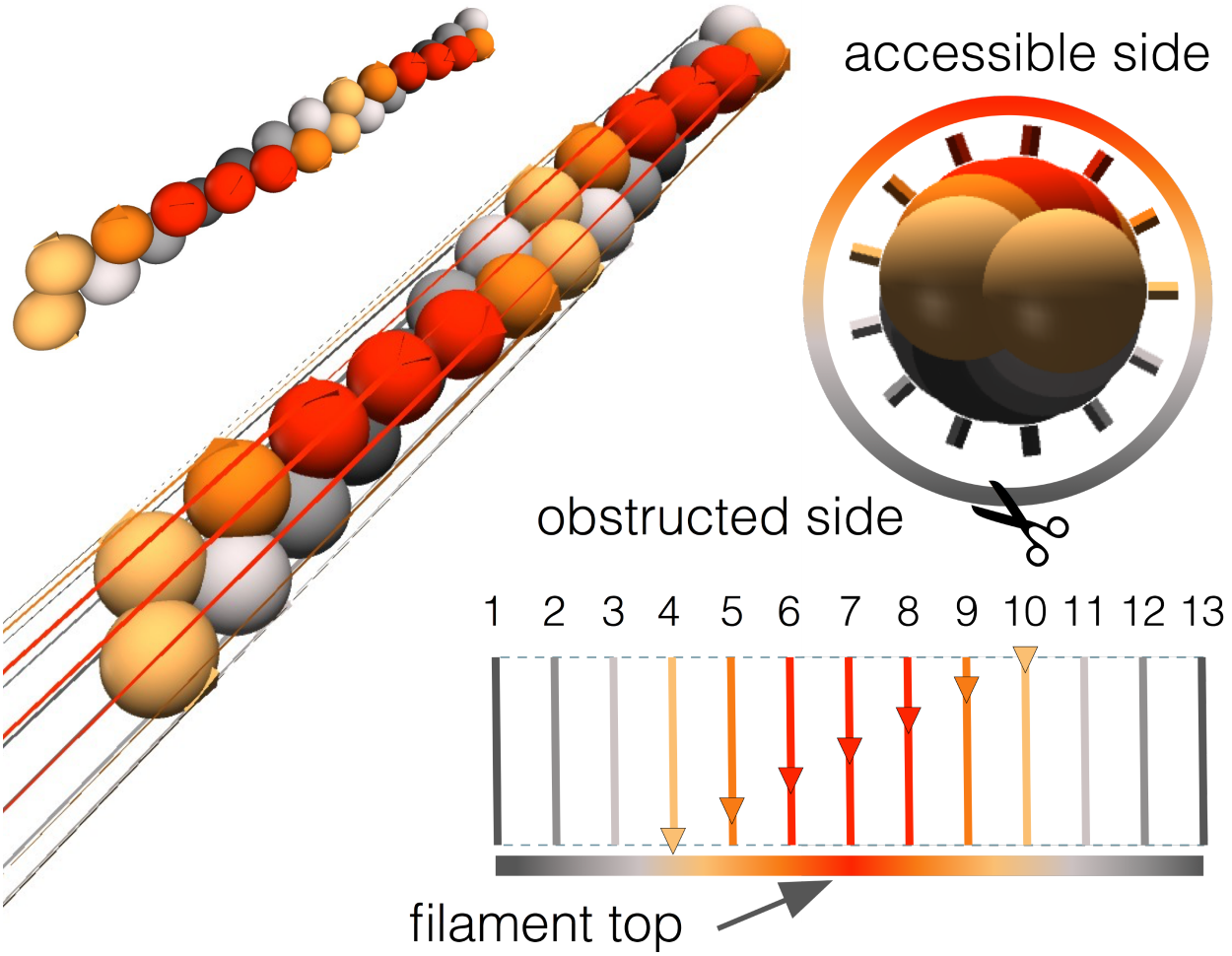


FIGURE 3.5 Visualization of accessible tracks for myosin walking along the filament
There are thirteen lanes encircling the filament, shown as lines connecting consecutive monomers along each lane in the left panel. A slice looking down the long axis of the filament is shown in the right panel. At the bottom, the unfurled cylinder is shown with its thirteen lanes. The red lanes are easily accessible for myosin binding, orange and yellow are less exposed, and gray indicate actin lanes that are likely obstructed by the coverslip surface.

3.4.Outcomes of encounters between myosin-5 and myosin-6

In experiments with myosin-5 and myosin-6 simultaneous motility, I observed 568 crossing events. For 521 collisions TMR phalloidin was present, sustaining ADP•Pi state of the filament and ensuring bright label withouth use of TMR actin. The remaining 47 collisions were reported on the filament with decaying phosphate state withouth phalloidin present.

3.4.1.Outcomes of 'head on' collisions

When the two myosins with opposite directionality meet traveling along a single actin filament, there are five possible outcomes that these encounters can result in. Both myosins can continue their runs uninterrupted, myosin-5 can detach while myosin-6 continues their run, myosin-6 can detach as myosin-5 crosses, both myosins meet and stall together or both detach upon encounter. These outcomes and representative kymographs parts of analyzed filaments are shown in Figure 3.6 and plotted on Figure 3.7. Velocities and runlengths of myosin motors as well as actin assembly rate are unaffected in the experiments and in agreement with the literature values (Ali et al., 2013).

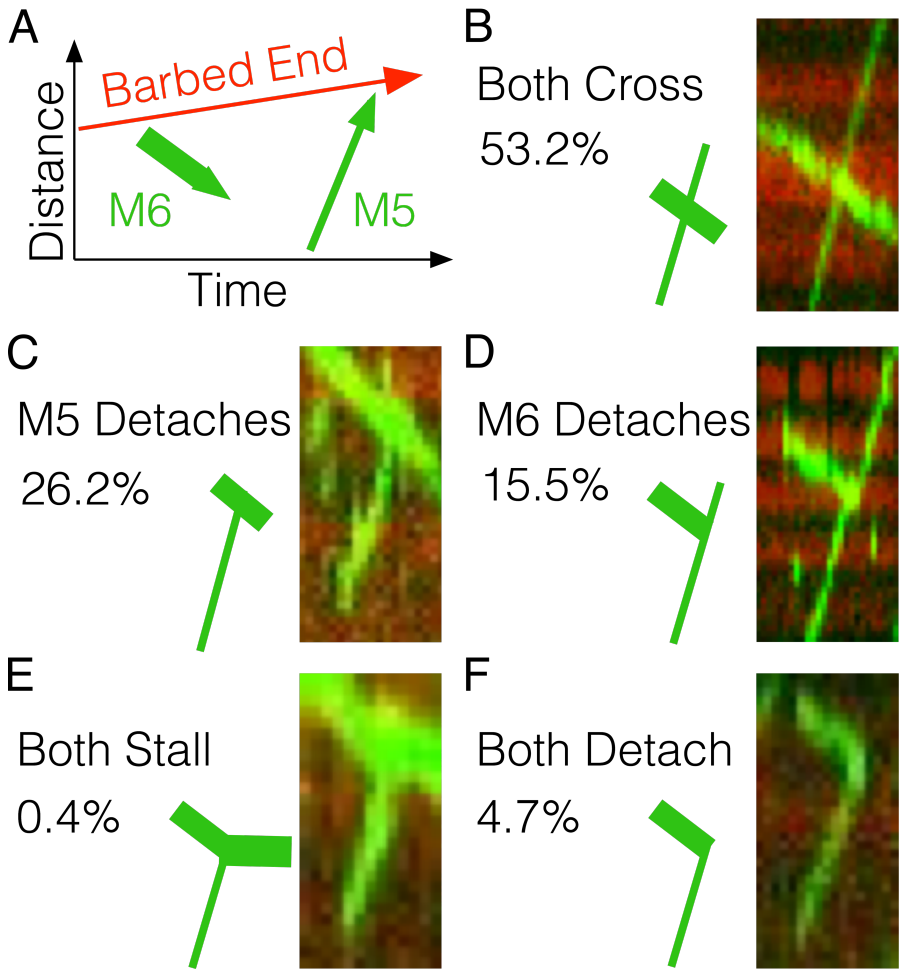


FIGURE 3.6 Collisions between myosin-5 and myosin-6 lead to five possible outcomes
(A) Scheme of kymograph analysis presented in (B-F). As in Figure 3.3, green diagonal lines from the lower left to the upper right are myosin-5, and lines from the upper right to the lower left are myosin-6. The red diagonal line represents the barbed end of growing actin filament. Five possible collision outcomes are reported with percent values that they account for among total number of collisions (568, out of 3636 total myosin runs). (B) The majority of the encounters allow both myosins to cross. (C-D) The second most common outcome is when one myosin continues while the other detaches at the site of the encounter. (E) Very few encounters result in both myosins stalling, indicated by a horizontal green line after the encounter. (F) A few encounters end with both myosins detaching.

3.4.2. Both myosins continue their runs after encountering each other

I observed a total of 568 crossings at equimolar concentrations of myosin-5 and myosin-6 based on my kymographs (Figure 3.3). The most common outcome is for

both of the myosins to continue their runs, passing by each other on the opposite sides of a filament; such events account for 53.2% of all encounters.

3.4.3. Only one motor continues the run after the collision

The second most common outcome is for at least one myosin to continue the run after the encounter; such events account for 41.7% of all encounters. Myosin-6 continues the run in 26.2% of encounters, while myosin-5 continues in 15.5% of encounters. These outcomes are likely a result of both myosins targeting the same favored binding sides along the actin filament. As such, they effect in one of the myosins succeeding in binding the the particular spot and the second myosins detachment.

3.4.4. Both myosins detach or stall

Collisions that result in detachment of both myosins or stall are rare, 4.5% and 0.4% respectively. Collisions that result in detachment of both myosins are rare (4.5%) and statistically can be a result of myosins ending the run right after an encounter, whether the opposite directionality myosin was in a way or not. Collisions that result in stall are extremely rare (0.4%) and could be an effect of the myosins running into other previously stalled motor. I do not observe extended pauses at the side of collision (with the exposure time 500ms).

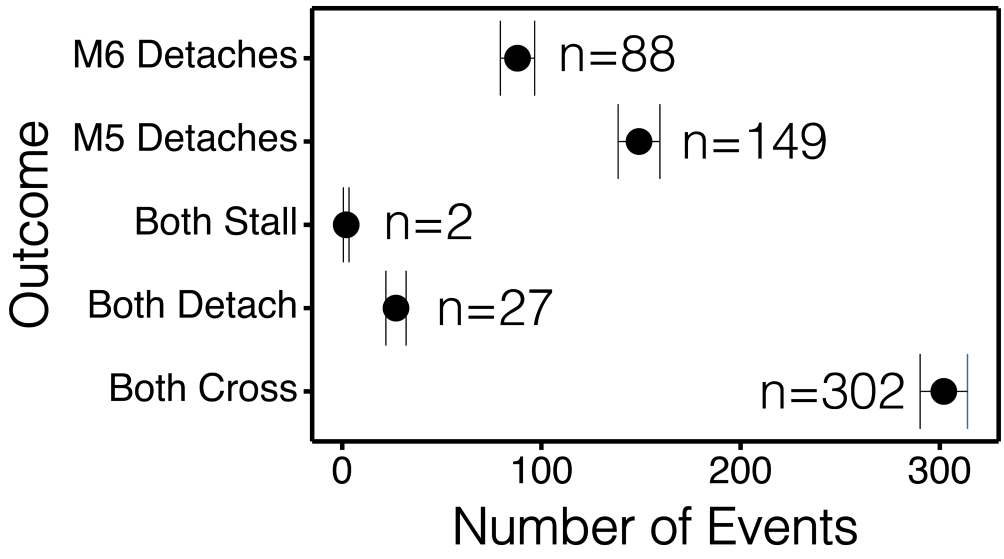


FIGURE 3.7. Collisions outcomes
The frequency of collision outcomes. Among events where one of the myosins detaches and the other myosin continues the run, myosin-5 detaches first almost twice as often as myosin-6. Error bars show standard deviations estimated from multinomial counting statistics.

3.4.5. Competition vs blocking

Just under half of the cases are collisions, where the myosins appear to interact at the encounter site. Collisions that result in detachment of both myosins are rare (4.5%) and can be a result of myosins ending the run right after an encounter, despite presence or absence of the opponent. Based upon the earlier runlength estimates for these myosins under these conditions (Zimmermann et al., 2015), I predict that 6.5% of encounters would have both myosins detach within a 200 nm window, a reasonable limit on our ability to resolve passing events. Collisions that result in stall are extremely rare (0.4%) and could be an effect of the myosins entangling with each other. The bulk of collisions result in one of the myosins detaching at the encounter site. The most straightforward explanation is that one myosin occupies actin binding sites required by

the other, in the head on collision scenario (Figure 3.4). In 63% of these cases, myosin-6 continues the run while myosin-5 detaches. I expect that this outcome is determined by a kinetic competition between each myosin for sites along actin.

In myosin-5 reach there is only one favorable binding spot with possibility to step on one closer or one further binding site. Additionally myosin-6 has the ability to take back steps, which not only lets it to step backwards when myosin-5 foot is bound, but also might lead to blocking the forward step of myosin-5. Both of the myosins have a high duty-ratio, however with slower kinetics for myosin-6. Therefore myosin-6 in rigor state might also be obstructing the next binding spot for myosin-5 leading foot. Apart from competing and blocking binding spots by myosin feet and kinetic differences between myosins there are also steric barriers resolving collision between myosin-5 and myosin-6 motility. 'One handed' walking with lever arm swing only in one side (Andrecka et al., 2015) would contribute to myosin-5 detachment caused by steric hindrance if myosin-6 molecule was in proximity at 'the wrong site' of myosin-5.

3.5. A stochastic simulation that predicts 'head on' collision outcomes

3.5.1. Gillespie's stochastic simulation algorithm

When collisions occur, I expect that at some point during the encounter the two myosins will compete for the same target binding site along actin. To further understand the nature of this competition, I performed a stochastic simulation of the approach process of the two myosins. Briefly, I describe a set of lattice sites that mark myosin positions on three actin monomers in one lane along the filament (Figure 3.8). In my model for behavior of myosins in 'head on' encounter I calculated the statistically

correct trajectory of the collision outcomes based on a set of lattice that mark myosin positions. Myosin-5 advances along sites 1→2→3→4→5, corresponding myosin-6 lattice has opposite direction 11→10→9→8→7, as the myosins approach each other. Lattice site 6 is always empty. There are also two separate sites on the lattice that mark myosin-5 or myosin-6 detachment. Odd numbers on the lattice mark sites where a motor domain is bound to actin, and even numbers for a free motor domain. Each odd site can transition to even site or to detachment (D). I set transition rates between these lattice sites to experimentally determined myosin-5 and myosin-6 values for ADP release (myosin detachment), and P_i release (myosin reattachment) (Altman et al., 2004; Cruz et al., 2001; Cruz et al., 1999; Rosenfeld & Sweeney, 2004; Sweeney et al., 2007). To sample the transitions between lattice sites I use Gillespie's direct method. The end of each simulation run occurs when one of the two myosins detaches.

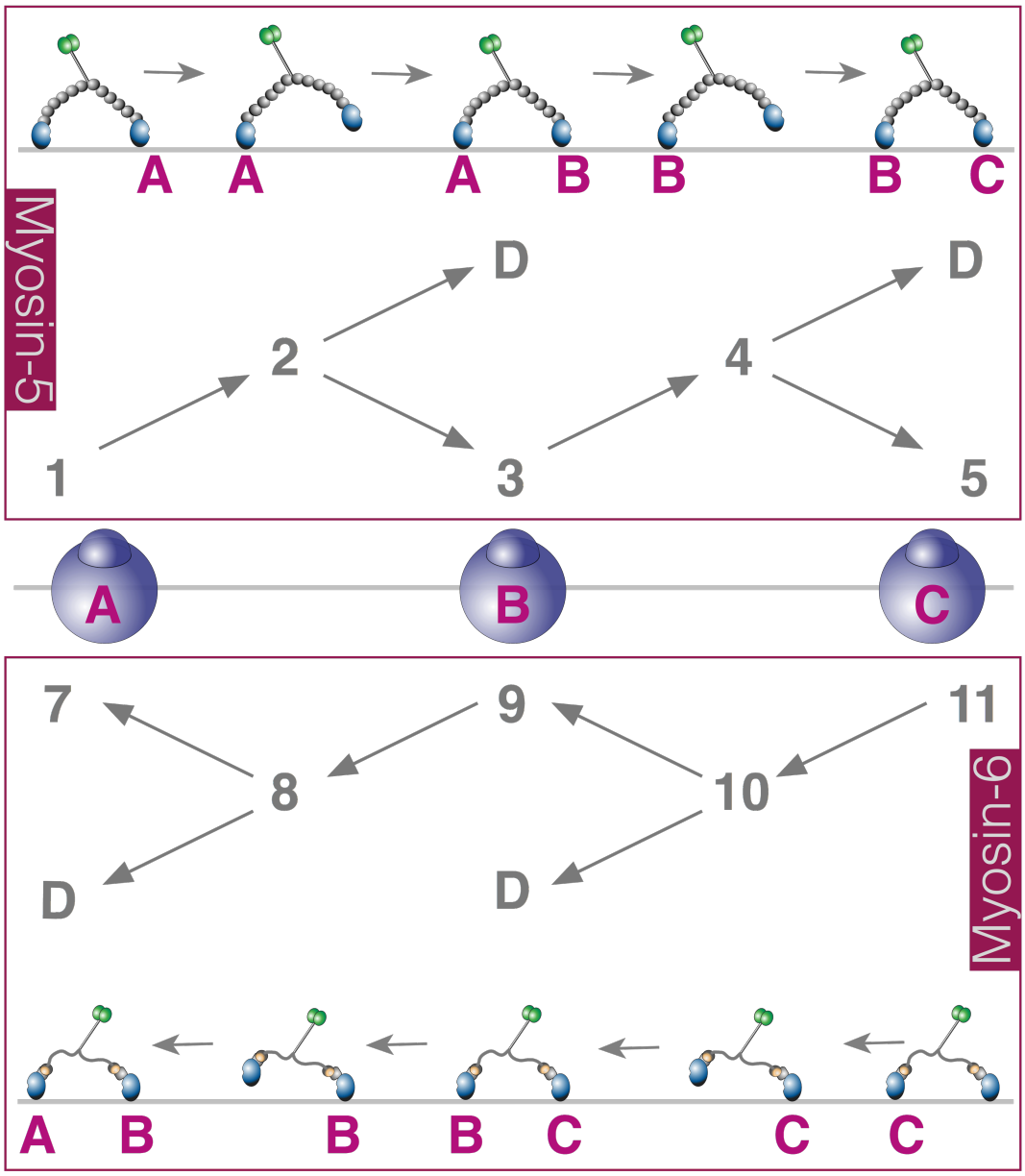


Figure 3.8. A stochastic simulation predicts that the faster myosin should detach more frequently when colliding with a slower myosin

For simulation I consider three actin monomers along one path on filament as well as one myosin-5 molecule and one myosin-6 molecule that approach each other from opposite directions using these three monomers. Assigned numbers represent a set of lattice that mark myosin-5 and myosin-6 positions. The myosin state is represented at the lattice site for its most advanced motor domain, where the free (even) sites are always ahead of the bound (odd) sites. I use the experimental ADP release rates for the odd-to-even numbered transitions, and for the even-to-D transitions. Likewise, I use the experimental myosin phosphate release rates to approximate actin rebinding rates in the even-to-odd transitions.

3.5.2. Outcome of collision series based on experimental kinetic rates

I ran a series of 10000 individual simulations to obtain statistically significant population of outcomes. I also provide a control with inputing equal rate constants for both myosins in 100000 simulations to obtain expected 0.5 probability of detachment for each of the myosins. In 75% of outcomes the first to detach is myosin-5. This compares favorably with my experimental value of 63%. Additionally, mean runlength of the motors changes the probability of falling off differently- ca 15% of myosin-5 and over 30% of myosin-6. Fall-off will not be noticed with our diffraction limitation with 500 ms exposure time. When this is taken under account the numbers shift towards 69% for myosin-5 detach and 31% for myosin-6 detach. Beyond the correction factor any further differences I account to actin filament conditions (eg. actin phosphate state enhancing myosin-5 and decreasing myosin-6 performance, curvature tension or biotin creating steric hindrance).

3.5.3. Analysis of collision outcomes with wide range of kinetic rates

I performed a sensitivity analysis to understand the relative importance of the kinetic parameters used in the simulation (Figure 3.9). Increased myosin-5 stepping rates relative to myosin-6 (to the right on the ADP release axis) strongly increase the myosin-5 detachment probability, while faster myosin-5 attachment rates relative to myosin-6 (to the top on the P_i release axis) cause a lesser decrease the myosin-5 detachment probability. Two sets of relative rate constants from the literature are indicated on the figure as cyan and orange circles. Although there is a range of literature values for myosin-6 attachment to actin (Cruz et al., 2001; Rosenfeld &

Sweeney, 2004; Rosenfeld & Sweeney, 2004; Sweeney et al., 2007), differences in this rate do not strongly affect the observed detachment probabilities.

Experimental values are indicated by circles, orange one represents set of kinetic rates reported in (Rosenfeld & Sweeney, 2004) (Sweeney et al., 2007), blue circle — rates from (Rosenfeld & Sweeney, 2004) (Cruz et al., 2001).

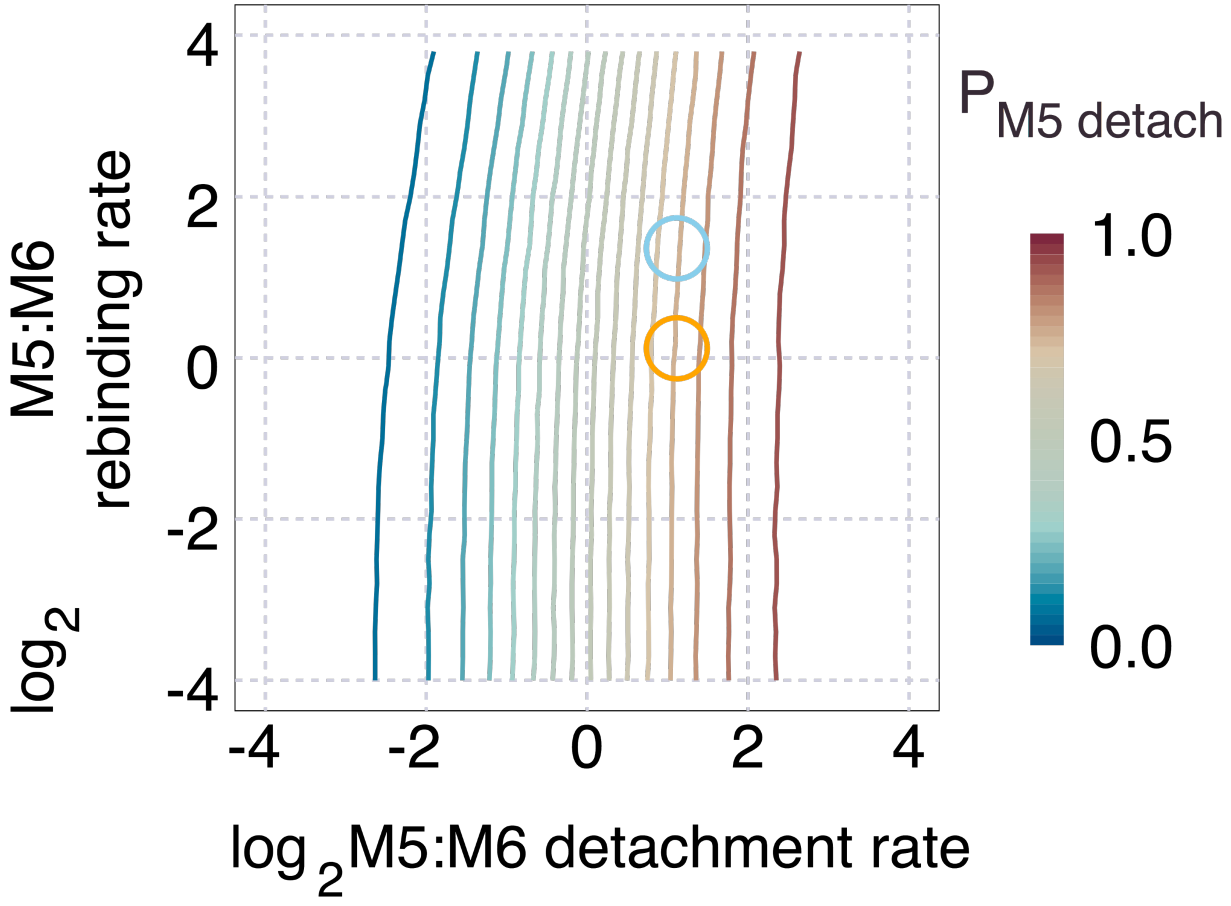


FIGURE 3.9 A contour plot of the probability of myosin-5 detaching first at a collision, detachment and rebinding rates
Rates are plotted as $\log_2(k_{m5}/k_{m6})$ values. Note that when both rates are equal (the point at the origin), each myosin is equally likely to detach as expected. Faster myosin-5 stepping rates (to the right) increase the myosin-5 detachment frequency, while faster myosin-5 attachment rates (to the top) decrease the myosin-5 detachment frequency. However, the effect is stronger for the former versus the latter. Experimental values are indicated by circles, orange one represents outcome when set of kinetic rates reported in (Rosenfeld & Sweeney, 2004; Sweeney et al., 2007) was used, cyan circle- outcomes when rates from (Rosenfeld & Sweeney, 2004; Cruz et al., 2001) were applied.

In most of the simulated encounters, the penultimate state has both myosins with one motor domain attached and one detached from actin. Thus, the slower myosin to detach would be more likely to continue its run while the faster myosin is more likely to fall off. Rarely, both myosins occupy these singly-attached states with a gap of one lattice site between them. In this case, the faster myosin is more likely to outcompete the slower to continue its run. But as shown in Figure 3.9, the detachment kinetics dominate the attachment kinetics.

3.6. Discussion

Myosin-5 and myosin-6 are both essential cellular transporters. When two way traffic occupies the same actin filament, these two myosin families would encounter each other and will occasionally occupy the same lane along a single actin filament. There is only one study that reports motility of myosin-5 and myosin-6 on the same filament (Yuan et al., 2013).Yuan et al focuses mainly on the methodology used to orient the filaments and sustaining myosin motility when orienting field was released. My approach is a less elaborate experimental method that provides comprehensive analysis of bidirectional myosin traffic on single filaments. I can dissect molecular details of multi motor interactions on actin avoiding additional intricacies of experimental method.

Myosin-6 is highly concentrated at the narrow bases of the stereocilia with a limited number of actin filaments, while myosin-5 is absent from stereocilia and is enriched only in afferent nerve cells that innervate hair cells (Hasson et al., 1997). Yet in stereocilia, barbed-end directed transport is preserved, suggesting that there are other means for the required cargoes to be carried e.g. by myosin-3 or myosin-15

classes (Ebrahim et al., 2016, Belyantseva et al., 2005). Microvilli in intestinal or renal epithelial cells are a related environment where two way traffic is maintained and both myosin-6 and myosin-5b are transporters (Chen et al., 2014; McDonough, 2009; Müller et al., 2008).

Here I examined encounters of myosins with opposite directionality on the molecular level, and find that the faster myosin frequently loses in the competition for actin binding sites. Since myosin-6 is the only known myosin class that moves toward the pointed end of actin, slower walking might enable it to plow through the many opposing myosin classes that would otherwise force it off of actin. Simultaneous bidirectional motility gives us insights on how multiple myosin families share actin tracks. Because myosins recognize each other as obstacles on a filament, my results also address the general idea of myosins encountering a stationary road block. As such, the results help in understanding the regulation of cellular multi-myosin traffic.

CHAPTER 4: CONCLUDING REMARKS

4.1. Synthesis of experimental findings

The first important aspect of this work was incorporating natural capacity of actin to polymerize in dynamic fashion into an *in vitro* assay for myosin motility tests. Constant rebuilding of the cellular mesh is a phenomenon essential for the physiology in every eukaryotic cell. Yet, this distinctive property of actin cytoskeleton has been omitted in previous single molecule studies of molecular motors. So far, *in vitro* single molecule motility experiments have used only static F-actin to obtain much desired assay simplicity. Filaments in these experiments have fixed lengths and are stabilized with the toxin phalloidin that disables one of the most characteristics to actin features — assembly and disassembly. Here, for the first time, I evaluated the impact of actin polymerization dynamics on myosin motor activity. On elongating F-actin I researched the behavior of representatives from various myosin classes, due to their distinct characteristic and functions performed in the cell. I recorded the behavior of fluorescently labeled myosins moving along elongating actin filaments via TIRF microscopy. Next I evaluated the impact of a toxin stabilizer, phalloidin, on myosin-actin interplay. The following experiments ultimately determined that the phosphate state of actin (i.e. the age of the actin) affects the interaction with myosin motors. I showed that actin age is one of the main clues for the motor to adjust their run length. Obtained results indicate that myosins behavior changes on ADP•Pi vs ADP actin. Myosin-5 has longer runs on ADP•Pi state, young, over ADP state, old F-actin. The tendency of myosin-6 is opposite; this motor takes longer runs on ADP actin tracks. Such results

were unexpected for me, as my hypothesis in the begging of the thesis research was that myosins motility and actin assembly will both have unchanged characteristic in this simple system. In fact testing myosins and elongating filaments was thought as the control experiment, where I was going to establish a baseline level of activity before reconstituting more complex cytoskeletal structures such as lammelipodia or filopodia by introducing more ABPs. The observations however showed that even such a basic feature of actin as phosphate state, omitted and not even reported as an experimental condition, was affecting the myosin activity. In here it is also worth a mention that the discovery of myosin preference for particular actin age would not be at all possible in the cellular context, where we still do not have tools to evaluate the exact composition of cytoskeletal F-actin in the actin age aspect. It would be indeed very interesting to investigate the age of actin within each cell during different phases, as well as different types of cells, as there might be a connection between the actin rearrangement rate and age with the overall transport direction in the cell. Following the discovery of actin age preference by myosis, I would expect myosin-5 being exhibiting higher activity in crawling cells, e.g. metastatic cancers, when the actin is rearranging more rapidly, whereas myosin-6 would exhibit high activity in more static cells with only subtle tread milling of actin meshwork.

Second major objective of this research project was investigating bidirectional effects between multiple myosin classes traveling along the same actin tracks. In here I also used single molecule techniques to reconstituting the simultaneous bidirectional motility of myosin-5 and myosin-6 on a single elongating filaments. I detected the encounter events between these two myosins. The experiment conditions resembles

cellular environment, where myosin-5 and myosin-6 motility may be supported by the same networks of actin filaments, with the two myosins traveling in opposite directions. First and foremost, I have found that in case of direct competition for binding site on actin, myosin-6 has almost twice more chances of attachment over myosin-5. Modeling *in silico* of the direct collision between myosin-5 and myosin-6 confirmed this results from *in vitro* experiments. Stochastic simulation based on kinetic constants established in literature has nearly the same outcome as the single molecule microscopy, with the strong tendency for myosin-6 be the winning motor. This finding, relying on a microscopic observation and a computational model of colliding myosins, points to the idea that pointed end transport by slower motor, myosin-6, is prioritized over the barbed end motility of faster myosin-5. I document encounters of the two myosin classes that end in both of the proteins continuing their runs. This indicates that two myosin motor classes can occupy the same actin filaments in a special and temporal close proximity withouth affecting each others ATPase activity. The summarized above findings are evident adaptations that regulate and ensure efficiency of bidirectional traffic within the cell.

In this project I integrated knowledge of actin dynamics, cytoskeleton associated proteins and myosin activity to understand how biological self-organization is achieved. The approaches taken here developed a pioneering strategy of 'bottom up' reconstitution of the cellular environment in an *in vitro* system. Knowledge obtained from experiments presented here serves as a bridge between classic *in vitro* studies and complex tissue culture observation. It helps to settle dissonances that embroil the

two conventional ways of cytoskeletal research and resolve questions that previous approaches could not answer.

4.2. Biological significance and applications

The main and possibly most important characteristic of myosin function is the motor's cellular distribution. Myosins carry cargos in a directed way, each transport run has a starting point to a destination. Each myosin is thought to have a specific destination, as its cargo needs to be delivered to a specific cellular destination. It has been a long standing hypothesis that myosin motors encounter on their way molecular 'road signs' that navigate them in the proper direction and help reaching the proper target region (Brawley & Rock, 2009). The findings of this thesis project are proving this hypothesis and manifest that tracks encode information about destinations and travel paths, making the directed cellular transport more efficient as opposed to motors taking random walks on actin networks. Random walks are in a way not more effective than a diffusion process, which can transport material, but does not satisfy the cells need for direct long distance transport. This idea can be also tied with adjusting functions of myosins that do not function as a transporter, but rather set tension. As a tethers these myosins also might exhibit similar preference to certain type of actin in order to pull in certain directions and avoid taking action in others.

In case of a disease, knowing how the motor is localized, confined or directed is a key to understanding the molecular basis of the disorder. Previous studies are pointing towards a number of conditions that are related to malfunction of molecular transport. Diseases connected with myosin motors studied have a broad range: from neurological disorders, deafness or heart conditions to cancer tumorigenesis and

metastasis. Let's take a look at the list of links between myosin motors malfunctions and associated abnormalities, some already mentioned in introductory Chapter 1. By emphasizing those in the summary chapter, I acknowledge the their number, versatility and a necessity to learn about them to address them pharmacologically.

Myosin-5 motor proteins have attracted attention of neuroscientists, since they are highly expressed in the central and peripheral nervous system. Absence of myosin-5a studied here, leads to a severe neurological disease — Griscelli syndrome (Griscelli et al., 1978; Pastural et al., 1997), also called Elejalde syndrome (Bahadoran et al., 2003; Elejalde et al., 1979). The isoforms myosin-5b and -5c are epithelial and secretory tissue related. Myosin-5b absence leads to an epithelial disorder called microvillus inclusion disease (Müller et al., 2008). The essential role of myosin-5a in cancer cell migration and metastasis was indicated in lung, colon, breast and prostate cancer derived cell lines (Lan et al., 2010).

The involvement of myosin-6 in human health disorders is even more impressive and diverse. Their mutations are associated with deafness in humans and mice (Avraham et al., 1995; Hertzano et al., 2008; Melchionda et al., 2001). Myosin-6 also plays a role in heart conditions, driving rapid trafficking in response to acute hypertension (Mohiddin et al., 2004; Yang et al., 2005). Due to its established role in cell migration, myosin-6 is related with maintaining the malignant properties of the majority of human prostate and ovarian cancers (Dunn et al., 2006; Yoshida et al., 2004). Last but not least, recent studies show myosin-6 co-localizing with fibrillary Tau protein in Alzheimer's disease indicating involvement of the motor in synaptic loss and neuronal death (Feuillette et al., 2010).

We must remember that apart from the role of myosins themselves, the abundance of ABPs that affect myosin motility are named one of main factors in various diseases including their role in cancer metastasis or heart failure (Hsu & Kao, 2013; Stefani et al., 2008; Yoder et al., 2005).

Linked to the major emerging health epidemic of 21st century: cancer, heart conditions or Alzheimer's disease, unconventional myosin motors are becoming a target of clinical approaches and are studied intensively over last decades. I contributed a reconstitution system that revealed behavioral changes of myosin motors when affected by age of actin or presence of other myosin classes. The discoveries reported here bring us closer to understanding how myosin based transport and tethering are governed. They also emphasize that to truly assess the influence of myosin motors, ABPs, and actin filaments on each other, it is essential to recreate the intracellular environment more precisely. Dissecting the cellular cytoskeleton is necessary to identify interactions that are important in the context of the living cell. The methods used for the pursues of my study allow to control the immense number of potential interactions by introducing one cytoskeletal component at a time, while maintaining the native-like dynamics of actin *in vitro* for testing myosin's responses.

4.3. Recommendations for future research

The method developed for the purposes of this project is an innovative *in vitro* approach that has a very broad aim to more accurately recreate cellular motility network structures. I focus on actin based transport by unconventional myosin motors. Thus far I have optimized protocols to successfully reconstitute filament formation with motility of single myosin class, myosin-5 and myosin-6, or simultaneous movement of

both of these two myosin classes on the same filament. There are, however, other myosins classes that could be tested with the method. Reconstituting motility of a set of single unconventional myosin classes on assembling filaments and comparing the phosphate state effect is the 'first-line' approach. By performing such experiments one could evaluate if actin age is a guidance signal for particular myosins and whether it enhances the performance of the motor towards targeted cellular compartments. By using multiple fluorophore labeling one can expand the number of myosins tested simultaneously and sharing the same actin tracks. In such experiment also myosins of the same directionality, but different speeds and stepping patterns could be examined against each other in environment that resembles native cytoskeleton.

Introducing other proteins associated with actin to assembling TIRF assay and tracking the changes in myosin motor activity is the next step. This is perhaps the single most appealing concept for reconstituting particular cellular compartments. Such experiments would lead to reconstituting actin formations found in the actin cytoskeleton. For example lammelipodium could be recreated by incorporating to assembling actin assay purified components, such as Arp2/3, which is a complex of seven protein subunits including two actin-related proteins (Arp2 and Arp3) that initiate branches of single filaments. Branching is especially predominant in the regions very close to the membrane, pushing the forefront of the cell membrane farward. Myosin-5 could be tested in such environment, with the emphasis on observing the motor behavior when approaching the branch. It would be very interesting to see if myosin-5 has a preferred way for turning on the branch or if for example detaches upon encounteinrg Arp2/3 along its track. The expectation would be that myosin-5 would be

processive along the branch, taking turns towards newly formed over the other filament. This mechanism would bring this exocytic transporter towards regions that are rich in newly assembled filaments next to the plasma membrane.

Also bundles that are main structure of stress fibers or filopodial protrusion could be induced by addition of actin bundlers such as filopodial marker fascin, espin, fimbrin or alpha-actinin. The advantages of this reconstitution approach is observing the actin track in real time, with knowledge of actin phosphate state, moments of branch formation or number of filaments and their orientation in forming ‘de novo’ bundle.

As presented in Appendix A, introducing fascin to assembling actin and tracking the number of participating filaments in the growing bundle is already auspicious in its preliminary phase. While the bundle is forming motility of selective for bundles myosin-10 can be tested, answering questions about minimal number of filaments required for myosin-10 motility or a preference for bundle phosphate state. With experiments described in Appendix A I give an example of multitude future directions for studying effect of the track on unconventional myosins motility.

Another direction is to use myosin themselves as convenient and sensitive reporters of actin structure and function. The idea would be to use motility of myosin on unperturbed, wild type actin filaments as a standard probe for testing the eventual effects of mutations and other alterations of actin itself. Example of application for this approach would be examining if myosin-5 and myosin-6 motility is altered on defective cardiac actin. Actin mutants involved in hypertrophic cardiomyopathy (HCM) and dilated cardiomyopathy (DCM) would be test subjects. Such experiment would reveal changes of motility behavior between skeletal, wild type cardiac and mutants of

cardiac actin. Myosin motility of cardiac actin mutants would most likely be impaired, possibly with high fraction of stalling motors, shorter runs and lower landing rates. With the established assay other cardiac actin mutants could be approached to establish weather they also affect overall myosin activity. That would provide the information about any subtle structural changes in filaments produced with those mutants. The strength of the effect on myosins will also provide with evaluation of to what extent given mutation may affect filament structure and interaction with other proteins. The mutants with the strongest structural changes and polymerization defects (e.g., Y166C) would most likely affect myosin motility to the most detectable extend. This work would guide future studies with cardiac myosins replacing the myosin-5 and myosin-6 and potentially lead to development of a new diagnostic tool.

Knowledge obtained from the experiments conducted as well as recommended here will serve as a bridge between classic *in vitro* studies and complex tissue culture observation. With advantages given by years of previous studies, recent pioneering work on the cytoskeletal matrix and advancements in single molecule techniques, the method developed during this dissertation work instigates means to 'put the pieces of the puzzle together'. By recreating native cytoskeleton more accurately I make the next step in understanding the complex metazoan cellular scaffolding and develop diagnostic tools to identify conditions that affect myosin motility. Further developments with the use of presented here method will advance the understanding of cellular transport regulation in healthy and diseased cells and provide diagnostic tools for identifying cytoskeletal component modifications that affect myosin based transport.

CHAPTER 5: METHOD RATIONALE AND DEVELOPMENT

5.1. Objectives of the assay

Standard motility assays use phalloidin-stabilized actin filaments that are prepared in advance (Kron & Spudich, 1986) (Sellers, 2001). As mentioned before phalloidin stimulates nucleation, what implies elevated number of filaments initiated in the sample. With a lot of seeds monomeric subunits get incorporated into high number of newly nascent filaments and the system quickly reaches steady state, where vast majority of G-actin is used up for composing short filaments. In order to avoid this effect and obtain long F-actin, phalloidin is typically added after the assembly reaction reaches equilibrium, although most of the myosin motility studies do not indicate when phalloidin was added, only that it was present. Here, I examined the motile properties of myosin-5 or myosin-6 on growing filaments with an ADP•Pi population gradient (''ADP•Pi decay''), compared to aged, phalloidin-stabilized actin that is in a uniform ADP state or F-actin in uniform ADP•Pi state preserved by phalloidin from the beginning of polymerization. (Figure 5.1).

Set of experiments described in Chapter 2 was performed with the actin polymerized with 5% TMR-actin for visualization. To ensure that effects that are observed in the study are not the result of using phalloidin as a stabilizer particularly, I utilized capping protein for obtaining desired phosphate state instead of the toxin. Next, I researched bidirectional motility of both myosin-5 and myosin-6, simultaneously utilizing the same growing actin filament. Results of this experimental setup are presented in Chapter 3. For the work on simultaneous motility of two myosin classes I

ensured that the ADP•Pi state is preserved uniformly along the whole length of the filament. I performed the experiment in the constant presence of phalloidin, also marked with TMR fluorescent molecule used for visualization. Via fluorescent imaging I observe the continuous growth of F-actin at the barbed end and directed myosins movements along the filament in both experimental setups (Figure 3.1 and Figure 4.1).

5.2. Construct design, protein purification and labeling

For all the experimental work presented here actin was purified from rabbit skeletal-muscle acetone powder (Peel Freez Biologicals) (Spudich & Watt, 1971) and further labeled on Cys374 with Tetramethylrhodamine-6-maleimide (TMR, Invitrogen-Molecular Probes) or biotin-maleimide as previously described (Pardee & Spudich, 1982; Rock et al., 2000) (Kudryashov & Reisler, 2003). Access of TMR after maleimide labeling reaction was removed with extensive dialysis and a subsequent weak anion exchange on DEAE Sepharose Fast Flow (HiTrap DEAE FF from GE Healthcare) via fast protein liquid chromatography (FPLC). To ensure monomeric form of subunits used in microscopy assays I performed gel filtration (size exclusion) with FPLC on HiPrep 16/60 Sephacryl S-200 HR prepacked column (GE Healthcare) on unlabeled and TMR actin (Figure 5.1). The G-actin used for assembly at 1 μM concentration contained 5% TMR-labeled actin monomers and 0.1% biotinylated actin monomers.

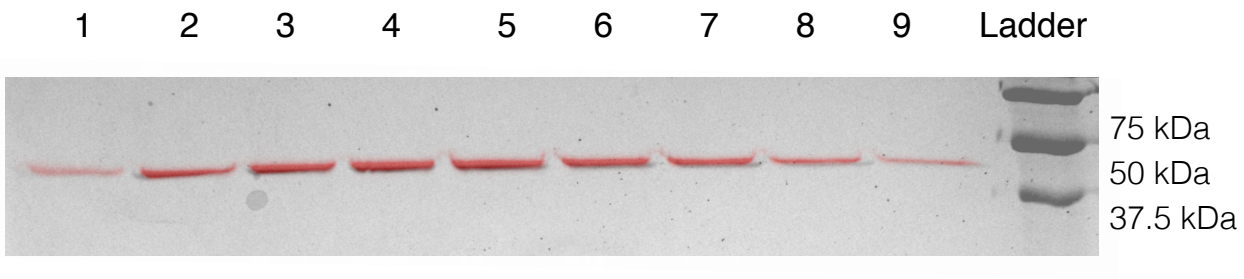


FIGURE 5.1 Fractions of TMR labeled actin via SDS-PAGE
TMR actin post gel filtration fractions (1-9) are shown as an overlay of SDS-PAGE gel images. The TMR label on the protein is shown in red over the gray commassie stain. To avoid nucleation a fraction past peak is used for the experiments.

The myosin-5-HMM-GCN4-YFP-Flag and myosin-5-HMM-GCN4-Flag-Ctag constructs contain the first 1107 amino acids of chicken myosin-5a, with a leucine zipper (GCN4) fused in frame to the native coiled-coil to ensure dimerization (Trybus et al., 1997) and YFP or C-tag fused to its C-terminus for fluorescent marking. To facilitate purification, a FLAG-tag epitope (GDYKDDDDK) was introduced at the N-terminus. Myosin-5 was expressed using recombinant baculovirus in Sf9 insect cells that were also co-infected with recombinant baculovirus expressing calmodulin and the specific light-chain MLC-1sa from human. The myosin-6-HMM-GCN4-Flag-Ctag contains the first 994 amino acids of porcine myosin-6, with a leucine zipper (GCN4) fused in frame to the native coiled-coil to ensure dimerization, a Flag-tag for purification, and a Ctag for Cy5 fluorescent labeling using separately expressed and labeled Clamp protein (Huang et al., 2009). Myosin-6 was cloned into the InsectDirect vector pBiEx3 (Novagen) or used to create recombinant baculovirus. For both vectors Sf9 insect cells were used in protein expression as previously described (Nagy & Rock, 2010; Ricca & Rock, 2010). All myosins were purified via Flag-tag affinity chromatography as previously described (Rock et al., 2001; Nagy et al., 2008) and dialyzed overnight at 4

°C against buffer containing 25 mM imidazole, pH 7.5, 50 mM KCl, 4 mM $MgCl_2$, 1 mM EGTA, 10 mM DTT, and 50% glycerol, and stored at -20 ° (Figure 5.2).

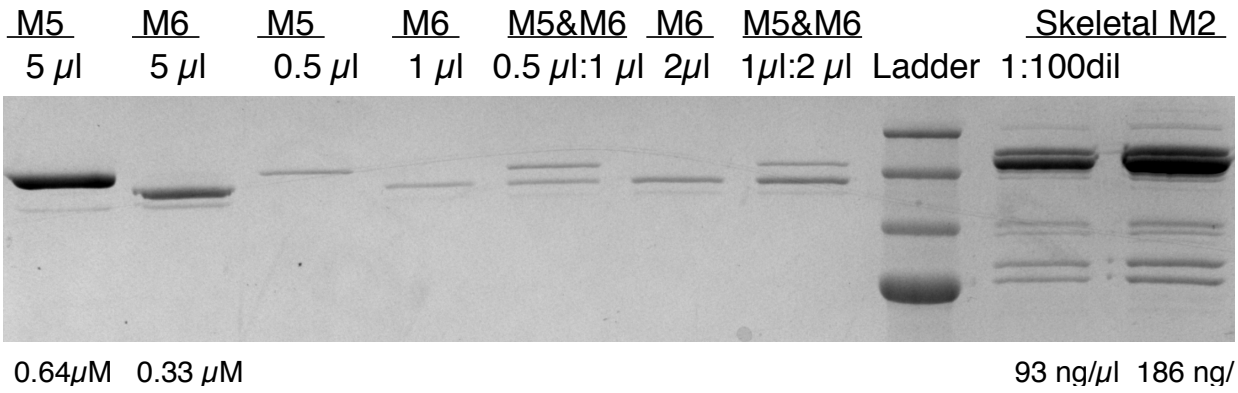


FIGURE 5.2 Concentrations of myosin-5 (M5) and myosin-6 (M6) by SDS-PAGE
Example of commassie stained gels of purified myosin-5 and myosin-6 are shown. Ladder lane separates myosin-5 and myosin-6 lanes (on the left) from a load/ concentration control: skeletal myosin-2 of established concentration at 9.3mg/ml, courtesy of Cooke lab (on the right). Concentrations estimates for myosin-5 and myosin-6 are based on band intensity and calculated with use of image-J. Myosin-5 stock is at 0.64 μM, myosin-6 at 0.33 μM. Third through seventh lanes are showing adjustment of motor concentration to equal ratio of myosin-5 with myosin-6. At ratio 1:2 of volume myosin-5 and myosin-6 have equal concentrations.

Affinity clamp protein with a single cysteine residue was expressed, purified and labeled with Cy5 as previously described (Huang et al., 2008; Huang et al., 2009). To label myosin-5 and myosin-6, Cy5-Clamp protein was used at a 5-fold molar excess over purified Ctag-labeled myosin. The established Ctag / affinity clamp system was chosen for reliable labeling each motor monomer with single fluorophore, what was especially significant in case of recording bidirectional myosin motility along the same filament (see Chapter 4). Because myosin-5 and myosin-6 travel in opposite directions, I could determine the identity of each motor based on directionality of movements in reference to the growing barbed end of actin and by the speed of the motor.

Mouse capping protein was expressed and purified as described previously (Falck et al., 2004), and was stored in buffer containing 10 mM Tris, pH 7.5, 40 mM KCl, 0.5 mM DTT, and 50% (w/v) glycerol.

5.3.Gliding filament assay and TIRF assay

Motility of each of the purified myosins was tested via gliding motility assay (Figure 5.3). In gliding filament assay I am testing ATPase activity of myosins attached to the surface via a tether, in my case Clamp protein for C-tag myosins. Movement of added atop fluorescently labeled actin filaments is visualized and is an indication of myosin feet performance quality. Stuck filaments are likely an effect of 'dead', non-functional myosin feet and eliminate such myosin protein prep from further experiments, as it might be contaminated with a set of 'out of order' motor domains.

One must note that gliding filament assay does not report myosin processvity, as the filaments are translocated also by the single headed motors as a collective quite efficiently. Only following single molecule microscopy performed via total internal reflection fluorescence (TIRF) assays indicate ability of myosin dimers to walk along actin filaments (Figure 5.3). TIRF movies show the continuous growth of F-actin at the barbed end and directed myosins movements along the filament in both experimental setups. I utilized dual-color TIRF, so I could observe motility of myosins as well as assembly of actin filament at exactly the same time.

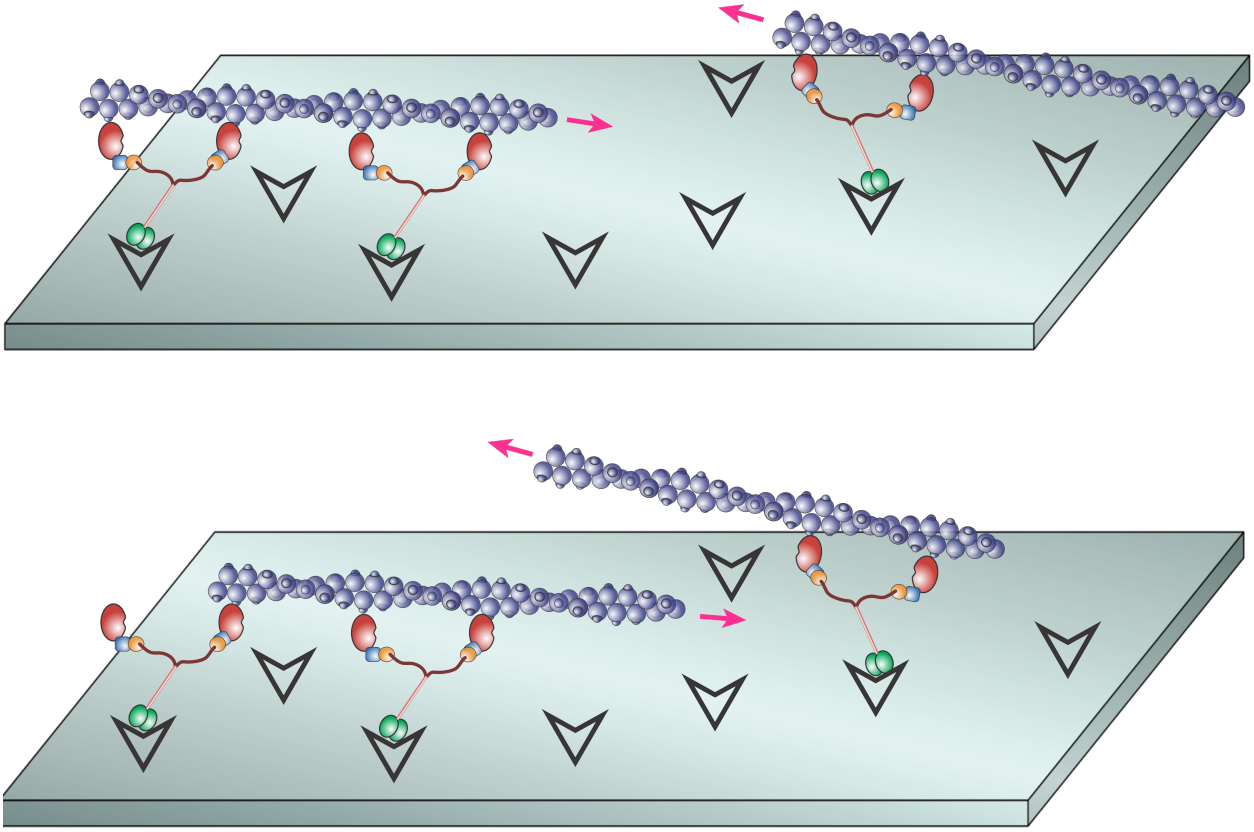


FIGURE 5.3 Gliding filament assay
Cartoon representation of the experiment. On the coverslip coated with a reagent binding to myosin tail, such as anti-GFP or Clamp protein, I have attached active myosins. After blocking step fluorescently labeled F-actin is introduced to the system together with ATP necessary for myosin catalytic cycle. Upon myosin motor domains collective activity the actin filaments are crowd-surfing by adhered myosin motors.

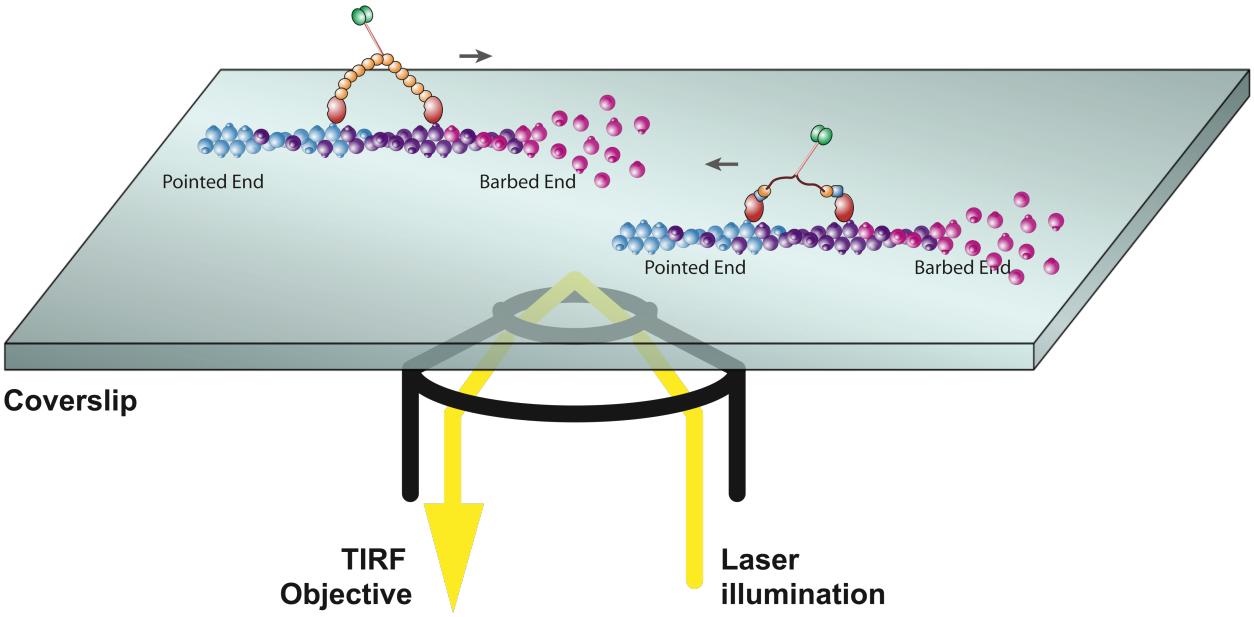


FIGURE 5.4 TIRF set-up to study myosin motility on elongating F-actin
Purified and fluorescently labeled myosin-5, myosin-6 and G-actin are perfused into a flow cell. The motility of single myosin molecules is studied using Total Internal Reflection Fluorescence (TIRF) microscopy on de novo assembling F-actin.

5.4. Data collection and analysis

Motility of myosin-5 and myosin-6 Ctag was imaged with use of a custom-built objective-type TIRF microscope. Images were collected with an EMCCD camera (iXon, Andor Technologies) and a 100×, 1.45 NA objective (Olympus and Zeiss). Frames were collected at 2 Hz with a pixel size of 60 nm for 1000 frames at 22 °C. Actin assembly was imaged simultaneously with the myosin motility with use of dual color imaging. TIRF microscopy images of TMR labeled actin and myosin-5 YFP were collected at 0.5s intervals with an iXon plus X-4818 EMCCD camera (Andor Technologies) using an Olympus IX-50 microscope equipped with a plan-apochromatic through-the-objective TIRFM illumination lens at 100x, 1.45 NA objective. Actin

assembly and myosin motility were imaged by switching illumination source frame by frame.

I projected actin filament tracings along the time axis to generate kymographs. I also separately traced the filament barbed and pointed ends in the kymographs. Myosin runs appear as diagonal lines with a slope that reports the speed and a projected y axis displacement that reports the run length. As expected, myosin-5 travels toward the growing barbed end at the top of kymographs, whereas myosin-6 travels toward the relatively static pointed end at the bottom of kymographs (Figure 3.3 & Figure 4.3).

Myosin run lengths were analyzed using Kaplan-Meier survival curves to correct for the finite length of the F-actin track (Kaplan & Meier, 1958). Motor run lengths were left truncated at 400 nm to handle missed events that were too short to detect. Myosin runs known to underestimate the true run length were treated as right censored in the Kaplan-Meier estimator. These artificially short runs occur when a myosin reaches the end of a filament, myosins that start at the beginning of a movie or terminate at the end, or myosins that cross the P(ADP•Pi) threshold indicated in (Figure 2.6).

For observing bidirectional motility of myosin-5 and myosin-6 on single filament motor runs (Figure 3.2 & Figure 3.3), filament ends and crossing events as well as collision outcomes were traced manually using ImageJ. Trajectory runlengths, velocities and landing events were extracted using custom scripts written in Julia (Bezanson et al., 2014).

APPENDIX A: MOTILITY OF MYOSIN-10 ON GROWING BUNDLE

A.1. Introduction

Myosin-10 is a third, after myosin-5 and myosin-6, molecular motor investigated in this thesis project. Alike myosin-5 and myosin-6, it is also an unconventional myosin, expressed ubiquitously in eukaryotic cells and functionally transporting cargoes as an active homodimer. Myosin-10 is present at the regions of dynamic actin: edges of lamellipodia, membrane ruffles, and the tips of filopodial actin bundles (Berg et al., 2000). Myosin-10 plays a role in intrafilopodial transport (Kerber et al., 2009; Tokuo & Ikebe, 2004), filopodial formation (Bohil et al., 2006; Tokuo et al., 2007), phagocytosis (Cox et al., 2002), spindle assembly (Weber et al., 2004; Woolner et al., 2008), epithelial junction formation (Liu et al., 2012) and neuronal development (Hwang et al., 2009; Sousa et al., 2006).

Over the last decade myosin-10 motility mechanism has been intensively studied, as this motor specific localization on rapidly rearranging regions of actin and co-localization with filopodial tips is a peculiar case in myosin world. Moreover, myosin-10 and its functional partner, fascin, are associated with functions in cell migration and are recognized as markers for cancer metastasis (Courson & Cheney, 2015). Myosin-10 has been shown to localize to the filopodial tip in a fascin dependent manner (Figure A.1) (Nagy et al., 2008). When over-expressed, it increases the number and length of filopodia (Bohil et al., 2006). Both, myosin-10 and partnering it fascin, are up-regulated in aggressive metastatic cancers and associated with metastatic cancer progression in animal models as well as clinical cases of human patients (Al-Alwan et

al., 2011; Alam et al., 2012; Arjonen et al., 2014; Cao et al., 2014). One revelation that tips towards explaining selectivity mechanism is a recent discovery of structural feature unique, over other myosin motors, only to myosin-10: anti-parallel dimerization domain (Lu et al., 2012). That way of dimerizing two monomers of myosin-10 results in more rigid separation between myosin feet and supports the 'straddle model' of motility along actin bundle for posed for the first time by Nagy et al. (Nagy et al., 2008).

In here I attempt to delineate the process of myosin-10 walking along freshly assembled and bundled F-actin. I hope to learn about minimal number of filaments in the bundle for supporting myosin-10 motility, as well as evaluate the influence of bundle age on myosin-10 performance.

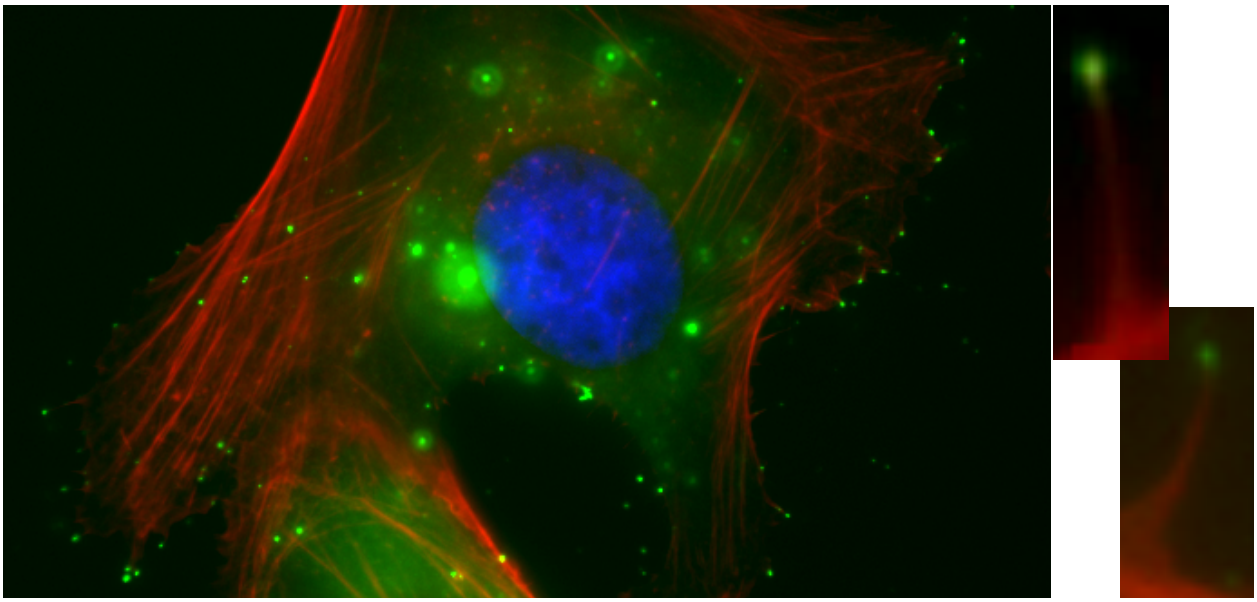


FIGURE A.1 Myosin-10 HMM localizes to the tips of filopodia and retraction fibers. Fluorescence micrographs of U2OS cells transfected with GFP-myosin-10 HMM (green), actin cytoskeletal stained with TMR-phalloidin (red), DNA stained with Hoechst dye (blue).The left image presents overlook on the cell where co-localization of myosin-10 is visible The images on the right are representative filopodia images enlarged in double color merge (actin red, myosin green).

A.2. Finding the way to cell's farthest ends: myosin-10 in filopodia

The co-localization with tips of filopodia is the most characteristic feature of myosin-10. Intriguingly, it was shown that myosin-10 is selecting for its motility fascin-actin bundles, a structure that makes filopodia (Nagy et al., 2008). That discovery sparked the debate in the field about how this selectivity for filopodia is achieved, with lead given to a stepping pattern that will be more efficient on bundle over single filaments (Ricca & Rock, 2010). In this 'straddle model' (Nagy et al., 2008; Nagy & Rock, 2010) myosin-10 would use two filaments for the processive movement, straddling them with the two motor feet binding to the parallel tracks and motor dimerization domain spread above the surface between the filaments. Structural features that will be discussed in the next part are of great meaning for feasibility of the 'straddle model'.

A.3. Evolutionary designation and unique structure of myosin-10

From structural point of view myosin-10 is much alike other unconventional myosin motors, however with remarkable evolutionary adaptations that make this motor very unique among the myosin superfamily. Myosin-10 contains all the canonical domains of the myosin motor: the motor domain followed by the leg region with IQ motifs that bind calmodulin or calmodulin-like light chain in calcium dependent manner, and finally the tail region with dimerization and cargo binding domains. Myosin-10 foot is relatively preserved among myosin superfamily with <45% protein sequence identity to other myosins (Berg et al., 2000). In the leg region that follows foot domain there are three IQ calmodulin biding motifs. Via IQ motifs myosin-10 interacts strongly with CALM3 and weakly with CAM (Rogers & Strehler, 2001), the CALM3 interaction is

specific to myosin-10 and essential for function in filopodial extension and motility (Bennett et al., 2009; Strehler, 2011). Next notable structure feature of myosin-10 after IQ motifs is the single α-helical domain (SAH), indicated to influence functional selectivity for bundled actin (Nagy & Rock, 2010). SAH domain is followed by tail with dimerization domain that is the most divergent structure for myosin-10 over the entire myosin superfamily: monomeric myosin-10 molecules form anti-parallel dimer (Lu et al., 2012; Vavra et al., 2016). As mentioned previously, this structural feature of myosin-10 is a key element for the bundle selectivity and function of myosin-10 as filopodial transporter. This unique anti-parallel coiled coil is followed by a specialized cargo binding portion of myosin-10. First there are three PEST motifs. PEST motifs are enriched in the amino acids P, E, S, and T and are implicated in cleavage by the Ca++ dependent protease calpain (Berg et al., 2000).This structure is thought to allow cleavage of the myosin tail, enabling efficient cargo release. The tail domain also includes three pleckstrin homology (PH) domains, which have been implicated in phosphatidylinositol phospholipid signaling (Lu et al., 2011; Plantard et al., 2010). Next is a myosin tail homology 4 (MyTH4) domain and a band four-point-one/ezrin/radixin/moesin (FERM) domain. The MyTH4 domain binds to microtubules linking *via* myosin-10 actin and tubulin during e.g. spindle formation (Weber et al., 2004). FERM domain binds to the netrin receptor Deleted in Colorectal Cancer (DCC) potentially linking internal cytoskeleton with the extracellular matrix (Hirano et al., 2011). Myosin-10 belongs therefore to the MyTH4-FERM family of myosins, an evolutionarily ancient family with key role in maintaining cytoskeleton interactions with the membrane (Kerber & Cheney, 2011).

A.4. Stepping mechanism adapted for bundle selectivity

With the structural nuance of antiparallel coiled-coil as dimerization domain, myosin-10 gains one of a kind properties among other myosins in terms of flexibility of the foot-leg region and the overall 'reach' during search for the proximal binding spot on actin. Antiparallel dimerization domain places myosin-10 feet 47 Å apart (Lu et al., 2012), with a moderate flexibility in between the feet in the SAH regions. With that spacing myosin-10 would be able to bind exposed sites on actin filament in the bundle much more efficiently than single filaments. The optimal distance for binding would be for the myosin-10 feet to be bound to at least three-filament , where one foot would track along the first filament, and the other foot would track along the third filament, straddling the second filament in between (Figure A.2). Two filament bundle would still accommodate myosin-10 motility better than a single filament, utilizing the flexibility of SAH. Single filament would not be optimal track for myosin-10, since SAH domain bending would not be enough to facilitate binding to proximal site on the actin. In fact when additional flexibility was induced to SAH domain, allowing the bends in the domain part to be more drastic, myosin-10 was no longer selective (Nagy & Rock et al., 2010). In the model proposed almost a decade ago by Nagy et al. myosin-10 is structurally constrained to straddle adjacent filaments along the bundle, with one foot binding along one filament while the second foot binds a second filament (Nagy et al., 2008) (Figure A.2). The straddle model explains the preference for bundled actin, over a single filament where flexibility of binding is restricted by the semi-rigid spacing induced by the anti-parallel dimerization. The requirement for at least two closely spaced filaments would allow myosin X to identify its target actin bundle in vivo.

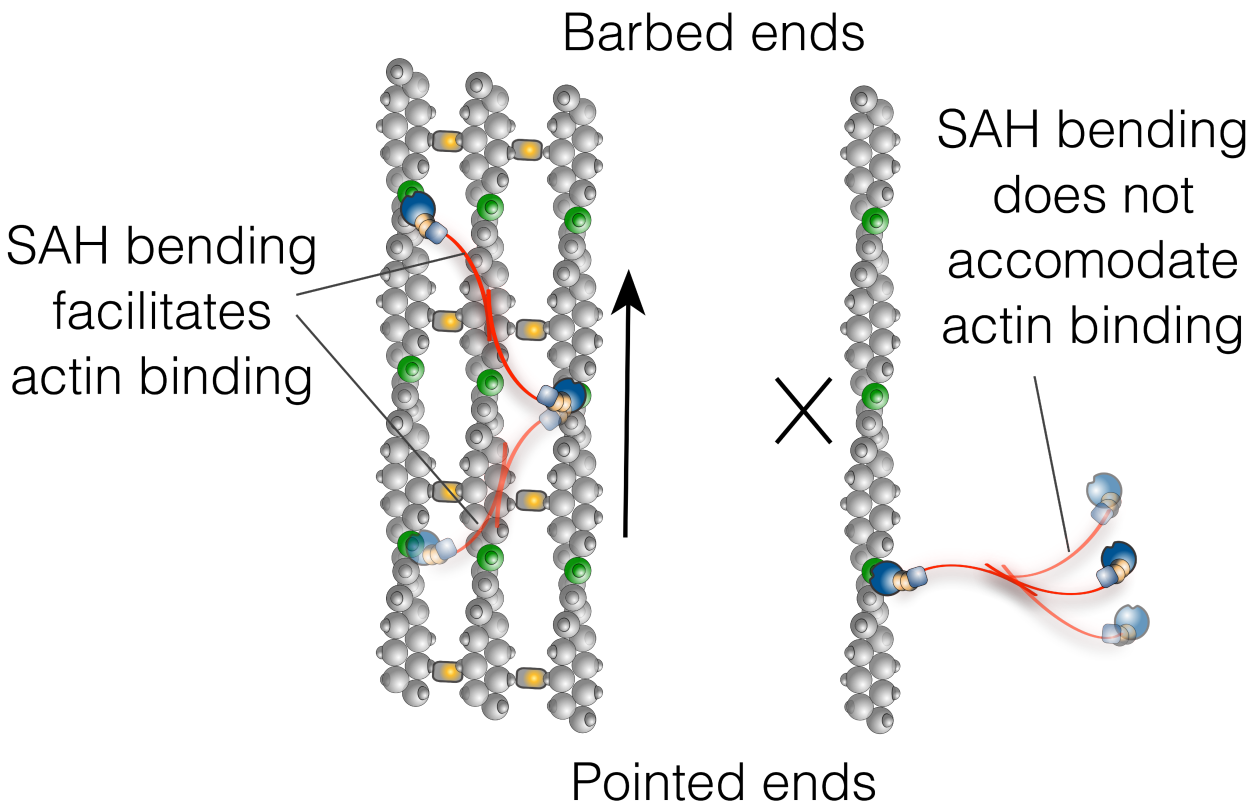


FIGURE A.1 A model of myosin-10 bundle selectivity mechanism. Adapted from *Nagy et al*. and *Vavra et al*.
(A) Myosin-10 straddles two actin filaments in an actin bundle. The stepping is shown by decreasing transparency of the myosin-10 graphic representation. Predicted sides of myosin-10 binding are shown in bright color. In this structural conformation anti-parallel spacing between motor feet is not constraining binding to either of actin filaments if accommodated with moderate bending of leg regions (B) Myosin-10 on a single actin filament, with one bound foot. The antiparallel coiled coil forces the free foot to project away from the only available actin filament. Even with moderate flexibility, illustrated using transparent graphic, still does not enable rebinding to actin.

A.5. Observation of bundle formation and elongation in real time

I am able to observe fascin-actin bundle formation and detect the composition of the bundle with multiple methods, such as for example bringing filaments together in presence of the bundler in the optical trap or adding the bundling protein to the gliding filament assay. These methods are however quite elaborate and challenging either in experiment execution and data analysis. With the adapted polymerizing actin assay (Zimmermann et al., 2015) I can observe the filaments form 'de novo' and come together into a bundle upon addition of actin binding protein- fascin (Figure A.2). I know the directionality, composition as well as the age of actin bundles that are created in real time and can serve as myosin-10 tracks. Depending on presence or absence of phalloidin I control actin phosphate state in the bundle. If phalloidin is added for the course of experiment, filaments will remain in ADP•Pi aka young state. If phalloidin is not added, the individual filaments in bundle undergo phosphate release, resulting in decay of phosphate state as shown in Figure 1.7.

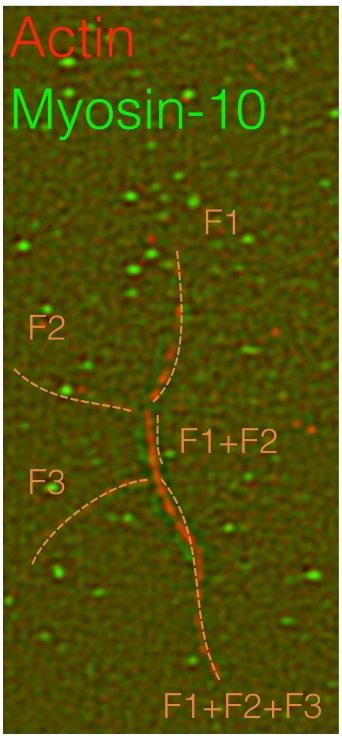


FIGURE A.2 A scheme of a bundle assembling from *de novo* polymerizing filaments
A final frame from a movie (Supplementary movie A.1) presenting newly nucleated filaments, as they elongate and get recruited to the bundle by fascin.Bundle is elongating from the top of the filed of view towards the bottom. Region F1, F2 and F3 show the single filaments that ultimately come together to form a bundle. F1, F2 and F3 parts of the filaments alone do not participate in the bundle and are considered a single filament. Region F1+F2 is a two filament bundle where filament F1 and filament F2 come tougher bound by fascin. Region F1+F2+F3 contains all three filaments: F1, F2 and F3 bundled together in parallel fashion by fascin.

A.6. Reconstitution of myosin-10 motility on assembling bundle

In order to test motility of myosin-10 on *de novo* formed fascin actin bundles I reconstituted bundle formation *in vitro* and introduced myosin-10 labeled with GFP. I used methods described in the main chapters of this dissertation and the details of the assay were as in the Chapter 5. The alteration made for the myosin-10 motility tests was introduction of fascin as a bundler at a concentration of 0.25-0.5 μM to preserve 1:4 ratio with G-actin.

A.7. Minimal requirement of filaments in the bundle for processivity

I hypothesize that myosin-10 will require at least two actin filaments, as it would straddle them in order to efficiently walk along the bundle. The preferred bundle structure however with the most efficient motility achieved would be consisting of at least three filaments. If I was to compare motility of myosin-10 on bundles that decayed their phosphate state and bundles that were assembled and elongated in presence of phalloidin, the latter would be more optical for myosin-10. I expect myosin-10 to have longer runlengths on the bundles with preserved ADP•Pi state, as *in vivo* this myosin was shown to be correlated with rapidly rearranging actin regions of ATP and ADP•Pi state. Myosin-10 is required for efficient initiation of filopodial growth, so the preference for the newly assembled actin in ATP and ADP•Pi state would be in this case an adaptation for performing this particular function.

When I reconstituted the motility of myosin-10 on a growing bundle I could observe that myosin-10 was in fact initiating more effective runs on bundles composed of three or even two filaments over the regions of single, unbundled filament.

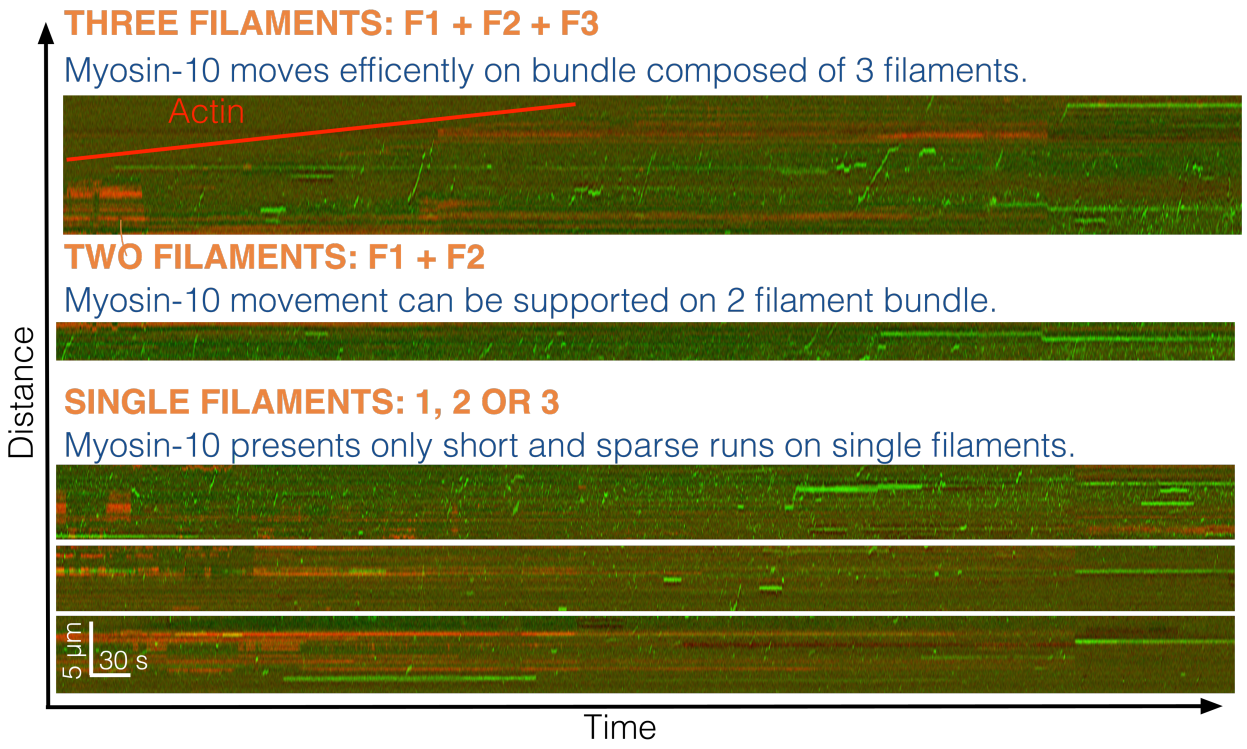


FIGURE A.3 Kymographs showing motility of myosin-10 HMM GCN4 construct across assembling fascin-actin bundle
Corresponding growing bundle presented on Figure A.2. Regions of the three filament bundle corresponds to F1+F2+F3 regions in Figure A.2, two filament bundle corresponds to F1+F2 regions and single, not yet bundled filaments corresponding to F1, F2 and F3 regions. Myosin-10 is labeled with GFP and moves towards the barbed end of parallel bundle from two or three individual filaments with velocity consistent with the literature. The most efficient motility is observed at the bundle composed of three filaments on the top kymograph. Portions of a single filament on three bottom kymographs do not support myosin-10 motility efficiently.

A.8. Conclusions and recommendations for future research

The pioneering reconstitution experiments featuring myosin-10 were performed as a proof of concept and are introducing a separate research project focusing on a minimal filament requirement for myosin motility. I show that myosin-10 motility can be reconstituted on a growing bundle. The motor takes longer and more frequent runs on bundles over single filaments. As predicted myosin-10 motility is supported on a

bundle consisting of two filaments, but reaches an optimal efficiency on a bundle of at least three filaments. These results are in support of the 'straddle model' of myosin-10 motility (Nagy et al. 2010) and help in understanding how myosin-10 is selectively choosing fascin-actin filopodia as a target cellular destination (Berg et al., 2000).

As a continuation of this project collecting and analyzing larger sets of data, both in presence and absence of phalloidin, would give an answer to the question for actin age preference of myosin-10. Filaments bundled with fascin and found in filopodia are some of the youngest in the cell, assembled from fresh monomers at the filopodial tip. The filopodial tip carries significant ATP cap from all the gathered in the bundle filaments, as well as ADP•Pi fraction. ATP hydrolysis and phosphate release from bundles have not been studied extensively and might differ from those on single filaments due to tension and structural differences between free and bundled filaments, thus actin age might have even more predominant effect on myosin-10 and may contribute significantly to this motors selectivity and filopodial tip co-localization. If myosin-10 motility is in fact enhanced on the young actin, it would be a second, along with bundle selectivity, mechanisms in which myosin-10 is co-localized with the filopodial structures. Such discovery would solidify the idea that myosins navigate actin cytoskeleton very effectively due to the intrinsic guidance provided by the track itself.

APPENDIX B: ACTIN FILAMENT BY ATOMIC FORCE MICROSCOPY (AFM)

B.1. Introduction

Actin is the most abundant protein in the cell and has been studied extensively for over half a century. Despite decades of research on this easily accessible protein, a high-resolution structure of F-actin is still missing. Although there are detailed structures of G-actin (Kabsch et al., 1990), F-actin structure was a long time only being modeled based on the monomeric actin information. It is so because due to variability in length of this polymer it is impossible to from uniform crystalline lattice form filamentous actin and obtain x-ray crystallography structure of the polymerized protein. The elaborate attempts to crystalized chemically modified timers of actin required quite severe modifications of the protein (Dawson et al., 2003; Zahm et al., 2013) and ultimately gave way to advanced microscopy techniques where heterogeneous nature of F-actin is not a problematic feature. Cryo-EM is constantly advancing and a powerful method overtaking the task of investigating detailed structure of filamentous actin to atomic resolution with a very good progress. There are already multiple structures of F-actin with various binding partners. A recent publication by Ecken et al. presents F-actin structure with resolution of 3.7 Å in complex with tropomyosin (Figure B.1) (Ecken et al., 2015). Other examples include an ADP-bound and ADP–beryllium fluoride F-actin at 8.6 Å resolution or 12 Å resolution of F-actin-fimbrin/plastin ABD2 complex (Ge et al., 2014) (Galkin et al., 2008). Next to cryo-EM, AFM emerges as an excellent tool for studying filamentous actin (Ando, 2013). High-speed AFM has lesser abilities in obtaining atomic resolution than cyro-EM, however major structural features of imaged

F-actin sample can be revealed to high detail (Narita et al., 2016). The AFM method has however advantages over cryo-EM that I hope to utilize in my experiments. The AFM sample preparation is not as elaborate as in case of EM. Imaging of biological probe can be performed in a fluid chamber, much like fluorescent microscopy. Filaments of actin are not constrained in the solid state, in layer of ice under the vacuum, like in case of EM. This allows me to use AFM to image elongation of actin filaments, observing the filament shape as the changes of phosphate state or assemble into a bundle occur. In fact there are exciting reports of recording myosin-5 walking along the actin filament via AFM (Kodera et al., 2010) and time-lapse AFM showing growth, shrinkage, branching and the interaction of actin filaments with endosomes performed on the material from single actin filaments in HeLa cell extracts (Lehto et al., 2003). The morphological features changing during *de novo* polymerization of actin or bundle assemble investigated by AFM are immensely informative. Also testing motility of other myosin motor, such as myosin-6 or myosin-10, via high-speed AFM is an appealing aim. Structural information revealed by use of this type of imaging is immense, and ability to track changes that the dynamic system undergoes is extremely desired in order to understand nuances of actin-myosin interaction nature.

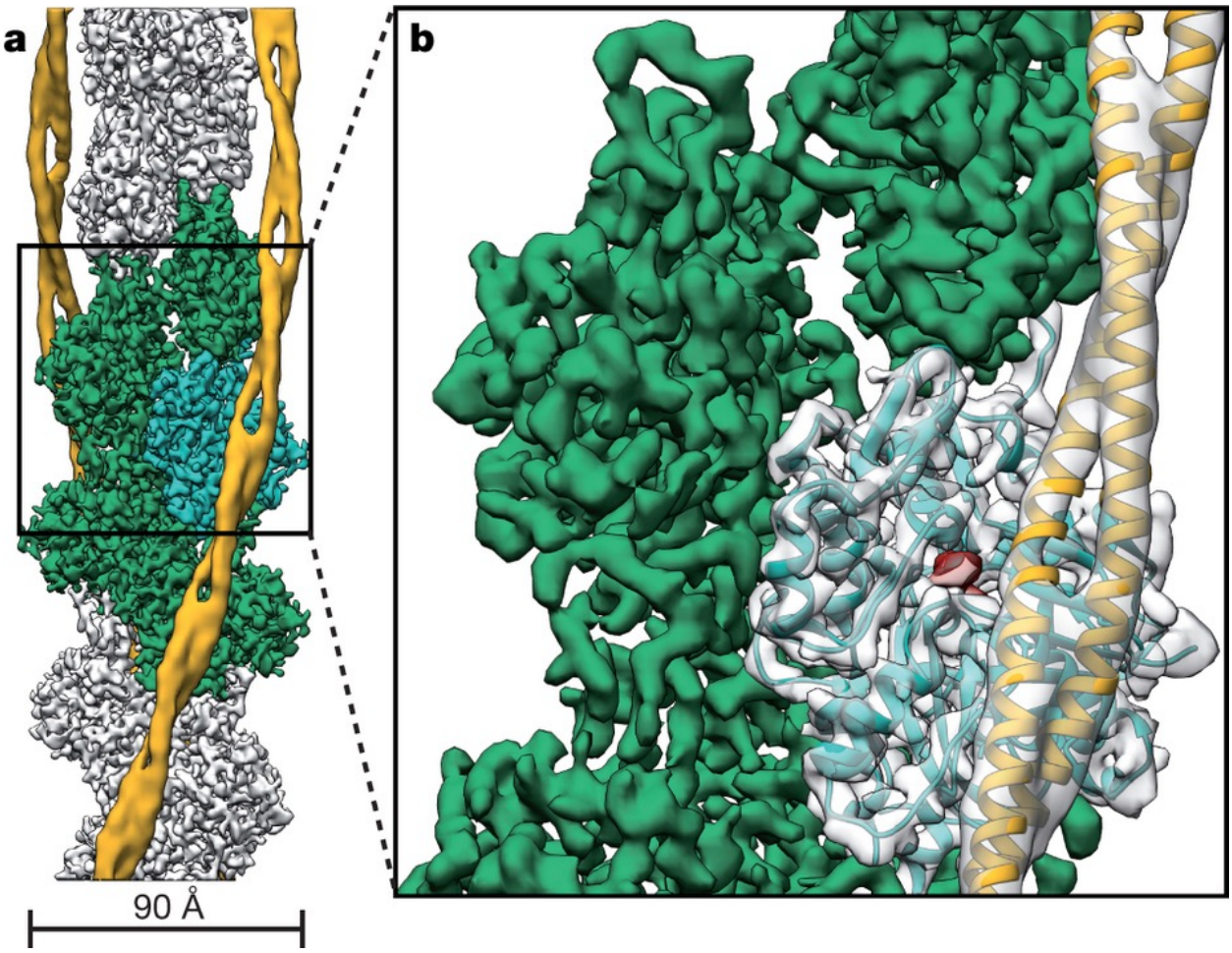


FIGURE B.1 Cryo-EM reconstruction of F-actin decorated with tropomyosin
F-actin is shown in grey, with five central subunits in green and one subunit in cyan, tropomyosin is shown yellow. The density corresponding to ADP is depicted in red.
SOURCE: (Ecken et al., 2015)

B.2. Details of sample preparation for AFM

To pursue the goals presented in the previous section I undertook primary tests of actin structure via AFM. This powerful technique does not present any major complications during the sample preparation, however it requires good quality, pure protein to avoid aggregation and stickiness on the surface that might interrupt he

cantilever. Images presented here are obtained in the air imaging chamber, meaning that the biological sample was attached on the surface and dried prior to imaging. As an AFM substrate I used mica, a non-conducting layered material that has been successfully used in numberless studies especially for AFM imaging of double stranded DNA and DNA-protein complexes, protein arrays, and densely packed proteins. Although the mechanism by which macromolecules absorb to mica still remains poorly understood, a large number of protein samples are tightly adhering to this surface (Silva, 2002).

Actin, polymerized and stabilized with phalloidin at 10 μM as described in Chapter 5, was spun down at 10 000g for 10 minutes at room temperature. A 100μl drop pipetted from near the bottom of eppendorf tube was applied on top of the freshly cleaved mica and incubated for 10 min. Next the sample mica surface was washed five times with F-buffer and air dried. High concentration of filamentous actin allowed deposition of numerous filaments on the surface of mica. Extensive washing ensured lack of loosely bound actin that could stick to the cantilever.

B.3. Principles of imaging by AFM

For imaging I used Asylum Cypher ES AFM that enables dynamic AFM measurements in diverse active systems and has abilities for environmental imaging, in air as well as in liquid chambers. AFM uses a cantilever with a tip that taps and samples the topography of tested surface. As the tip approaches the surface, the close-range, attractive force between the surface and the tip cause the cantilever to bend towards the surface. However, as the cantilever is brought even closer to the surface, such that the tip does not touch the surface but enters the increasingly

repulsive force distance, the cantilever deflects away from the surface. In order to detect cantilever deflections towards or away from the surface, a laser beam is used to reflect form cantilever surface and track the changes of the reflection with a position-sensitive photo diode (PSPD). When the cantilever is tapping over elevated surfaces on the sample, the resulting cantilever deflection is recorded by the PSPD. A feedback loop from the cantilever position recorded by PSPD allows to control the height of the cantilever tip above the surface and maintenance of the constant laser position (Figure B.1) (Binnig et al., 1986; Engel & Müller, 2000; Müller & Dufrêne, 2008).

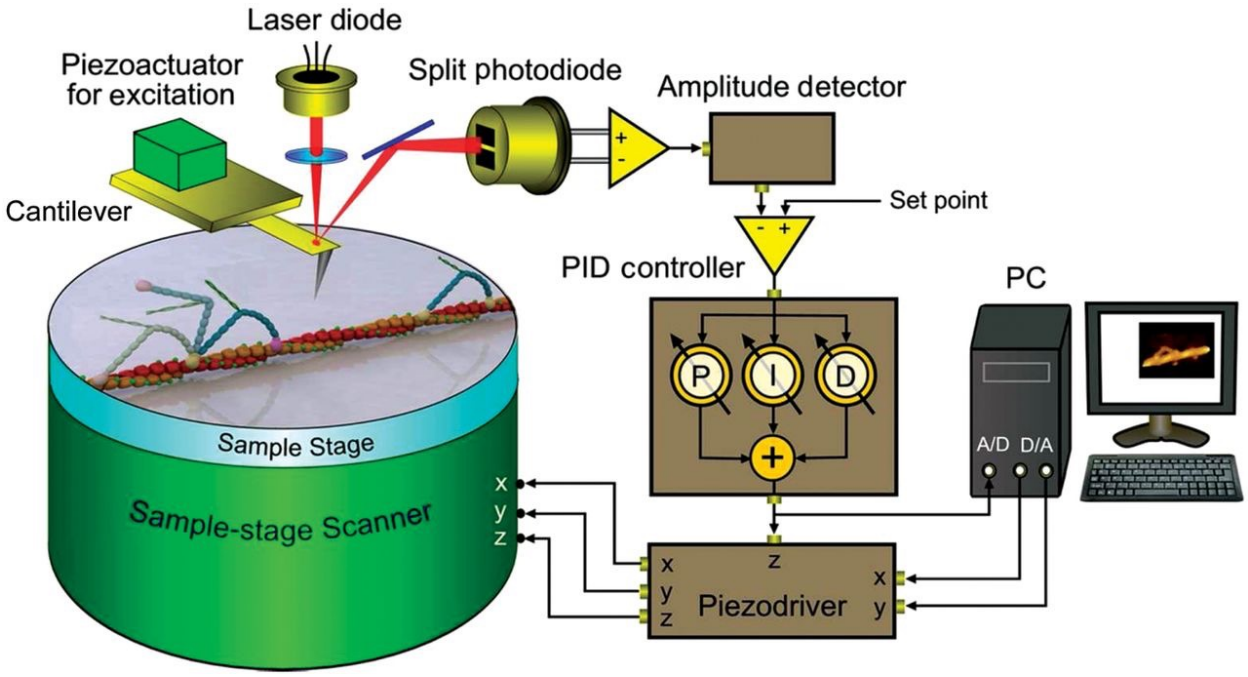


FIGURE B.2 Schematic of tapping-mode AFM setup
The cantilever is vertically oscillating above the surface of the tested sample. The the laser beam reflected from deflecting cantilever is detected by the optical beam detector. The signal given by the cantilever deflection is translated to the PID feedback controller that regulates the oscillation amplitude of the cantilever. SOURCE: (Ando, 2013).

B.4. Structural details of actin filament captured by AFM imaging

A typical images of F-actin obtained by AFM are presented in Figure B.3 and Figure B.4. Filamentous actin has 13 actin molecules arranged on six left-handed turns repeating every 36 nm. The rise per subunit is 2.75 nm. The morphology of the actin helix is two intertwined, long- pitch, right-handed helices. Along each of the morphological helices, the actin monomers are spaced by 5.5 nm. Actin filaments ranges from 5-9 nm in diameter (Egelman, 1985; Egelman, 2003).

The F-actin shown in figure B.4 has the hight of ca. 6 nm, that corresponds to the proper diameter of a filament. Filaments at certain areas seem to be aligned in together, other regions of the images show single filament portion of the proper width of ca. 6-8 nm. However, determination of the thickness of the filaments may be not reliable because the tip diameter and the position of the cantilever needle in the z axis has, unlike light in fluorescence microscopes, special limitation. It is noticeable as an unevenness on the transitions form the flat mica surface to the elevated part of the actin filament on the Figure B.4.

Remarkably, the pitch of actin filament can be observed as the regularly separated in space bulges on the top edge of the filaments. The intervals between the bulges correspond to the distances between the top monomer at each 36 nm distance. Figure B.4 also features a model of an actin filament with main dimensions marked for the reference.

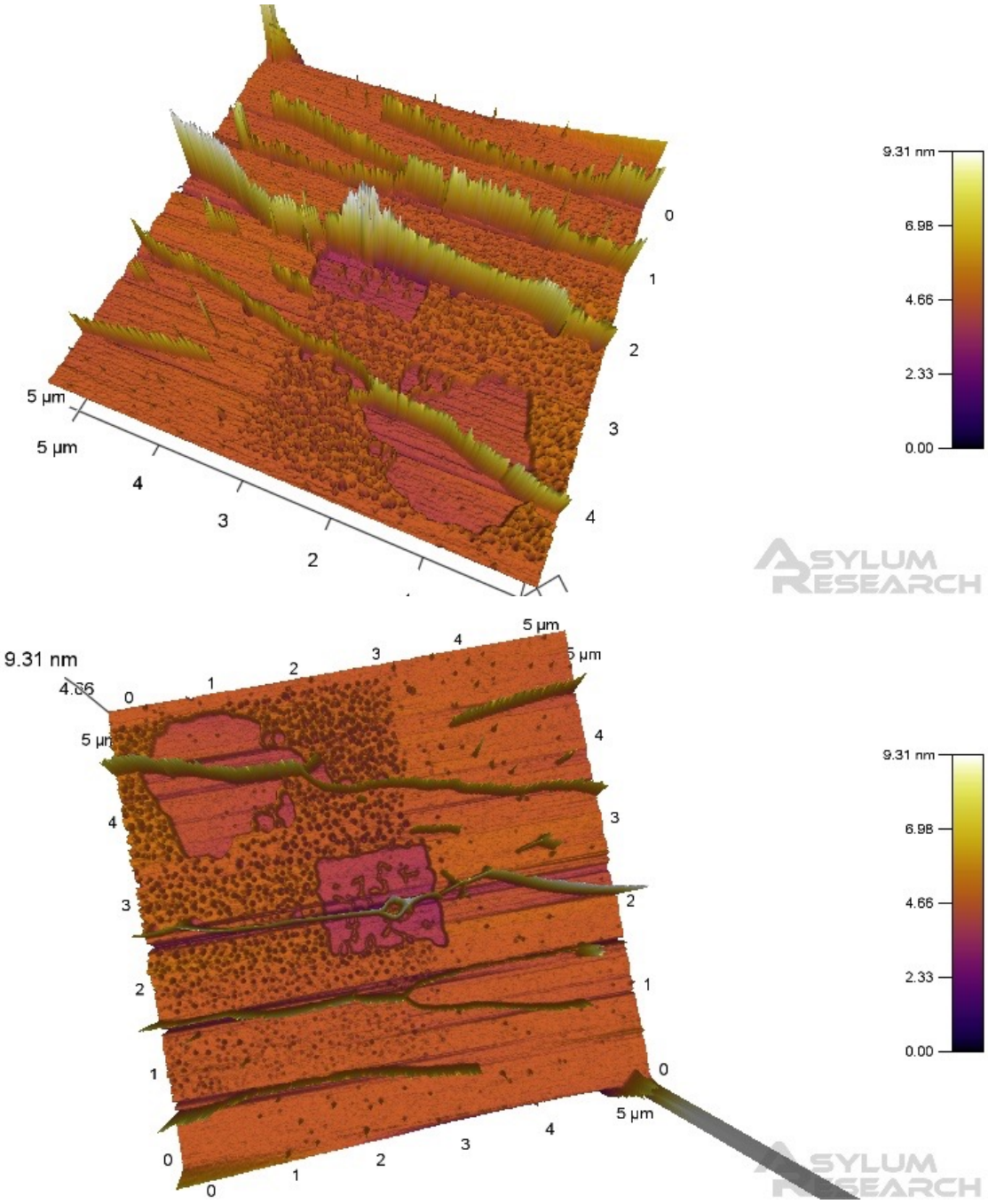


FIGURE B.3 The topography of actin filaments via AFM
AFM images of the surface covered with F-actin by scanning the cantilever over a region 5 µm by 5 µm region. The raised and lowered features on the surface are colored accordingly to color heat map on the right side, with yellow color representing the raised surfaces and purple color indicating the lowered surfaces. Long strings of filamentous actin are visible as elevated structures across the whole field of scan, with pink and purple regions that are a result of extensive imaging with the increased amplitude to obtain images of higher resolution (compare Figure B.4).

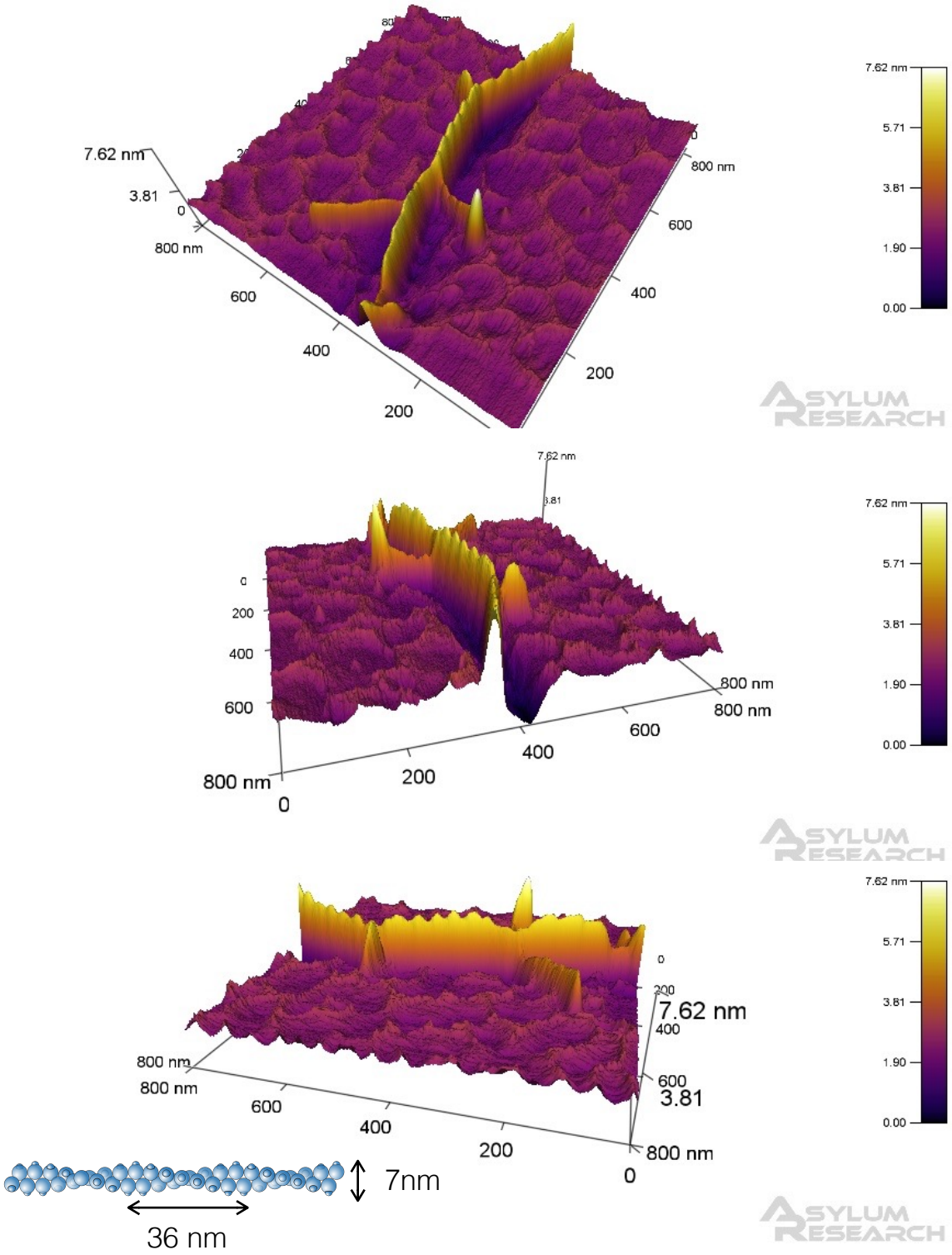


FIGURE B.4 Series of close-up images of the region along actin filaments *via* AFM
Series of three angle views on the topography of a region of interest. The scan area spans region of 0.8 μm by 0.8 μm. The raised and lowered features on the surface are colored accordingly to color heat maps on the right side, with yellow color representing

FIGURE B.4 Caption Continuation
the elevated surfaces and purple color indicating the lowered surfaces. Actin filaments are visible as long elevated structures with dimensions corresponding to literature values. In the lower left side model of an actin filament with main dimensions marked for the reference.

B.5. Conclusions and recommendations for future research

In here I was able to image filamentous actin *via* the AFM. The molecular features of this polymeric protein are well refined on the obtained images and reflect the literature dimensions of actin filaments. As in the case of Appendix A, experiments presented in this part serve as a proof of concept, as the procedures requires optimization and further experimental work. With the images presented here I learnt the reference topography of the filaments as seen *via* the AFM instrument and established a ground for a method of visualizing the dynamic actin filaments and bundles. The transition of the experimental setup form air to liquid environmental chamber will be done initially with pre-assembled filaments to compare filament structure obtained in these two different environments. Next the advantages of imaging with high-speed AFM will be utilized to observe the assemble of actin filaments. That will provide me with extra information on the filament polarity. As the method is optimized and I can efficiently image assume of actin filaments, I can introduce one higher lever of complexity- add actin binding proteins. By adding fascin or other actin bundling protein I will be able to observe the formation of the actin bundle. If myosin is added, imaging the motor bound or even walking along the actin track is an desirable goal. The tip-scan AFM represents satisfactory spatial resolution and frame rate and is suitable for the coupling of this AFM system with a high-resolution light microscope. Such approach of combining microscopy techniques is called correlative microscopy

and is a future goal for imaging of biological samples explored in recent years by EM field (Grabenbauer et. al, 2012; Loussert-Fonta et al, 2015). Achieving this goal with AFM is a bit more challenging, as oil immersion required for high-resolution light microscopy is performed on the thin glass that tends to vibrate owing to the AFM needle oscillation and limits AFM resolution. Overcoming the use of thin glass will enable to observe the cytoskeletal system activity via topography scan, as well as imaging the fluorescently labeled proteins.

Al-Alwan, M., Olabi, S., Ghebeh, H., Barhoush, E., Tulbah, A., Al-Tweigeri, T., Ajarim, D., and Adra, C. (2011). Fascin is a key regulator of breast cancer invasion that acts via the modification of metastasis-associated molecules. PLoS One, 6(11), e27339.

Alam, H., Bhate, A. V., Gangadaran, P., Sawant, S. S., Salot, S., Sehgal, L., Dange, P. P., Chaukar, D. A., D'cruz, A. K., Kannanl, S., Gude, R., Kane, S., Dalal, S. N., and Vaidya, M. M. (2012). Fascin overexpression promotes neoplastic progression in oral squamous cell carcinoma. BMC Cancer, 12, 32.

Ali, M. Y., Previs, S. B., Trybus, K. M., Sweeney, H. L., and Warshaw, D. M. (2013, Jan). Myosin VI has a one track mind versus myosin Va when moving on actin bundles or at an intersection. Traffic, 14(1), 70-81.

Altman, D., Goswami, D., Hasson, T., Spudich, J. A., and Mayor, S. (2007, Aug). Precise positioning of myosin VI on endocytic vesicles in vivo. PLoS Biol, 5(8), e210.

Altman, D., Sweeney, H. L., and Spudich, J. A. (2004, Mar). The mechanism of myosin VI translocation and its load-induced anchoring. Cell, 116(5), 737-49.

Ando, T. (2013, Feb). High-speed atomic force microscopy. Microscopy (Oxf), 62(1), 81-93.

Andrecka, J., Arroyo, J. O., Takagi, Y., Wit, G. d., Fineberg, A., MacKinnon, L., Young, G., Sellers, J. R., and Kukura, P. (2015, March). Structural dynamics of myosin 5 during processive motion revealed by interferometric scattering microscopy. eLife, 4, e05413.

Arjonen, A., Kaukonen, R., Mattila, E., Rouhi, P., Högnäs, G., Sihto, H., Miller, B. W., Morton, J. P., Bucher, E., Taimen, P., Virtakoivu, R., Cao, Y., Sansom, O. J., Joensuu, H., and Ivaska, J. (2014, Mar). Mutant p53-associated myosin-X upregulation promotes breast cancer invasion and metastasis. J Clin Invest, 124(3), 1069-82.

Avraham, K. B., Hasson, T., Steel, K. P., Kingsley, D. M., Russell, L. B., Mooseker, M. S., Copeland, N. G., and Jenkins, N. A. (1995, Dec). The mouse Snell's waltzer deafness gene encodes an unconventional myosin required for structural integrity of inner ear hair cells. Nat Genet, 11(4), 369-75.

Bahadoran, P., Ortonne, J.-P., Ballotti, R., and de Saint-Basile, G. (2003, Feb). Comment on Elejalde syndrome and relationship with Griscelli syndrome. Am J Med Genet A, 116A(4), 408-9.

Belmont, L. D., Orlova, A., Drubin, D. G., and Egelman, E. H. (1999). A change in actin conformation associated with filament instability after Pi release. Proceedings of the National Academy of Sciences, 96(1), 29–34.

Belyantseva, I. A., Boger, E. T., Naz, S., Frolenkov, G. I., Sellers, J. R., Ahmed, Z. M., Griffith, A. J., and Friedman, T. B. (2005, Feb). Myosin-XVa is required for tip localization of whirlin and differential elongation of hair-cell stereocilia. Nat Cell Biol, 7(2), 148-56.

Bennett, R. D., Mauer, A. S., Pittelkow, M. R., and Strehler, E. E. (2009, Mar). Calmodulin-like protein upregulates myosin-10 in human keratinocytes and is regulated during epidermal wound healing in vivo. J Invest Dermatol, 129(3), 765-9.

Berg, J. S. and Cheney, R. E. (2002). Myosin-X is an unconventional myosin that undergoes intrafilopodial motility. Nature cell biology, 4(3), 246–250.

Berg, J. S., Derfler, B. H., Pennisi, C. M., Corey, D. P., and Cheney, R. E. (2000, Oct). Myosin-X, a novel myosin with pleckstrin homology domains, associates with regions of dynamic actin. J Cell Sci, 113 Pt 19, 3439-51.

Berg, J. S., Powell, B. C., and Cheney, R. E. (2001, Apr). A millennial myosin census. Mol Biol Cell, 12(4), 780-94.

Bezanson, J., Edelman, A., Karpinski, S., and Shah, V. B. (2014). Julia: A fresh approach to numerical computing. arXiv preprint arXiv:1411.1607, .

Bindschadler, M., Osborn, E. A., Dewey, Jr, C. F., and McGrath, J. L. (2004, May). A mechanistic model of the actin cycle. Biophys J, 86(5), 2720-39.

Binnig, Quate, and Gerber (1986, Mar). Atomic force microscope. Phys Rev Lett, 56(9), 930-933.

Blanchoin, L., Boujemaa-Paterski, R., Sykes, C., and Plastino, J. (2014, January). Actin Dynamics, Architecture, and Mechanics in Cell Motility. Physiological Reviews, 94(1), 235–263.

Bohil, A. B., Robertson, B. W., and Cheney, R. E. (2006, Aug). Myosin-X is a molecular motor that functions in filopodia formation. Proc Natl Acad Sci U S A, 103(33), 12411-6.

Bond, L. M., Peden, A. A., Kendrick-Jones, J., Sellers, J. R., and Buss, F. (2011, Jan). Myosin VI and its binding partner optineurin are involved in secretory vesicle fusion at the plasma membrane. Mol Biol Cell, 22(1), 54-65.

Brawley, C. M. and Rock, R. S. (2009, Jun). Unconventional myosin traffic in cells reveals a selective actin cytoskeleton. Proc Natl Acad Sci U S A, 106(24), 9685-90.

Brownstein, Z., Abu-Rayyan, A., Karfunkel-Doron, D., Sirigu, S., Davidov, B., Shohat, M., Frydman, M., Houdusse, A., Kanaan, M., and Avraham, K. B. (2014, Jun). Novel myosin mutations for hereditary hearing loss revealed by targeted genomic capture and massively parallel sequencing. Eur J Hum Genet, 22(6), 768-75.

Buss, F., Spudich, G., and Kendrick-Jones, J. (2004). Myosin VI: cellular functions and motor properties. Annu Rev Cell Dev Biol, 20, 649-76.

Cao, R., Chen, J., Zhang, X., Zhai, Y., Qing, X., Xing, W., Zhang, L., Malik, Y. S., Yu, H., and Zhu, X. (2014, Jul). Elevated expression of myosin X in tumours contributes to breast cancer aggressiveness and metastasis. Br J Cancer, 111(3), 539-50.

Caremani, M., Dantzig, J., Goldman, Y. E., Lombardi, V., and Linari, M. (2008, Dec). Effect of inorganic phosphate on the force and number of myosin cross-bridges during the isometric contraction of permeabilized muscle fibers from rabbit psoas. Biophys J, 95(12), 5798-808.

Carlier, M. F. (1991, Jan). Actin: protein structure and filament dynamics. J Biol Chem, 266(1), 1-4.

Carlier, M. F., Laurent, V., Santolini, J., Melki, R., Didry, D., Xia, G. X., Hong, Y., Chua, N. H., and Pantaloni, D. (1997, Mar). Actin depolymerizing factor (ADF/cofilin) enhances the rate of filament turnover: implication in actin-based motility. J Cell Biol, 136(6), 1307-22.

Carlier, M.-F. (1987). Measurement of P i dissociation from actin filaments following ATP hydrolysis using a linked enzyme assay. Biochemical and biophysical research communications, 143(3), 1069–1075.

Chen, T., Hubbard, A., Murtazina, R., Price, J., Yang, J., Cha, B., Sarker, R., and Donowitz, M. (2014, Aug). Myosin VI mediates the movement of NHE3 down the microvillus in intestinal epithelial cells. J Cell Sci, 127(Pt 16), 3535-45.

Chieregatti, E., Gärtner, A., Stöffler, H. E., and Bähler, M. (1998, Dec). Myr 7 is a novel myosin IX-RhoGAP expressed in rat brain. J Cell Sci, 111 (Pt 24), 3597-608.

Chu, J.-W. and Voth, G. A. (2005, Sep). Allostery of actin filaments: molecular dynamics simulations and coarse-grained analysis. Proc Natl Acad Sci U S A, 102(37), 13111-6.

Chuan, P., Spudich, J. A., and Dunn, A. R. (2011, Jan). Robust mechanosensing and tension generation by myosin VI. J Mol Biol, 405(1), 105-12.

Coluccio, L. M. and Tilney, L. G. (1984). Phalloidin enhances actin assembly by preventing monomer dissociation. The Journal of cell biology, 99(2), 529–535.

Coureux, P.-D., Sweeney, H. L., and Houdusse, A. (2004, Nov). Three myosin V structures delineate essential features of chemo-mechanical transduction. EMBO J, 23(23), 4527-37.

Coureux, P.-D., Wells, A. L., Ménétrey, J., Yengo, C. M., Morris, C. A., Sweeney, H. L., and Houdusse, A. (2003, Sep). A structural state of the myosin V motor without bound nucleotide. Nature, 425(6956), 419-23.

Courson, D. S. and Cheney, R. E. (2015, May). Myosin-X and disease. Exp Cell Res, 334(1), 10-5.

Cox, D., Berg, J. S., Cammer, M., Chinegwundoh, J. O., Dale, B. M., Cheney, R. E., and Greenberg, S. (2002, Jul). Myosin X is a downstream effector of PI(3)K during phagocytosis. Nat Cell Biol, 4(7), 469-77.

Cruz, E. M. D. L., Ostap, E. M., and Sweeney, H. L. (2001, August). Kinetic Mechanism and Regulation of Myosin VI. J. Biol. Chem., 276(34), 32373–32381.

Cruz, E. M. D. L., Wells, A. L., Rosenfeld, S. S., Ostap, E. M., and Sweeney, H. L. (1999, November). The kinetic mechanism of myosin V. PNAS, 96(24), 13726–13731.

Dancker, P., Löw, I., Hasselbach, W., and Wieland, T. (1975). Interaction of actin with phalloidin:: Polymerization and stabilization of F-actin. Biochimica et Biophysica Acta (BBA)-Protein Structure, 400(2), 407–414.

Dancker, P. and Hess, L. (1990). Phalloidin reduces the release of inorganic phosphate during actin polymerization Phalloidin reduces the release of inorganic phosphate during actin polymerization. Biochimica et Biophysica Acta,

De La Cruz, E. M. and Ostap, E. M. (2004, Feb). Relating biochemistry and function in the myosin superfamily. Curr Opin Cell Biol, 16(1), 61-7.

De La Cruz, E. M., Ostap, E. M., and Sweeney, H. L. (2001, Aug). Kinetic mechanism and regulation of myosin VI. J Biol Chem, 276(34), 32373-81.

De La Cruz, E. M., Roland, J., McCullough, B. R., Blanchoin, L., and Martiel, J.-L. (2010, Sep). Origin of twist-bend coupling in actin filaments. Biophys J, 99(6), 1852-60.

De La Cruz, E. M., Wells, A. L., Rosenfeld, S. S., Ostap, E. M., and Sweeney, H. L. (1999, Nov). The kinetic mechanism of myosin V. Proc Natl Acad Sci U S A, 96(24), 13726-31.

Dawson, J. F., Sablin, E. P., Spudich, J. A., and Fletterick, R. J. (2003, Jan). Structure of an F-actin trimer disrupted by gelsolin and implications for the mechanism of severing. J Biol Chem, 278(2), 1229-38.

Dunn, A. R., Chuan, P., Bryant, Z., and Spudich, J. A. (2010, Apr). Contribution of the myosin VI tail domain to processive stepping and intramolecular tension sensing. Proc Natl Acad Sci U S A, 107(17), 7746-50.

Dunn, T. A., Chen, S., Faith, D. A., Hicks, J. L., Platz, E. A., Chen, Y., Ewing, C. M., Sauvageot, J., Isaacs, W. B., De Marzo, A. M., and Luo, J. (2006, Nov). A novel role of myosin VI in human prostate cancer. Am J Pathol, 169(5), 1843-54.

Ebrahim, S., Avenarius, M. R., Grati, M., Krey, J. F., Windsor, A. M., Sousa, A. D., Ballesteros, A., Cui, R., Millis, B. A., Salles, F. T., Baird, M. A., Davidson, M. W., Jones, S. M., Choi, D., Dong, L., Raval, M. H., Yengo, C. M., Barr-Gillespie, P. G., and Kachar, B. (2016). Stereocilia-staircase spacing is influenced by myosin III motors and their cargos espin-1 and espin-like. Nat Commun, 7, 10833.

von der Ecken, J., Müller, M., Lehman, W., Manstein, D. J., Penczek, P. A., and Raunser, S. (2015, Mar). Structure of the F-actin-tropomyosin complex. Nature, 519(7541), 114-7.

Elejalde, B. R., Holguin, J., Valencia, A., Gilbert, E. F., Molina, J., Marin, G., and Arango, L. A. (1979). Mutations affecting pigmentation in man: I. Neuroectodermal melanolysosomal disease. Am J Med Genet, 3(1), 65-80.

Engel, A. and Müller, D. J. (2000, Sep). Observing single biomolecules at work with the atomic force microscope. Nat Struct Biol, 7(9), 715-8.

Egelman, E. H. (1985, Apr). The structure of F-actin. J Muscle Res Cell Motil, 6(2), 129-51.

Egelman, E. H. (2003, Aug). A tale of two polymers: new insights into helical filaments. Nat Rev Mol Cell Biol, 4(8), 621-30.

Estes, J. E., Selden, L. A., and Gershman, L. C. (1987, Apr). Tight binding of divalent cations to monomeric actin. Binding kinetics support a simplified model. J Biol Chem, 262(11), 4952-7.

Falck, S., Paavilainen, V. O., Wear, M. A., Grossmann, J. G., Cooper, J. A., and Lappalainen, P. (2004, Aug). Biological role and structural mechanism of twinfilin-capping protein interaction. EMBO J, 23(15), 3010-9.

Fanning, A. S., Wolenski, J. S., Mooseker, M. S., and Izant, J. G. (1994). Differential regulation of skeletal muscle myosin-II and brush border myosin-I

enzymology and mechanochemistry by bacterially produced tropomyosin isoforms. Cell Motil Cytoskeleton, 29(1), 29-45.

Feuillette, S., Deramecourt, V., Laquerriere, A., Duyckaerts, C., Delisle, M.-B., Maurage, C.-A., Blum, D., Buée, L., Frébourg, T., Campion, D., and Lecourtois, M. (2010, Jul). Filamin-A and Myosin VI colocalize with fibrillary Tau protein in Alzheimer's disease and FTDP-17 brains. Brain Res, 1345, 182-9.

Frieden, C. (1983, Nov). Polymerization of actin: mechanism of the Mg2+-induced process at pH 8 and 20 degrees C. Proc Natl Acad Sci U S A, 80(21), 6513-7.

Galkin, V. E., Orlova, A., Cherepanova, O., Lebart, M.-C., and Egelman, E. H. (2008, Feb). High-resolution cryo-EM structure of the F-actin-fimbrin/plastin ABD2 complex. Proc Natl Acad Sci U S A, 105(5), 1494-8.

Ge, P., Durer, Z. A. O., Kudryashov, D., Zhou, Z. H., and Reisler, E. (2014, Dec). Cryo-EM reveals different coronin binding modes for ADP- and ADP-BeFx actin filaments. Nat Struct Mol Biol, 21(12), 1075-81.

Geisbrecht, E. R. and Montell, D. J. (2002, Aug). Myosin VI is required for E-cadherin-mediated border cell migration. Nat Cell Biol, 4(8), 616-20.

Goodson, H. V., Anderson, B. L., Warrick, H. M., Pon, L. A., and Spudich, J. A. (1996, Jun). Synthetic lethality screen identifies a novel yeast myosin I gene (MYO5): myosin I proteins are required for polarization of the actin cytoskeleton. J Cell Biol, 133(6), 1277-91.

Graceffa, P. and Dominguez, R. (2003, Sep). Crystal structure of monomeric actin in the ATP state. Structural basis of nucleotide-dependent actin dynamics. J Biol Chem, 278(36), 34172-80.

Grabenbauer M (2012) Correlative light and electron microscopy of GFP. Methods Cell Biol. 111: 117–138.

Griscelli, C., Durandy, A., Guy-Grand, D., Daguillard, F., Herzog, C., and Prunieras, M. (1978, Oct). A syndrome associating partial albinism and immunodeficiency. Am J Med, 65(4), 691-702.

Grissom, P. M., Fiedler, T., Grishchuk, E. L., Nicastro, D., West, R. R., and McIntosh, J. R. (2009, Feb). Kinesin-8 from fission yeast: a heterodimeric, plus-end-directed motor that can couple microtubule depolymerization to cargo movement. Mol Biol Cell, 20(3), 963-72.

Hancock, W. O. and Howard, J. (1998, Mar). Processivity of the motor protein kinesin requires two heads. J Cell Biol, 140(6), 1395-405.

Hartman, M. A., Finan, D., Sivaramakrishnan, S., and Spudich, J. A. (2011). Principles of unconventional myosin function and targeting. Annu Rev Cell Dev Biol, 27, 133-55.

Hasson, T. (2003, Sep). Myosin VI: two distinct roles in endocytosis. J Cell Sci, 116(Pt 17), 3453-61.

Hasson, T., Gillespie, P. G., Garcia, J. A., MacDonald, R. B., Zhao, Y., Yee, A. G., Mooseker, M. S., and Corey, D. P. (1997, Jun). Unconventional myosins in inner-ear sensory epithelia. J Cell Biol, 137(6), 1287-307.

Hertzano, R., Shalit, E., Rzadzinska, A. K., Dror, A. A., Song, L., Ron, U., Tan, J. T., Shitrit, A. S., Fuchs, H., Hasson, T., Ben-Tal, N., Sweeney, H. L., de Angelis, M. H., Steel, K. P., and Avraham, K. B. (2008). A Myo6 mutation destroys coordination between the myosin heads, revealing new functions of myosin VI in the stereocilia of mammalian inner ear hair cells. PLoS Genet, 4(10), e1000207.

Hirano, Y., Hatano, T., Takahashi, A., Toriyama, M., Inagaki, N., and Hakoshima, T. (2011, Jul). Structural basis of cargo recognition by the myosin-X MyTH4-FERM domain. EMBO J, 30(13), 2734-47.

Hodges, A. R., Krementsova, E. B., Bookwalter, C. S., Fagnant, P. M., Sladewski, T. E., and Trybus, K. M. (2012). Tropomyosin is essential for processive movement of a class V myosin from budding yeast. Current Biology, 22(15), 1410–1416.

Hsu, K.-S. and Kao, H.-Y. (2013). Alpha-actinin 4 and tumorigenesis of breast cancer. Vitam Horm, 93, 323-51.

Huang, J., Koide, A., Makabe, K., and Koide, S. (2008, May). Design of protein function leaps by directed domain interface evolution. Proc Natl Acad Sci U S A, 105(18), 6578-83.

Huang, J., Nagy, S. S., Koide, A., Rock, R. S., and Koide, S. (2009). A peptide tag system for facile purification and single-molecule immobilization. Biochemistry, 48(50), 11834–11836.

Hwang, Y.-S., Luo, T., Xu, Y., and Sargent, T. D. (2009, Oct). Myosin-X is required for cranial neural crest cell migration in Xenopus laevis. Dev Dyn, 238(10), 2522-9.

Ikezaki, K., Komori, T., and Yanagida, T. (2013). Spontaneous detachment of the leading head contributes to myosin VI backward steps. PLoS One, 8(3), e58912.

Isambert, H., Venier, P., Maggs, A. C., Fattoum, A., Kassab, R., Pantaloni, D., and Carlier, M.-F. (1995). Flexibility of actin filaments derived from thermal

fluctuations. Effect of bound nucleotide, phalloidin, and muscle regulatory proteins. Journal of Biological Chemistry, 270(19), 11437–11444.

Kabsch, W., Mannherz, H. G., Suck, D., Pai, E. F., and Holmes, K. C. (1990, Sep). Atomic structure of the actin:DNase I complex. Nature, 347(6288), 37-44.

Kang, H., Bradley, M. J., McCullough, B. R., Pierre, A., Grintsevich, E. E., Reisler, E., and De La Cruz, E. M. (2012, Oct). Identification of cation-binding sites on actin that drive polymerization and modulate bending stiffness. Proc Natl Acad Sci U S A, 109(42), 16923-7.

Kaplan, E. L. and Meier, P. (1958). Nonparametric estimation from incomplete observations. Journal of the American statistical association, 53(282), 457–481.

Kerber, M. L. and Cheney, R. E. (2011, Nov). Myosin-X: a MyTH-FERM myosin at the tips of filopodia. J Cell Sci, 124(Pt 22), 3733-41.

Kerber, M. L., Jacobs, D. T., Campagnola, L., Dunn, B. D., Yin, T., Sousa, A. D., Quintero, O. A., and Cheney, R. E. (2009, Jun). A novel form of motility in filopodia revealed by imaging myosin-X at the single-molecule level. Curr Biol, 19(11), 967-73.

Kinoshita, K., Arnal, I., Desai, A., Drechsel, D. N., and Hyman, A. A. (2001, Nov). Reconstitution of physiological microtubule dynamics using purified components. Science, 294(5545), 1340-3.

Kodera, N., Yamamoto, D., Ishikawa, R., and Ando, T. (2010, Nov). Video imaging of walking myosin V by high-speed atomic force microscopy. Nature, 468(7320), 72-6.

Koide, H., Kinoshita, T., Tanaka, Y., Tanaka, S., Nagura, N., Meyer zu Hörste, G., Miyagi, A., and Ando, T. (2006, Sep). Identification of the single specific IQ motif of myosin V from which calmodulin dissociates in the presence of Ca2+. Biochemistry, 45(38), 11598-604.

Kron, S. J. and Spudich, J. A. (1986). Fluorescent actin filaments move on myosin fixed to a glass surface. Proceedings of the National Academy of Sciences, 83(17), 6272–6276.

Kudryashov, D. S. and Reisler, E. (2003, Oct). Solution properties of tetramethylrhodamine-modified G-actin. Biophys J, 85(4), 2466-75.

Kudryashov, D. S. and Reisler, E. (2013). ATP and ADP actin states. Biopolymers, 99(4), 245–256.

Lan, L., Han, H., Zuo, H., Chen, Z., Du, Y., Zhao, W., Gu, J., and Zhang, Z. (2010, Jan). Upregulation of myosin Va by Snail is involved in cancer cell migration and metastasis. Int J Cancer, 126(1), 53-64.

Lehto, T, Miaczynska, M, Zerial, M, Müller, DJ and Severin, F. (2003). Observing the growth of individual actin filaments in cell extracts by time-lapse atomic force microscopy. FEBS letters, 551(1-3), 25-8.

Li, X.-D., Ikebe, R., and Ikebe, M. (2005, May). Activation of myosin Va function by melanophilin, a specific docking partner of myosin Va. J Biol Chem, 280(18), 17815-22.

Li, X.-d., Jung, H. S., Mabuchi, K., Craig, R., and Ikebe, M. (2006, Aug). The globular tail domain of myosin Va functions as an inhibitor of the myosin Va motor. J Biol Chem, 281(31), 21789-98.

Liu, K. C., Jacobs, D. T., Dunn, B. D., Fanning, A. S., and Cheney, R. E. (2012, May). Myosin-X functions in polarized epithelial cells. Mol Biol Cell, 23(9), 1675-87.

Liu, X. Z., Walsh, J., Mburu, P., Kendrick-Jones, J., Cope, M. J., Steel, K. P., and Brown, S. D. (1997, Jun). Mutations in the myosin VIIA gene cause non-syndromic recessive deafness. Nat Genet, 16(2), 188-90.

Lorenz, M. and Holmes, K. C. (2010). The actin-myosin interface. Proceedings of the National Academy of Sciences, 107(28), 12529–12534.

Loussert-Fonta, C, and Humbel, BM, (2015 Sept) Correlative microscopy. Arch Biochem Biophys. 581(98-110)

Lu, Q., Ye, F., Wei, Z., Wen, Z., and Zhang, M. (2012, Oct). Antiparallel coiled-coil-mediated dimerization of myosin X. Proc Natl Acad Sci U S A, 109(43), 17388-93.

Lu, Q., Yu, J., Yan, J., Wei, Z., and Zhang, M. (2011, Nov). Structural basis of the myosin X PH1(N)-PH2-PH1(C) tandem as a specific and acute cellular PI(3,4,5)P(3) sensor. Mol Biol Cell, 22(22), 4268-78.

McDonough, A. A. (2009, Dec). Motoring down the microvilli. Focus on "PTH-induced internalization of apical membrane NaPi2a: role of actin and myosin VI". Am J Physiol Cell Physiol, 297(6), C1331-2.

McVicker, D. P., Chrin, L. R., and Berger, C. L. (2011, Dec). The nucleotide-binding state of microtubules modulates kinesin processivity and the ability of Tau to inhibit kinesin-mediated transport. J Biol Chem, 286(50), 42873-80.

Mehta, A. D., Rock, R. S., Rief, M., Spudich, J. A., Mooseker, M. S., and Cheney, R. E. (1999, Aug). Myosin-V is a processive actin-based motor. Nature, 400(6744), 590-3.

Melchionda, S., Ahituv, N., Bisceglia, L., Sobe, T., Glaser, F., Rabionet, R., Arbones, M. L., Notarangelo, A., Di Iorio, E., Carella, M., Zelante, L., Estivill, X., Avraham, K. B., and Gasparini, P. (2001, Sep). MYO6, the human homologue of the gene responsible for deafness in Snell's waltzer mice, is mutated in autosomal dominant nonsyndromic hearing loss. Am J Hum Genet, 69(3), 635-40.

Melki, R., Fievez, S., and Carlier, M. F. (1996, Sep). Continuous monitoring of Pi release following nucleotide hydrolysis in actin or tubulin assembly using 2-amino-6-mercapto-7-methylpurine ribonucleoside and purine-nucleoside phosphorylase as an enzyme-linked assay. Biochemistry, 35(37), 12038-45.

Ménasché, G., Ho, C. H., Sanal, O., Feldmann, J., Tezcan, I., Ersoy, F., Houdusse, A., Fischer, A., and de Saint Basile, G. (2003, Aug). Griscelli syndrome restricted to hypopigmentation results from a melanophilin defect (GS3) or a MYO5A F-exon deletion (GS1). J Clin Invest, 112(3), 450-6.

Ménétrey, J., Llinas, P., Mukherjea, M., Sweeney, H. L., and Houdusse, A. (2007, Oct). The structural basis for the large powerstroke of myosin VI. Cell, 131(2), 300-8.

Mohiddin, S. A., Ahmed, Z. M., Griffith, A. J., Tripodi, D., Friedman, T. B., Fananapazir, L., and Morell, R. J. (2004, Apr). Novel association of hypertrophic cardiomyopathy, sensorineural deafness, and a mutation in unconventional myosin VI (MYO6). J Med Genet, 41(4), 309-14.

Mukherjea, M., Llinas, P., Kim, H., Travaglia, M., Safer, D., Ménétrey, J., Franzini-Armstrong, C., Selvin, P. R., Houdusse, A., and Sweeney, H. L. (2009, Aug). Myosin VI dimerization triggers an unfolding of a three-helix bundle in order to extend its reach. Mol Cell, 35(3), 305-15.

Müller, D. J. and Dufrêne, Y. F. (2008, May). Atomic force microscopy as a multifunctional molecular toolbox in nanobiotechnology. Nat Nanotechnol, 3(5), 261-9.

Müller, T., Hess, M. W., Schiefermeier, N., Pfaller, K., Ebner, H. L., Heinz-Erian, P., Ponstingl, H., Partsch, J., Röllinghoff, B., Köhler, H., Berger, T., Lenhartz, H., Schlenck, B., Houwen, R. J., Taylor, C. J., Zoller, H., Lechner, S., Goulet, O., Utermann, G., Ruemmele, F. M., Huber, L. A., and Janecke, A. R. (2008, Oct). MYO5B mutations cause microvillus inclusion disease and disrupt epithelial cell polarity. Nat Genet, 40(10), 1163-5.

Murphy, C. T. and Spudich, J. A. (1999). The sequence of the myosin 50-20K loop affects Myosin's affinity for actin throughout the actin-myosin ATPase cycle and its maximum ATPase activity. Biochemistry, 38(12), 3785–3792.

Nagy, S., Ricca, B. L., Norstrom, M. F., Courson, D. S., Brawley, C. M., Smithback, P. A., and Rock, R. S. (2008, Jul). A myosin motor that selects bundled actin for motility. Proc Natl Acad Sci U S A, 105(28), 9616-20.

Nagy, S. and Rock, R. S. (2010). Structured post-IQ domain governs selectivity of myosin X for fascin-actin bundles. Journal of Biological Chemistry, 285(34), 26608–26617.

Narita, A., Usukura, E., Yagi, A., Tateyama, K., Akizuki, S., Kikumoto, M., Matsumoto, T., Maéda, Y., Ito, S., and Usukura, J. (2016, May). Direct observation of the actin filament by tip-scan atomic force microscopy. Microscopy (Oxf), .

Ng, K. P., Kambara, T., Matsuura, M., Burke, M., and Ikebe, M. (1996, Jul). Identification of myosin III as a protein kinase. Biochemistry, 35(29), 9392-9.

Oda, T., Iwasa, M., Aihara, T., Maéda, Y., and Narita, A. (2009, Jan). The nature of the globular- to fibrous-actin transition. Nature, 457(7228), 441-5.

Odronitz, F. and Kollmar, M. (2007). Drawing the tree of eukaryotic life based on the analysis of 2,269 manually annotated myosins from 328 species. Genome Biol, 8(9), R196.

Oosawa, F. and Kasai, M. (1962, Jan). A theory of linear and helical aggregations of macromolecules. J Mol Biol, 4, 10-21.

Orlova, A. and Egelman, E. H. (1993, Jul). A conformational change in the actin subunit can change the flexibility of the actin filament. J Mol Biol, 232(2), 334-41.

Ostap, E. M. and Pollard, T. D. (1996, Apr). Overlapping functions of myosin-I isoforms? J Cell Biol, 133(2), 221-4.

Pardee, J. D. and Spudich, J. A. (1982). Purification of muscle actin. Methods Enzymol, 85 Pt B, 164-81.

Pashkova, N., Catlett, N. L., Novak, J. L., Wu, G., Lu, R., Cohen, R. E., and Weisman, L. S. (2005, Jan). Myosin V attachment to cargo requires the tight association of two functional subdomains. J Cell Biol, 168(3), 359-64.

Pastural, E., Barrat, F. J., Dufourcq-Lagelouse, R., Certain, S., Sanal, O., Jabado, N., Seger, R., Griscelli, C., Fischer, A., and de Saint Basile, G. (1997, Jul). Griscelli disease maps to chromosome 15q21 and is associated with mutations in the myosin-Va gene. Nat Genet, 16(3), 289-92.

Plantard, L., Arjonen, A., Lock, J. G., Nurani, G., Ivaska, J., and Strömblad, S. (2010, Oct). PtdIns(3,4,5)P_3 is a regulator of myosin-X localization and filopodia formation. J Cell Sci, 123(Pt 20), 3525-34.

Pollard, T. D. (1986). Rate constants for the reactions of ATP-and ADP-actin with the ends of actin filaments. The Journal of cell biology, 103(6), 2747–2754.

Pollard, T. D. and Cooper, J. A. (2009, Nov). Actin, a central player in cell shape and movement. Science, 326(5957), 1208-12.

Pollard, T. D. and Weeds, A. G. (1984). The rate constant for ATP hydrolysis by polymerized actin. FEBS letters, 170(1), 94–98.

Porter, J. A. and Montell, C. (1993, Aug). Distinct roles of the Drosophila ninaC kinase and myosin domains revealed by systematic mutagenesis. J Cell Biol, 122(3), 601-12.

Prochniewicz, E., Chin, H. F., Henn, A., Hannemann, D. E., Olivares, A. O., Thomas, D. D., and De La Cruz, E. M. (2010, Feb). Myosin isoform determines the conformational dynamics and cooperativity of actin filaments in the strongly bound actomyosin complex. J Mol Biol, 396(3), 501-9.

Prochniewicz, E., Pierre, A., McCullough, B. R., Chin, H. F., Cao, W., Saunders, L. P., Thomas, D. D., and De La Cruz, E. M. (2011, Oct). Actin filament dynamics in the actomyosin VI complex is regulated allosterically by calcium-calmodulin light chain. J Mol Biol, 413(3), 584-92.

Prochniewicz, E. and Yanagida, T. (1990, Dec). Inhibition of sliding movement of F-actin by crosslinking emphasizes the role of actin structure in the mechanism of motility. J Mol Biol, 216(3), 761-72.

Pylypenko, O., Song, L., Shima, A., Yang, Z., Houdusse, A. M., and Sweeney, H. L. (2015, Mar). Myosin VI deafness mutation prevents the initiation of processive runs on actin. Proc Natl Acad Sci U S A, 112(11), E1201-9.

Reck-Peterson, S. L., Provance Jr., D. W., Mooseker, M. S., and Mercer, J. A. (2000, March). Class V myosins. Biochimica et Biophysica Acta (BBA) - Molecular Cell Research, 1496(1), 36–51.

Ricca, B. L. and Rock, R. S. (2010, Sep). The stepping pattern of myosin X is adapted for processive motility on bundled actin. Biophys J, 99(6), 1818-26.

Riemslag, E. E. F., Janson, M. E., and Dogterom, M. (2004, Dec). Active motor proteins can couple cargo to the ends of growing microtubules. Phys Biol, 1(3-4), C5-11.

Rock, R. S., Ramamurthy, B., Dunn, A. R., Beccafico, S., Rami, B. R., Morris, C., Spink, B. J., Franzini-Armstrong, C., Spudich, J. A., and Sweeney, H. L. (2005, Feb). A flexible domain is essential for the large step size and processivity of myosin VI. Mol Cell, 17(4), 603-9.

Rock, R. S., Rice, S. E., Wells, A. L., Purcell, T. J., Spudich, J. A., and Sweeney, H. L. (2001, November). Myosin VI is a processive motor with a large step size. PNAS, 98(24), 13655–13659.

Rock, R. S., Rief, M., Mehta, A. D., and Spudich, J. A. (2000, December). In Vitro Assays of Processive Myosin Motors. Methods, 22(4), 373–381.

Rodriguez, O. C. and Cheney, R. E. (2002, Mar). Human myosin-Vc is a novel class V myosin expressed in epithelial cells. J Cell Sci, 115(Pt 5), 991-1004.

Rogers, M. S. and Strehler, E. E. (2001, Apr). The tumor-sensitive calmodulin-like protein is a specific light chain of human unconventional myosin X. J Biol Chem, 276(15), 12182-9.

Roland, J. T., Kenworthy, A. K., Peranen, J., Caplan, S., and Goldenring, J. R. (2007, Aug). Myosin Vb interacts with Rab8a on a tubular network containing EHD1 and EHD3. Mol Biol Cell, 18(8), 2828-37.

Rosenfeld, S. S. and Sweeney, H. L. (2004, September). A Model of Myosin V Processivity. J. Biol. Chem., 279(38), 40100–40111.

Sahlender, D. A., Roberts, R. C., Arden, S. D., Spudich, G., Taylor, M. J., Luzio, J. P., Kendrick-Jones, J., and Buss, F. (2005, Apr). Optineurin links myosin VI to the Golgi complex and is involved in Golgi organization and exocytosis. J Cell Biol, 169(2), 285-95.

Sakamoto, T., Webb, M. R., Forgacs, E., White, H. D., and Sellers, J. R. (2008, Sep). Direct observation of the mechanochemical coupling in myosin Va during processive movement. Nature, 455(7209), 128-32.

Santos, A.; Joanna M. Kalita; Rock, R. (2016, Nov). Slow and steady wins the race: encounters of myosin-5 and myosin-6 on shared actin filaments. Pre-printed in bioRxiv 087940, in submission to peer reviewed journal.

Sellers, J. R. (2001). In Vitro Motility Assay to Study Translocation of Actin by Myosin. .

Sellers, J. R. and Goodson, H. V. (1995). Motor proteins 2: myosin. Protein Profile, 2(12), 1323-1423.

Semenova, I., Burakov, A., Berardone, N., Zaliapin, I., Slepchenko, B., Svitkina, T., Kashina, A., and Rodionov, V. (2008). Actin dynamics is essential for myosin-based transport of membrane organelles. Current Biology, 18(20), 1581–1586.

Sept, D. and McCammon, J. A. (2001, Aug). Thermodynamics and kinetics of actin filament nucleation. Biophys J, 81(2), 667-74.

da Silva, L. P. (2002, Apr). Atomic force microscopy and proteins. Protein Pept Lett, 9(2), 117-26.

Sckolnick, M., Krementsova, E. B., Warshaw, D. M., and Trybus, K. M. (2016, Aug). Tropomyosin isoforms bias actin track selection by vertebrate myosin Va. Mol Biol Cell, .

Sousa, A. D., Berg, J. S., Robertson, B. W., Meeker, R. B., and Cheney, R. E. (2006, Jan). Myo10 in brain: developmental regulation, identification of a headless isoform and dynamics in neurons. J Cell Sci, 119(Pt 1), 184-94.

Spudich, J. A., Kron, S. J., and Sheetz, M. P. (1985). Movement of myosin-coated beads on oriented filaments reconstituted from purified actin. .

Spudich, J. A. and Sivaramakrishnan, S. (2010, Feb). Myosin VI: an innovative motor that challenged the swinging lever arm hypothesis. Nat Rev Mol Cell Biol, 11(2), 128-37.

Spudich, J. A. and Watt, S. (1971, August). The Regulation of Rabbit Skeletal Muscle Contraction I. Biochemical studies of the interaction of the tropomyosin-troponin complex with actin and the proteolytic fragments of myosin. J. Biol. Chem., 246(15), 4866–4871.

Stefani, M., Tsubakihara, M., Hambly, B. D., Liew, C. C., Allen, P. D., Macdonald, P. S., and dos Remedios, C. G. (2008). Actin and Its Binding Proteins in Heart Failure. , 318–334.

Strehler, E. E. (2011, Apr). Emanuel Strehler's work on calcium pumps and calcium signaling. World J Biol Chem, 2(4), 67-72.

Suarez, C., Roland, J., Boujemaa-Paterski, R., Kang, H., McCullough, B. R., Reymann, A.-C., Guérin, C., Martiel, J.-L., De la Cruz, E. M., and Blanchoin, L. (2011, May). Cofilin tunes the nucleotide state of actin filaments and severs at bare and decorated segment boundaries. Curr Biol, 21(10), 862-8.

Svitkina, T. M. and Borisy, G. G. (1999, May). Arp2/3 complex and actin depolymerizing factor/cofilin in dendritic organization and treadmilling of actin filament array in lamellipodia. J Cell Biol, 145(5), 1009-26.

Sweeney, H. L., Park, H., Zong, A. B., Yang, Z., Selvin, P. R., and Rosenfeld, S. S. (2007, Jun). How myosin VI coordinates its heads during processive movement. EMBO J, 26(11), 2682-92.

Swiatecka-Urban, A., Talebian, L., Kanno, E., Moreau-Marquis, S., Coutermarsh, B., Hansen, K., Karlson, K. H., Barnaby, R., Cheney, R. E., Langford, G. M., Fukuda, M., and Stanton, B. A. (2007, Aug). Myosin Vb is required for trafficking of the cystic fibrosis transmembrane conductance regulator in

Rab11a-specific apical recycling endosomes in polarized human airway epithelial cells. J Biol Chem, 282(32), 23725-36.

Tang, N. and Ostap, E. M. (2001, Jul). Motor domain-dependent localization of myo1b (myr-1). Curr Biol, 11(14), 1131-5.

Tokuo, H. and Ikebe, M. (2004, Jun). Myosin X transports Mena/VASP to the tip of filopodia. Biochem Biophys Res Commun, 319(1), 214-20.

Tokuo, H., Mabuchi, K., and Ikebe, M. (2007). The motor activity of myosin-X promotes actin fiber convergence at the cell periphery to initiate filopodia formation. The Journal of cell biology, 179(2), 229–238.

Trybus, K. M. (2008, May). Myosin V from head to tail. Cell Mol Life Sci, 65(9), 1378-89.

Trybus, K. M., Freyzon, Y., Faust, L. Z., and Sweeney, H. L. (1997, Jan). Spare the rod, spoil the regulation: necessity for a myosin rod. Proc Natl Acad Sci U S A, 94(1), 48-52.

Trybus, K. M., Gushchin, M. I., Lui, H., Hazelwood, L., Krementsova, E. B., Volkmann, N., and Hanein, D. (2007, Aug). Effect of calcium on calmodulin bound to the IQ motifs of myosin V. J Biol Chem, 282(32), 23316-25.

Tumbarello, D. A., Kendrick-Jones, J., and Buss, F. (2013, Jun). Myosin VI and its cargo adaptors - linking endocytosis and autophagy. J Cell Sci, 126(Pt 12), 2561-70.

Tumbarello, D. A., Waxse, B. J., Arden, S. D., Bright, N. A., Kendrick-Jones, J., and Buss, F. (2012, Oct). Autophagy receptors link myosin VI to autophagosomes to mediate Tom1-dependent autophagosome maturation and fusion with the lysosome. Nat Cell Biol, 14(10), 1024-35.

Uemura, S., Higuchi, H., Olivares, A. O., De La Cruz, E. M., and Ishiwata, S. (2004, Sep). Mechanochemical coupling of two substeps in a single myosin V motor. Nat Struct Mol Biol, 11(9), 877-83.

Vale, R. D. (2003, Nov). Myosin V motor proteins: marching stepwise towards a mechanism. J Cell Biol, 163(3), 445-50.

Vavra, K. C., Xia, Y., and Rock, R. S. (2016, Jun). Competition between Coiled-Coil Structures and the Impact on Myosin-10 Bundle Selection. Biophys J, 110(11), 2517-27.

Volkmann, N., Liu, H., Hazelwood, L., Krementsova, E. B., Lowey, S., Trybus, K. M., and Hanein, D. (2005, Sep). The structural basis of myosin V processive movement as revealed by electron cryomicroscopy. Mol Cell, 19(5), 595-605.

Weber, K. L., Sokac, A. M., Berg, J. S., Cheney, R. E., and Bement, W. M. (2004, Sep). A microtubule-binding myosin required for nuclear anchoring and spindle assembly. Nature, 431(7006), 325-9.

Wei, M.-Y., Leon, L. J., Lee, Y., Parks, D., Carroll, L., and Famouri, P. (2011, Apr). Selective attachment of F-actin with controlled length for developing an intelligent nanodevice. J Colloid Interface Sci, 356(1), 182-9.

Wells, A. L., Lin, A. W., Chen, L.-Q., Safer, D., Cain, S. M., Hasson, T., Carragher, B. O., Milligan, R. A., and Sweeney, H. L. (1999, September). Myosin VI is an actin-based motor that moves backwards. Nature, 401(6752), 505–508.

Woolner, S., O'Brien, L. L., Wiese, C., and Bement, W. M. (2008, Jul). Myosin-10 and actin filaments are essential for mitotic spindle function. J Cell Biol, 182(1), 77-88.

Yamashita, R. A. and May, G. S. (1998, Jun). Constitutive activation of endocytosis by mutation of myoA, the myosin I gene of Aspergillus nidulans. J Biol Chem, 273(23), 14644-8.

Yang, L. E., Maunsbach, A. B., Leong, P. K. K., and McDonough, A. A. (2005, Oct). Redistribution of myosin VI from top to base of proximal tubule microvilli during acute hypertension. J Am Soc Nephrol, 16(10), 2890-6.

Yengo, C. M. and Sweeney, H. L. (2004). Functional role of loop 2 in myosin V. Biochemistry, 43(9), 2605–2612.

Yoder, B. J., Tso, E., Skacel, M., Pettay, J., Tarr, S., Budd, T., Tubbs, R. R., Adams, J. C., and Hicks, D. G. (2005, Jan). The expression of fascin, an actin-bundling motility protein, correlates with hormone receptor-negative breast cancer and a more aggressive clinical course. Clin Cancer Res, 11(1), 186-92.

Yoshida, H., Cheng, W., Hung, J., Montell, D., Geisbrecht, E., Rosen, D., Liu, J., and Naora, H. (2004, May). Lessons from border cell migration in the Drosophila ovary: A role for myosin VI in dissemination of human ovarian cancer. Proc Natl Acad Sci U S A, 101(21), 8144-9.

Yu, C., Feng, W., Wei, Z., Miyanoiri, Y., Wen, W., Zhao, Y., and Zhang, M. (2009, Aug). Myosin VI undergoes cargo-mediated dimerization. Cell, 138(3), 537-48.

Yuan, J., Pillarisetti, A., Goldman, Y. E., and Bau, H. H. (2013, Jan). Orienting actin filaments for directional motility of processive myosin motors. Nano Lett, 13(1), 79-84.

Zahm, J. A., Padrick, S. B., Chen, Z., Pak, C. W., Yunus, A. A., Henry, L., Tomchick, D. R., Chen, Z., and Rosen, M. K. (2013, Oct). The bacterial effector VopL organizes actin into filament-like structures. Cell, 155(2), 423-34.

Zimmermann, D., Santos, A., Kovar, D. R., and Rock, R. S. (2015, Aug). Actin age orchestrates myosin-5 and myosin-6 run lengths. Curr Biol, 25(15), 2057-62.